DYE SENSITIZED SOLAR CELLS WITH TEMPLATED TiO_2 COATINGS

by

SARIKA A. PHADKE

A Dissertation submitted to the

Graduate School-New Brunswick

Rutgers, The State University of New Jersey

In partial fulfillment of the requirements

for the degree of

Doctor of Philosophy

Graduate Program in Materials Science and Engineering

Written under the direction of

Dr. Dunbar P. Birnie, III

And approved by

_____

_____

_____

_____

New Brunswick, New Jersey

[January, 2010]

ABSTRACT OF THE DISSERTATION

DYE SENSITIZED SOLAR CELLS WITH TEMPLATED TiO_2 COATINGS

By SARIKA A. PHADKE

Dissertation Director:

Dr. Dunbar P. Birnie, III

Photovoltaic (PV) technology can make a significant contribution in energy production if it becomes more economical and technologically more competitive with other renewable and conventional energy sources. Dye sensitized solar cell (DSSC) is a third generation PV technology which utilizes easily available raw material and low cost manufacturing methods. The performance of the DSSC technology is not yet at par with the existing crystalline silicon and thin film based photovoltaic technologies. Therefore to realize the real potential of DSSC, fundamental research in understanding the device physics and identifying the most promising cell material and configuration is necessary. This research focuses on the titanium dioxide coating, which is used as the photoanode in the DSSC. The titania coating transfers the electrons injected from the adsorbed dye to the electrode. For efficient regeneration of the dye, the redox electrolyte present in between the two electrodes of the cell has to be in intimate contact with the titania nanoparticles. This requires the titania coating to contain interpenetrating network of meso and macro pores. The present research employs sacrificial templating technique to incorporate porosity into the titania coating. Oil in water emulsions have been primarily

used as the templating material and they provide a very cost effective and simple way to produce the porous coatings. Different commercial techniques have been used to produce the emulsion templated titania coatings such as blade coating, spin coating and roll to roll coating. Their microstructures were analyzed and compared in detail. Mercury porosimetry and BET surface area measurements were also employed to characterize the pore size distribution and surface area of the emulsion templated coatings. To understand the effect of the added porosity on the internal resistances and kinetics of the TiO_2/dye/electrolyte interface, electrochemical impedance spectroscopic (EIS) analysis was performed. EIS analysis showed that the templated coatings had lower impedances and they provided faster diffusion of ionic species through the titania coating. The current-voltage characterization of the emulsion templated dye sensitized solar cells showed an increase in the photocurrent and photovoltage as compared to the nontemplated cells. Cells templated with the 20 wt% oil in water emulsion had twice the efficiency as compared to the non-templated solar cells.

ACKNOWLEDGEMENT

I dedicate this thesis to my family- my parents and my husband. They have been my constant support and encouragement during my doctoral study and especially during the writing of this thesis.

I owe my deepest gratitude to my advisor, Dr. Dunbar P. Birnie, III, for his guidance and continuous support to my PhD study and research. He was always accessible and willing to help me during all the difficult times. I could not have imagined having a better advisor and mentor for my doctoral study. I would also like to thank all my fellow groupmates at Rutgers University for all the stimulating discussions and for being so cooperative while I was away on my maternity leave. I especially want to thank my undergraduate group mates, Jerome, Jay, Mike and Brian for helping me in all the mundane lab work.

Along with my thesis advisor, I would like to thank the rest of my committee members, Dr. Richard Haber, Dr. Lisa Klein and Dr. James Guiheen for their guidance and support.

I think Dr. James Guiheen deserves a special mention, as he has been my true mentor during last two years. During my internship at Honeywell Specialty Materials, I learned so much through the stimulating discussions with him. This experience broadened my perspective on different aspects of industry. I thank Jim sincerely for all his insightful comments.

I want to thank all the faculty members at the Materials Science department for their guidance and encouragement. My deepest gratitude goes to Dr. Greenhut who showed immense confidence in me and convinced me to pursue doctoral

studies. I also want to thank the postdocs Andrei Jitianu, Mihaela Jitianu and Swanand Patil for training me on various equipments and for helping me resolve (often silly) experimental problems. I also want to thank Phyllis Cassel, Phillip Grill and Claudia Cuchinow for their help in sorting out all the administrative issues.

TABLE OF CONTENTS

LIST OF TABLES

LIST OF FIGURES

CHAPTER 1: INTRODUCTION

The present dissertation is concerned with photovoltaic technology (PV). Improved dye sensitized solar cells (DSSC) were developed with an eye toward methods that would have the potential to allow cells to be produced at low cost. PV technology is expected to play a more significant role in future global energy production. The present research work is aimed at making enhanced microstructures that will enable lower cost processing – and therefore more affordable solar power.

Fossil fuels have long served as the main source of energy for mankind. With increasing population and advances in technology, the energy consumption of the world is increasing tremendously [1]. Since fossil fuels cannot be reused or renewed and also because they are thought to cause global warming, there is a pressing need for renewable, environmentally safe, alternative energy sources. Therefore, alternate renewable energy sources such as wind, hydroelectricity, biomass and photovoltaics (PV) have received a great deal of attention. Photovoltaics convert energy from the Sun to electricity. The Sun provides around 100,000 terawatts of energy to the Earth and by covering 0.1% of the Earth's surface with photovoltaic installations having a conversion efficiency of 10%, the present energy needs of the entire world could be met [2] . Thus photovoltaic technology has great potential to be a sustainable energy source for the future.

Since the 1960's, the photovoltaic market has been dominated by mono- and poly-crystalline silicon solar cells with more than 90% market share [3]. These first generation solar cells are based on p-n junction semiconductor devices. In silicon solar cells electron-hole pairs are generated by absorption of the sunlight and the

electric field generated across the p-n junction helps to collect the photo-induced carriers by attracting the minority carriers across the junction. This generates a net photocurrent. The maximum photo-voltage corresponds to the potential difference that is set up in the dark at the p-n junction. So far crystalline silicon based solar cells have been able to offer the maximum conversion efficiency among all single junction photovoltaic technologies (at about 25%) [3]. Although this technology is quite mature now, it has some disadvantages that limit the pace of installation. The major issue about the crystalline silicon technology is that it is highly capital intensive. It uses extremely clean Si wafers requiring very stringent processing conditions, therefore the material and processing costs are very high. Another drawback, from the scientific point of view, is that silicon has a slight mismatch of absorption edge with the solar spectrum, so the sunlight does not get as efficiently used; a slightly larger band-gap would be better. Also, it is difficult to use Si when making flexible solar cells because many Si deposition techniques involve processes which are harsh or not compatible with the flexible, polymer substrates. This limits the application areas where silicon solar cells can be used.

Since the 1970's, a second generation of photovoltaics, based on thin film technology, has emerged. Cells using II-VI semiconductors such as Cadmium Telluride (CdTe) or having chalcopyrite structure such as Copper Indium Gallium Diselenide (CIGS) are the most common in thin film solar cell technology. Currently the market share of these second generation photovoltaics is still small but they are being increasingly employed as they offer relatively good conversion efficiency (10-15%) at a lower cost-per-Watt. Among the main challenges the thin film solar cells

face are, the use of vacuum deposition techniques to produce the thin films (which involve high processing costs) and the scarcity of the raw materials such as indium, tellurium and selenium. There are also valid worries about the toxicity of cadmium and selenium, even though relatively small quantities are used.

Considering all the key issues with these technologies, there is a sustained need for developing new materials and concepts with lower production costs for photovoltaic conversion. Recently, different types of organic, inorganic, nanoparticle systems have emerged as new candidates for photovoltaic devices. The most well known among these “third-generation” PVs are dye-sensitized solar cells (DSSC) based on TiO_2 nanoparticles and light harvesting organic dye molecules. Dye sensitized cells are technically and economically strong competitors to the established crystalline silicon and other thin film II-V compound solar cells [4]. Although the solar cell efficiencies obtained so far with DSSCs (11-12%) are somewhat lower than achieved by the first and second generation PV technologies, they still offer many advantages such as:

- Fabrication without expensive and energy-intensive high temperature and high vacuum processes,
- Compatibility with rigid as well as flexible substrates and the ability to be produced in a variety of appearances to enter markets for domestic devices and architectural or decorative applications,
- Effective and stable operation under diffused light conditions and lower sensitivity to the angle of incidence [3],
- Easy availability of raw materials, and

- Low health and environmental issues and good recyclability.

In spite of offering all these advantages, dye sensitized solar cells still need to improve technically and economically [3]. Some of the challenges where dye sensitized cells require further research and improvement are as follows:

- Improvement of TiO_2 particle surfaces for better dye and electrolyte permeation,
- Exploration of new dye photo-sensitizers with optimum HOMO/LUMO and broader spectrum of photon to current efficiency, and
- Exploration of new room temperature ionic liquids to replace the existing electrolytes containing volatile solvents, which could improve the long-term stability of these cells.

The goal of the present research was to improve the properties of the TiO_2 coating, which serves as the photoanode in the dye sensitized solar cell. The hypothesis was to template the TiO_2 coating with suitable materials to incorporate interconnected pore structures having a size-scale of a few hundred nanometers. The porous structure would provide better electrolyte permeation and dye absorption into the titania coating and enhance the conduction during solar cell operation. The templated coatings were deposited onto rigid glass substrates as well as on flexible polymer substrates using various commercial methods such as blade coating, spin coating and roll coating. The effect of adding porosity into the titania coatings was studied using microstructural analysis, surface area analysis, porosimetry, impedance spectroscopy, and solar cell performance analysis. Although this research mainly focused on the photovoltaic application, the templating techniques developed to produce coatings with interconnected porous structures could be useful in many other

applications which involve permeation of a liquid into a porous coating to improve diffusion of one or more species.

The thesis has been organized as follows. Chapter 2 contains a literature review, in which the basic structure and operation mechanism of the dye sensitized solar cells are discussed. Chapter 2 also describes various templating methods used so far to produce macroporous structures. In this dissertation, the primary method of producing porous titania coatings was “emulsion templating”. The background of this method has also been presented in Chapter 2. Chapter 3 describes the overall plan of approach for this dissertation. All the main tasks of the research were divided into four basic categories, as presented in Chapter 3. Chapter 4 contains all the detailed experimental procedures and methods used to perform various tasks described in Chapter 3. The results of all the experiments have been presented in Chapter 5 in detail, followed by the conclusions in Chapter 6. Chapter 7 presents some ideas where this work can be extended in future.

References:

1. http://en.wikipedia.org/wiki/World_energy_resources_and_consumption.
2. Gratzel, M. *Photovoltaic and photoelectrochemical conversion of solar energy*. Philosophical Transactions of the Royal Society A 2007, 365: p. 993-1005.
3. Luque, A., Hegedus,S. *Handbook of Photovoltaic Science and Engineering* 2003: John Wiley & Sons, p. 32-36.
4. Gratzel, M. *Perspectives for dye-sensitized nanocrystalline solar cells.* Progress in Photovoltaics: Research and Applications 2000, 8: p. 171-185.

CHAPTER 2: LITERATURE REVIEW

2.1 Photovoltaic technology (PV)

Electricity is a necessity in everyday life. Having cheap and available power plays a very crucial role in the economic development of the industrialized nations. With the increase in world population and tremendous advances in technology, the need for electricity is ever rising [1]. At the beginning of the twenty first century, more than 80% of electricity is generated by burning fossil fuels (coal, gas and oil) [2]. Due to the limited supply of fossil fuels and the growing concerns about global warming, use of more and more renewable energy sources in energy production is being encouraged in many parts of the world [3]. Among the various sources of renewable energy, solar energy has been considered to have great potential because of the virtually unlimited (100KTW) supply of sunlight on the Earth [4]. The technology which harnesses the solar energy and converts it into electrical energy is known as photovoltaic (PV) technology.

2.1.1 History

The first solar cell was made by Fritts [5] in 1883 using a flat sheet of Selenium deposited on a metal sheet. But the modern era of photovoltaics began in 1954 when researchers at Bell AT&T labs observed that under light, p-n junction diodes generated some voltage [6]. Until the 1980s most solar cells were based on doped crystalline silicon semiconductor diodes. These were the first generation photovoltaic cells and they gave an efficiency of around 10 % [2]. In 1980, a second generation of photovoltaics emerged. This technology was based on thin films of amorphous silicon and II-VI binary semiconductors (CIGS,

CdTe). The scale up effort of the thin film PV was found to be far more complicated and expensive than envisioned, therefore many big companies such as IBM, GE, Motorola gave up their research and development in photovoltaics [2]. In the 1990s, through mergers and acquisitions of some key solar cell manufacturers, companies such as United Solar Systems Corp. (USA, Japan), Siemens Solar (Germany), BP solar (UK) emerged. This triggered further research in photovoltaics and initiated its commercialization [2]. By this time, the first generation silicon solar cells had achieved around 25% efficiency and the second generation thin film solar cells were at approximately 15% efficiency.

The basic structure of these systems is illustrated in Figure 2.1 and Figure 2.2, respectively. The working mechanism of these cells is the same as the p-n junction diode. After illumination of the solar cell by sunlight, electron-hole pairs are generated and separated by the built-in electric field across the p-n junction's depletion region. This separation of the charges produces electrical current.

While the operation mechanism is well understood, the extremely high costs involved in the production and deposition of the active semiconductor material are serious challenges faced by these PV technologies. This provides broad incentive for further research in new types of solar cells and lower cost processing techniques. Third generation cells involve new materials and concepts, which many people believe will allow for substantially lower cost systems while maintaining reasonable efficiency. Systems under development now include: dye sensitized solar cells, organic polymer cells, ultra-high efficiency PV (based on quantum dots and nanostructured devices), and solar

concentrator systems. Except for the concentrator systems, all other third generation PV systems are still at the prototype stage. Figure 2.3 gives an overview of the performance of different PV systems over the last thirty years. Figure 2.4 presents the market share of first and second generation PV systems in the world in 2008.

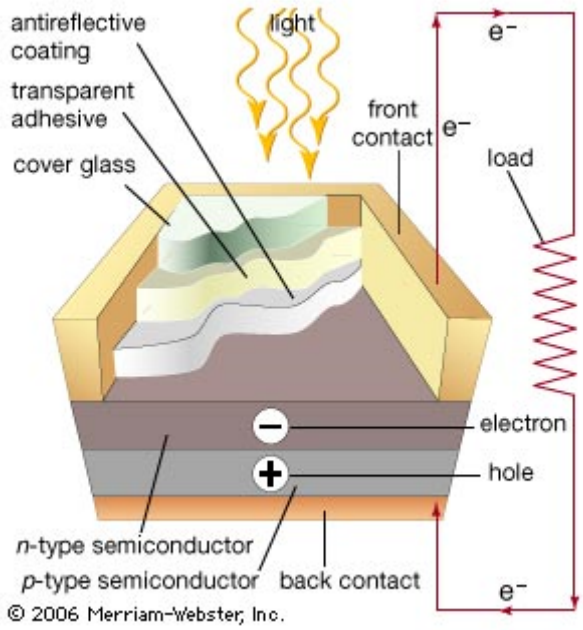

Figure 2.1: Structure of a typical crystalline silicon solar cell [7]

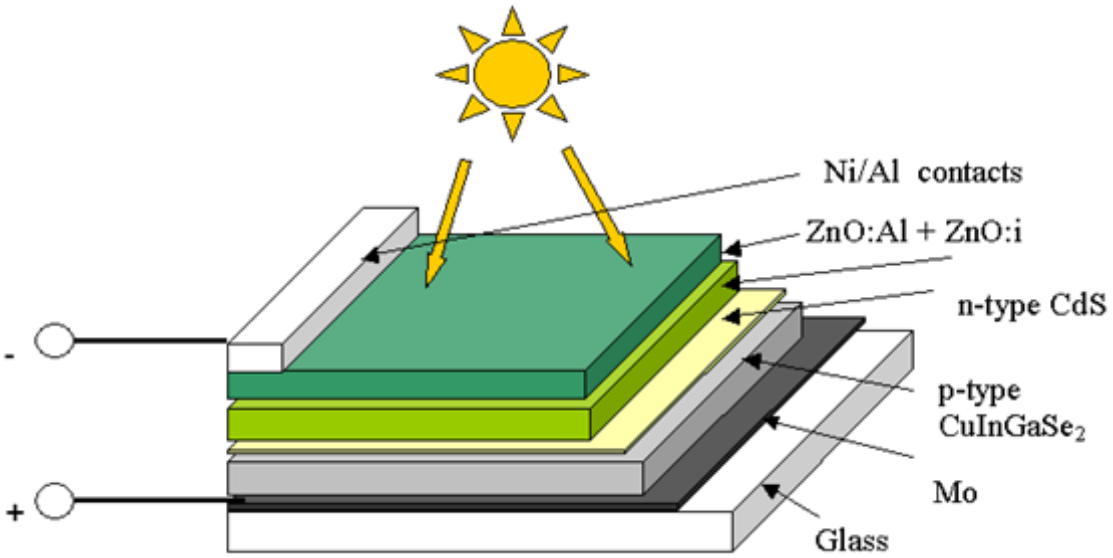

Figure 2.2: Structure of a typical CIGS solar cell [8]

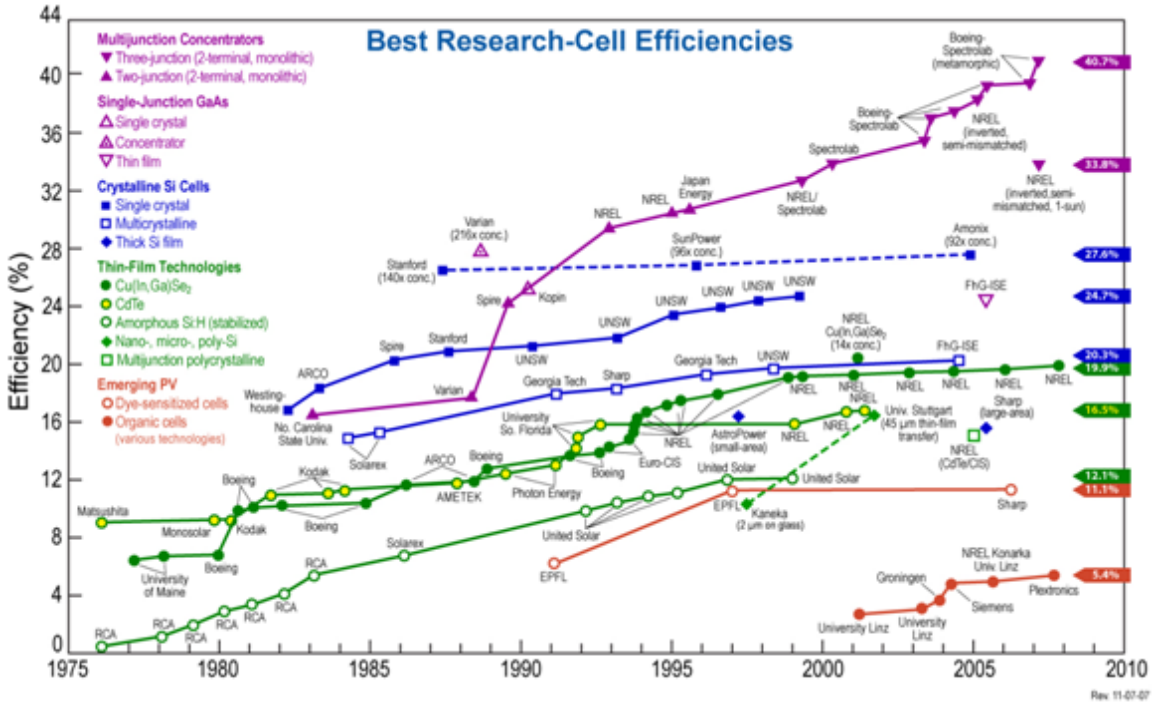

Figure 2.3: The state of different photovoltaic systems at the end of 2007[9]

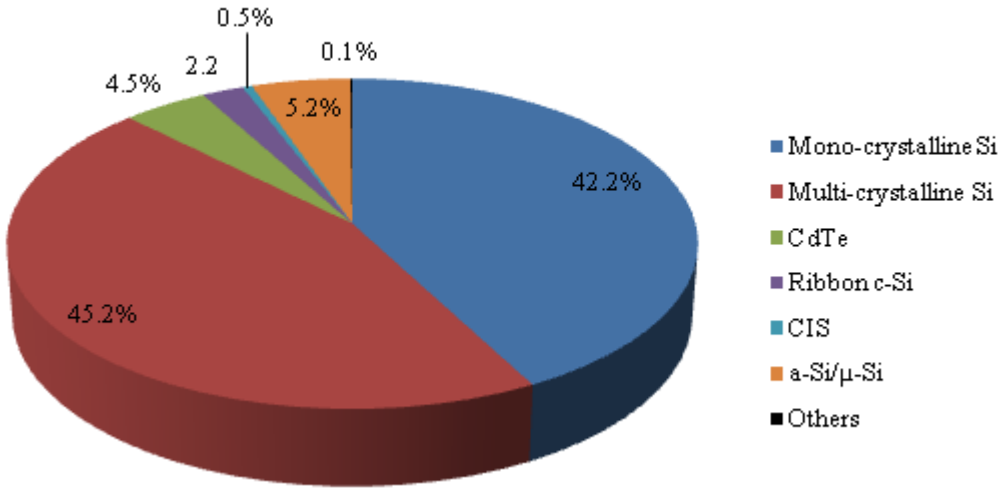

Figure 2.4: 2008 market share of installed PV technologies [3]

2.1.2 Trends

Through the 1980s the main emphasis of research in photovoltaics was to increase efficiency. Substantial improvements in cell and module efficiency were made. But since the 1990s the trend has shifted to the production of low cost photovoltaic systems[1]. Figure 2.5 illustrates the trend in the cost-performance relationship in the three generations of the PV systems. First generation silicon solar cells are mainly high-cost/high-efficiency type cells, thin film cells can come under medium-cost/medium-efficiency cells and all the new types of solar cells try to achieve the low-cost/high-efficiency scenario. In general, the future of PV is mainly going to be decided by the following three factors:

- Cost reduction: Figure 2.6 presents the current and future costs of the existing photovoltaic technologies. It is expected that with high volume production and improvements in the processes, the overall PV cost can reach grid price parity (~$0.15 /kWh) within 5 to 7 years [3, 10]. Some third generation PV systems such as dye sensitized solar cells have the potential to bring the cost at par with the utility grid power earlier than this [2].
- Efficiency improvement: 25% to 30% efficiency is foreseeable for crystalline silicon solar cells [11]. Non-silicon thin film PV also has the potential to go up to 16-17% efficiency [2]. The third generation photovoltaic systems are trying to achieve or exceed these efficiency levels at lower cost.
- Storage networks: If PV is to contribute substantially more of the total electricity required then development of compatible energy storage systems is

1- The important figure of merit for cost is dollars per peak-Watt ($\$/W_p$) where Wp is the power generated by the solar module when illuminated with 1 kW/m2 of luminous power at ambient temperature.

essential to be able to accommodate seasonal and day/night variations in power output.

The present dissertation is focused mainly on the cost reduction aspect of dye sensitized solar and partly on efficiency improvement issues for these cells. Among the third generation PV technologies, dye sensitized solar cell technology is considered to have excellent prospects for low cost, high volume commercialization since it makes use of readily available, low cost raw materials and non-vacuum, solution based coating methods. In the next part of this chapter a literature review of dye sensitized solar cells is presented, identifying areas where further improvements can be made. A detailed review of the focus area of this research is also presented.

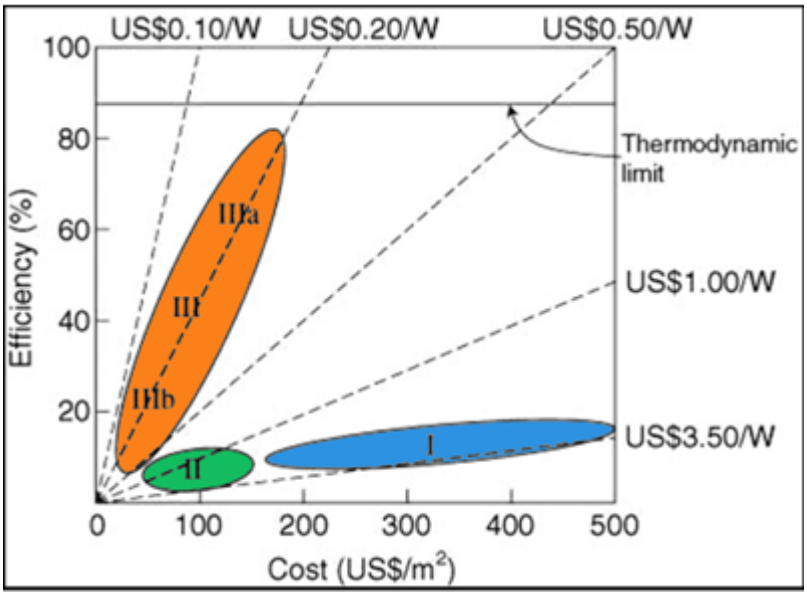

Figure 2.5: Trend in cost-performance relationship in all three generations of PV systems [9]

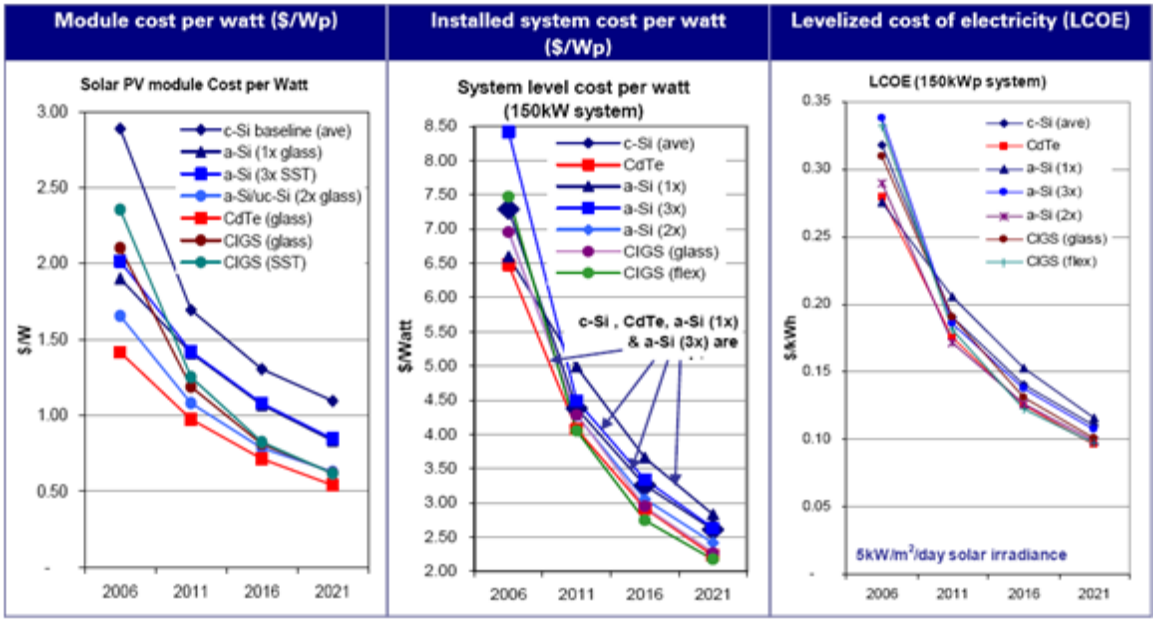

Figure 2.6: Model, system and electricity costs for existing photovoltaic technologies for a 150kWp roof mounted system [10]

2.2 Dye Sensitized Solar Cells

2.2.1 Background

Dye sensitized solar cells (DSSC) are photoelectrochemical cells. The photoelectrode in DSSC is sensitized with an organic dye which interacts with light. The excited state of the dye injects its electron into the anode material and provides charge for conduction in the circuit. The negative charge carriers are transported to the anode via a semiconductor layer, and the positive charge carriers are transported to the counter electrode via a redox electrolyte. DSSCs are also known as Grätzel cells, commemorating their discovery by Professor Michael Grätzel from École Polytechnique Fédérale de Lausanne, Switzerland, who published the first scientific paper on DSSCs in 1991 [12].

The active material in most dye sensitized solar cells is a few-micron-thick coating of nanocrystalline titanium dioxide, which acts as the photoanode. Titanium dioxide is a wide bandgap semiconductor, and therefore has low absorption in visible light. To capture the visible light energy of the solar spectrum efficiently, the titania coating is chemisorbed with photosensitizers which can get excited upon irradiation and then inject electrons into the conduction band of the semiconductor. For this reason these cells are called “dye sensitized” solar cells. Since oxide materials often have good stability in many solutions, many have been investigated for DSSC anodes [2]. Oxides such as TiO_2, ZnO, SnO_2, all having moderate-to-wide band gaps, have been demonstrated to operate as photoanode materials in DSSCs [12-16]. Of these,

TiO_2 has proven to be the most successful (highest efficiency and most stable) candidate of them all.

Figure 2.7 illustrates the basic operation mechanism of a dye sensitized solar cell. The cell is built between two surfaces of transparent conductive oxide (TCO) deposited on transparent glass or polymer film. On one of the TCO substrates, a few μm thick coating of nanocrystalline TiO_2 is deposited. The TiO_2 nanoparticles are sintered together and then coated by a layer of chemisorbed dye molecules, which act as photosensitizers. Upon irradiation, the dye molecules get excited by the sunlight and inject electrons into the conduction band of TiO_2. This electron injection process occurs faster (picoseconds) than the electron relaxation process taking place back to the sensitizer (microseconds), allowing charge separation to take place with high efficiency [2]. The nanometer sized, sintered TiO_2 particles allow electronic conduction towards the transparent conductive oxide. The dye molecules continually recover their initial electronic state by oxidizing the electrolyte, which is usually based an iodide/tri-iodide redox couple in some kind of organic solvent. In response, the iodide recovers its initial electronic state by reduction of tri-iodide at the counter electrode, completing the circuit by electron transport through the external load – delivering power to the external system. The difference in the Fermi level of the TiO_2 and the redox potential of the counter electrode corresponds to the maximum achievable output voltage of the cell. Figure 2.8 illustrates the journey of the electrons in each step when the cell is illuminated by sunlight.

Grätzel's research group has obtained the maximum solar conversion efficiency of the dye sensitized solar cells (11%) under air mass 1.5 solar spectral irradiance (AM 1.5) [17] using nanocrystalline titania as the photoanode, a novel ruthenium-bipyridyl complex as the dye sensitizer and an iodine redox electrolyte [2, 12, 18]. Recently the National Renewable Energy Labs (NREL) sponsored by the US Department of Energy (DOE) have developed a roadmap for dye sensitized solar cell research in the future [19]. The roadmap concluded that fundamental research in understanding the device physics and identifying the most promising cell materials and configurations for DSSC needs to be a focus of research. These studies also need to emphasize processing improvements that can help lower the cost of making these third-generation cells.

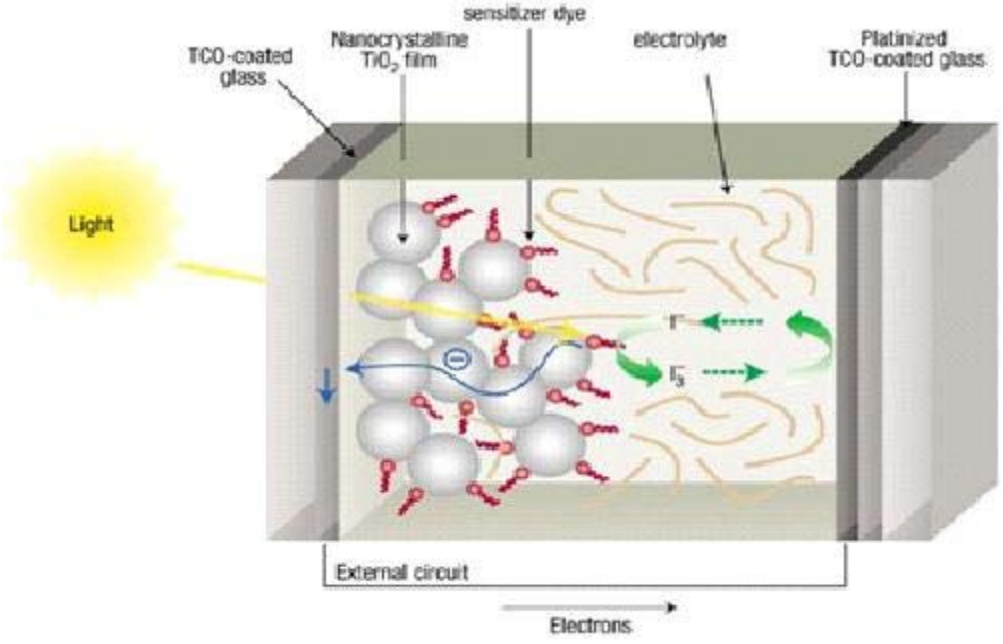

Figure 2.7 : Schematic diagram of a dye sensitized solar cell showing basic operational mechanism [20].

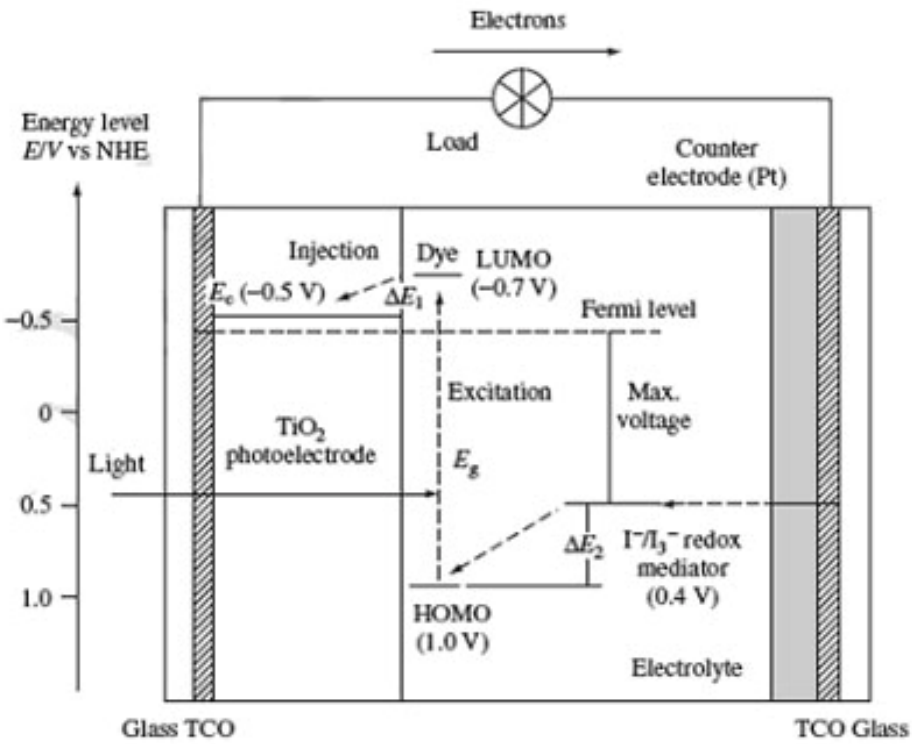

Figure 2.8 : Energy diagram of dye sensitized solar cell showing transfer of electrons during the cell operation [2]. (LUMO: Lowest Unoccupied Molecular Orbital, HOMO: Highest Occupied Molecular Orbital)

$TiO_2|S + h\upsilon \rightarrow TiO_2|S^*$ Excitation of dye upon irradiation (1)

$TiO_2|S^* \rightarrow TiO_2|S^+ + e^-$ Oxidation of dye due to injection of electrons into TiO_2 (2)

$TiO_2|S^+ + e^- \rightarrow TiO_2|S$ Dye recovers its original ground state (3)

$TiO_2|S^+ + 3/2I^- \rightarrow TiO_2|S + 1/2I_3^-$ Oxidization of the electrolyte (4)

$1/2I_3^- + e^- \rightarrow 3/2I^-$ Restoration of electrolyte at the counter electrode (5)

$I_3^- + 2e^- \rightarrow 3I^-$ Redox reaction (6)

S: Dye sensitizer; *: excitation upon irradiation ; +: Oxidation

2.2.2 Structure and Materials

Figure 2.9 illustrates the structure of the dye sensitized solar cell. The dye sensitized solar cell consists of 5 main components: substrate, transparent conductive oxide coating (TCO), semiconductor oxide coating, dye and electrolyte. This section describes the functions and properties of all the components.

1. **Substrate:** The electrode substrate is usually a transparent glass or a polymer film with higher than 90% transparency. It provides mechanical integrity to the solar cell and protects it from the environment. Usually the photoanode side of the cell is exposed to the incident light. It is observed that the cell gives lower efficiency if cathode side is illuminated instead, because then the electrons have to travel a greater distance and can get trapped more easily [21]. The cathode side of the cell is sputtered with platinum. The selection of Pt to coat the back electrode is mainly due to its high work function. Platinum has 5.6 eV work function which is higher than most other metals. For example gold has 5.1 eV, which will give 0.5 eV lower output voltage of the solar cell than platinum. Figure 2.10 depicts these differences in the output voltage in the electron configuration diagram.

   Recently, transparent polymer films such as PET (polyethylene terephthalate) and PEN (polyethylene naphthalate) have been used as substrates. They may allow people to make the solar cell lightweight and flexible [22-24]. The main issue with using polymer substrates is that they lose dimensional stability if heat treated above 150 ^{0}C processing

temperatures, therefore additional low temperature processing methods need to be employed to achieve good interparticle connection in the titania coating [22, 25-26].

2. **Transparent Conductive Oxide (TCO):** The TCO is deposited on the glass or polymer substrate for anode as well as cathode sides of the cell. It maintains the transparency of the substrates as well as improves the adhesion of the deposited titania (on anode) and platinum (on cathode) coating on the substrate. as well as maintains the mechanical strength and transparency of the substrates. The TCO film should have very low sheet resistance and high transparency. Depending upon the thickness of the TCO film the resistivity of the TCO can be varied. The photoanode is usually heat treated up to 450-500 ^{0}C to achieve sintering of TiO_2 nanoparticles, therefore the TCO film resistance should be stable with respect to temperature at least up to 500 ^{0}C. Most commonly used TCOs are fluorine doped tin oxide (FTO) and indium doped tin oxide (ITO). Both materials can have around 85 to 90 % transparency. To have 8-10 Ω/sq resistance of the FTO coating, approximately 500 nm thick coating is required [21]. ITO resistance is a strong function of temperature at higher temperatures therefore FTO is usually preferred over ITO [2].

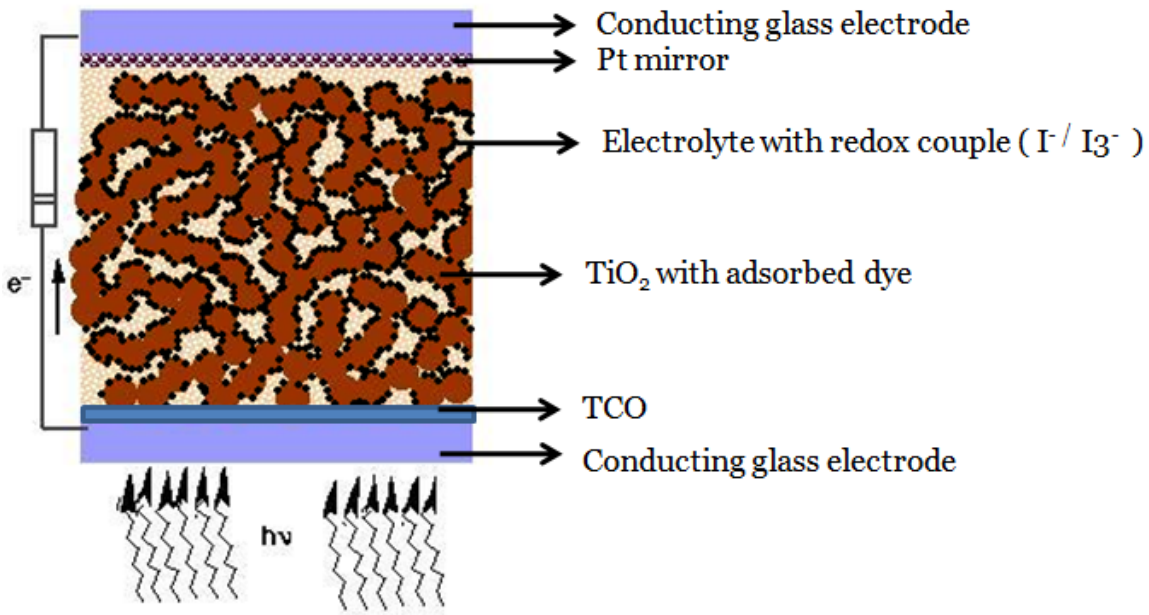

Figure 2.9: Structure of a dye sensitized solar cell [27]

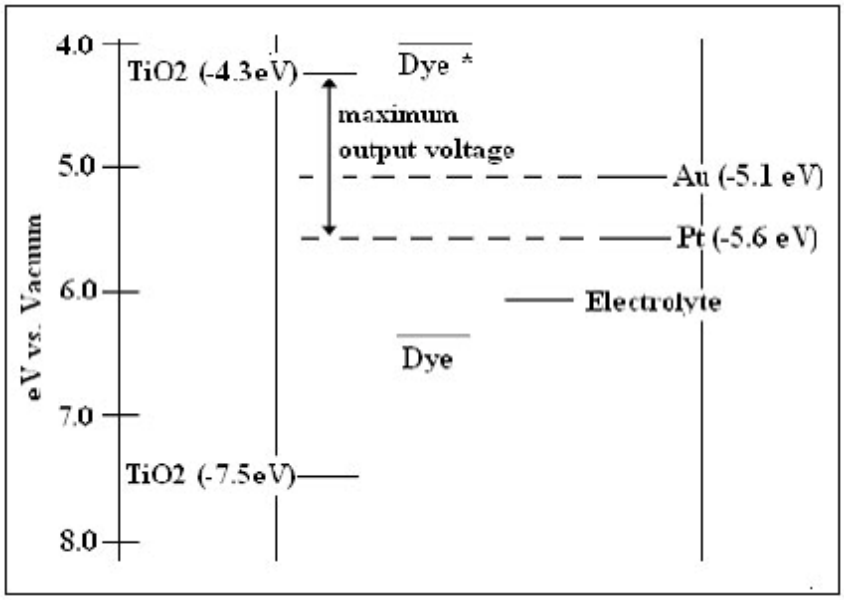

Figure 2.10 : Illustrative diagram of electron configuration in DSSC. Changes in output voltage with respect to the metal deposited on the counter electrode are depicted [28]

3. **Semiconductor Oxide Layer:** The semiconductor oxide coating is deposited on the top of the TCO to act as the photoanode in the dye sensitized solar cell. For most DSSCs, the semiconductor of choice is TiO_2. Zinc Oxide has also been tried by some researchers but it takes more time to adsorb dye molecules and the cells give lower conversion efficiency [14, 29]. SnO_2[13, 16], Fe_2O_3[30], Nb_2O_5[15] and CdS[31-32] have also been researched as possible electrode materials. Although they do produce photocurrents, their efficiencies are not as high as titanium dioxide. Additionally, TiO_2 is a very easily available material that has minimal environmental or health issues [2]. It is also very stable in the electrolyte solution under visible irradiation.

   The TiO_2 layer performs four major functions in the cell,

   - provides a surface for the dye adsorption,
   - accepts electrons from the excited dye
   - conducts electrons to the TCO.
   - helps regeneration of the dye by permeating the electrolyte through its structure

   In order to perform these functions, the TiO_2 coating has to possess specific electronic and physical properties as described below:

   Mesoporosity: The TiO_2 layer needs to be *mesoporous* (2-50 nm range of pores) to allow effective adsorption of dye molecules across the TiO_2 surface [33-35]. The photocurrent output of the solar cell is directly related to the light harvesting efficiency of the dye which in turn depends on the amount of dye adsorbed on the surface of TiO_2. Electron injection into the TiO_2

conduction band takes place only through the chemically bonded carboxylate ligands on the dye sensitizer [2] ; hence usually only one layer of dye adsorption on the surface of semiconductor coating is active. Although thicker layers of dye show excitation upon illumination, electron injection takes place only from the dye molecules which are chemically bonded with the semiconductor. Tsubomura, et al reported that efficiencies of solar cells with a flat surface of zinc oxide are considerably lower than a porous or rough surface [29].

To obtain mesoporosity, nanocrystalline TiO_2 particles are used because they drastically increase the roughness factor and surface area of the coating [36]. The effective surface of TiO_2 is increased by a factor of 1000 in a nanoporous structure [37] as compared to a dense or flat structure. Many times small particles (~20 nm) are mixed with larger (~200nm) particles to increase incident light scattering which increases the net light absorption in the TiO_2 film [38].

The use of nanocrystalline TiO_2 provides an additional advantage. In order to conduct electrons through a bulk titania film, it has to be n-doped [36]. However, the presence of conduction band electrons in the doped TiO_2 might quench the excited dye by energy transfer. In the nanocrystalline TiO_2 film, the injection of one single electron from the surface adsorbed sensitizer into the TiO_2 conduction band is sufficient to switch the TiO_2 into conductive state [36].Therefore doping is not required. The use of nanoparticles may increase the recombination losses due to trapping of electrons at grain boundaries and

surface states, but if the charge separation and reduction of dye is rapid enough, these losses may not be significant enough to affect the solar cell performance [36, 39-41]. Also due to the screening effect of the electrolyte on the surface of the nanoparticles with the negative charge, electrons can travel through the semiconductor without experiencing much recombination loss [40, 42].

Various methods have been used to produce nanocrystalline titania. Among these, sol-gel methods [43-44], dispersion methods[18] and hydrothermal growth methods [45] are quite successful.

TiO_2 Morphology and Crystal Structure: The morphology and crystalline structure of TiO_2 play an important role in the dye adsorption as it provides different bonding configurations. The anatase (101) surface leaves mostly Ti atoms to bond to carboxylate ligands, and therefore allows higher dye adsorption and gives higher photocurrents. Also, bulk anatase has a wider bandgap (3.2 eV) than rutile (3eV) which gives higher output voltage. For nanocrystalline TiO_2 particles, quantum size effects can further increase the bandgap. Sol-gel produced titania is usually completely anatase but if a commercial dispersion like Degussa's "P25" is used, which is 70% anatase and 30% rutile, then heat treatment above 450^0 C is often required to convert rutile phase to anatase to achieve better performance [46].

A desirable morphology of the TiO_2 film is to have nanorods or nanotubes aligned in parallel to each other and vertically with respect to TCO to facilitate faster electron diffusion and avoid grain boundaries [36].

Mechanical Properties: The TiO_2 film should have good mechanical strength and good adhesion to the TCO coated substrate. The film should also be of uniform thickness. Optimum thickness is very important as a thinner coating does not absorb the incident light completely and thicker coatings do not allow complete penetration of the light. Usually it is observed that 10 to 15 μm thick film is optimum [12].

TiO_2 Macroporosity: To achieve higher solar conversion efficiency, the TiO_2 layer should possess macroporosity (50 nm or greater size pores). These pores allow the redox electrolyte to permeate into the entire structure of the TiO_2 coating and be in intimate contact with the TiO_2 nanoparticles [33-35]. The diffusion coefficient of the ionic species in the electrolyte increases with the porosity of the electrode [47]. This improves the dye regeneration rate and in turn increases the efficiency of the cells. According to Ni et al. [48], the optimum porosity of the TiO_2 electrode should be around 40%. Figure 2.11 shows the effect of porosity on the photocurrent and photovoltage of the dye sensitized solar cell. From the plot it is observed that, although photovoltage plateaus at higher porosities, photocurrent goes through an optimum value. This is mainly due to the decrease in the dye concentration with lowering of specific surface area at high porosities. Also at high porosities (above 70%) the light absorption in the titania coating decreases which decreases the charge carrier concentration in the cell. In another study [49], TiO_2 film porosity is correlated to the electron transport dynamics through TiO_2 particle network geometry, using percolation theory. Again it is observed that the

performance of the solar cell goes through an optimum point as the porosity is increased. In this study, the porosity of the films was varied from 52 to 71% and it was observed that as the porosity increases above 52%, the distribution of the particle coordination number shifts to lower values which slows down the electron transport. Also very high porosities increases the fraction of terminating TiO_2 particles or dead ends which affects the photocurrent adversely as many electrons gets stuck at dead end titania particles and cannot reach the TCO coated substrate. This subject will be reviewed in more detail in section 2.3.

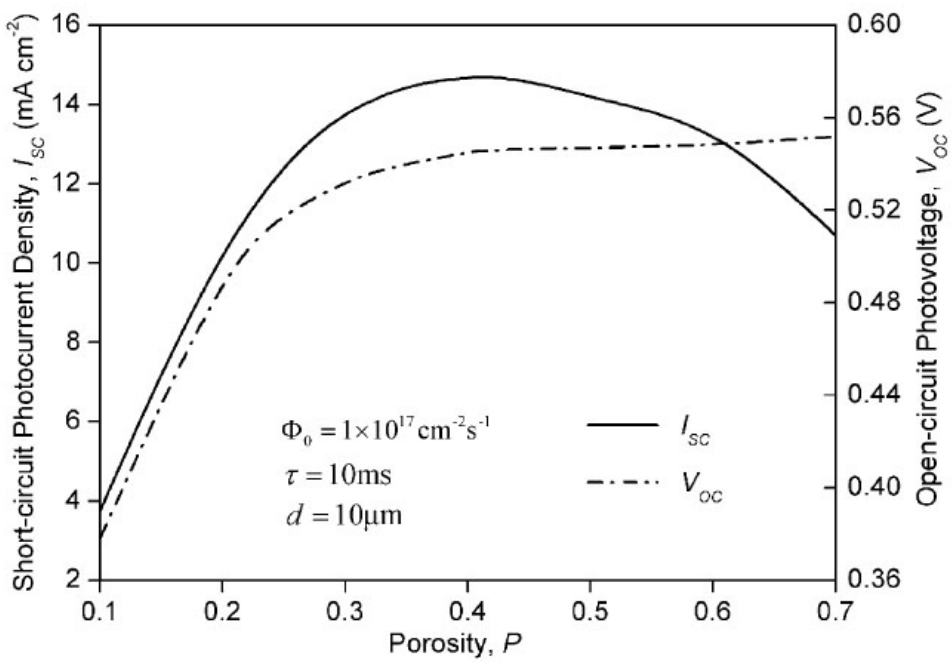

Figure 2.11 : Effect of photoelectrode porosity on short circuit current and open circuit voltage [48]

4. **The Dye Sensitizer:** The sensitizer, or dye monolayer, is the layer which interacts with the sunlight and therefore is a very important part of the DSSC. Upon interaction with the light, electrons from the dye molecules jump from the ground state to the excited state and get transferred onto the conduction band of TiO_2. An efficient photosensitizer must have
    - high light absorption in the visible region,
    - strong chemical adsorption onto the semiconductor surface, and
    - efficient electron injection into the conduction band of the semiconductor.

    The dye should also be rapidly regenerated by the electrolyte in order to avoid electron recombination processes and should be chemically stable in the ground and excited states. Usually the semiconductor coating is soaked into the dye solution for 10 to 12 hours for chemisorption. Excessive soaking does not improve the adsorption once the surface is saturated [29, 50]. For effective electron injection to take place, the energy levels of the sensitizer and the semiconductor should be well matched, such that the excited state of the sensitizer should lie just above the conduction band of the semiconductor. The ground state energy level should be just below that of the electrolyte and be of sufficient reduction potential to be easily reduced by the redox electrolyte. Figure 2.8 illustrates the ground (HOMO) and excited (LUMO) electron states in the electron configuration diagram.

    The most commonly used photosensitizer is called the 'N3 dye' having chemical formula cis-Ru(2,2'-bipyridal-4,4'-dicarboxylate)$_2$(NCS)$_2$ which is

shown in Figure 2.12 [18, 36]. The absorption maxima of N3 lie at 518 and 380 nm with extinction coefficients of 1.3 and 1.33 M^{-1}/cm, and the dye emits at 750 nm with a 60 s lifetime (much longer than its lifetime with respect to its injection into the conduction band). Usually the dye degrades in water, therefore needs to be stored in an airtight container. Novel sensitizers utilize quaterpyridyl derivatives and may demonstrate increased incident photon to current efficiency (IPCE) values for a larger region of wavelengths [51]. Fine tuning of dye characteristics continues to be a fertile area for research and might help improve the present efficiency values obtained in DSSCs.

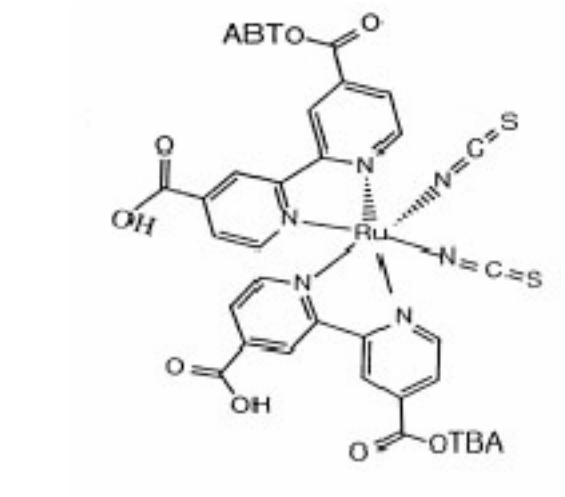

Figure 2.12 : Molecular cartoon of N3 dye

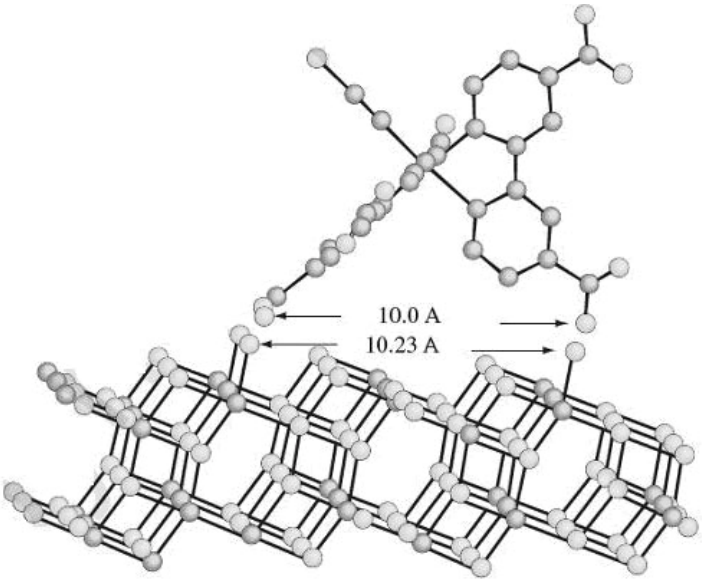

Figure 2.13 : Bonding of N3 dye molecule on (101) surface of TiO_2 [2]

5. **The Electrolyte:** The electrolyte is a reduction-oxidation (redox) system of molecules, typically based on iodine and iodide. The electrolyte reduces the dye sensitizer after photoexcitation and in turn gets reduced at the counter electrode. In order to have effective electron transport, the redox potential of the electrolyte should lie between the platinum work function and the sensitizer reduction potential (see Figure 2.10). The iodine/iodide electrolyte is produced simply by mixing iodine with an iodide salt in an appropriate solvent, such as acetonitrile or methoxypropionitrile. The liquid phase of the electrolyte helps to fill all of the pores and small crevices in the mesoporous electrode, allowing for rapid reduction of the dye in all places. But at the same time the solvent based electrolyte gets degraded in air and evaporates at higher temperatures (80-85C) requiring perfect sealing of the cell [2].

   A lot of research is being done in producing quasi-solid-state and solid state electrolytes to avoid degradation and leakage in DSSC, for example, p-type semiconductors [29], organic hole-transport materials [13, 16], low molecular weight gels [30], ionic liquid-based gel electrolytes [15, 31-33], polymer gel electrolytes [34-38, 52], plastic crystal electrolyte [39-41] and solid polymer electrolytes [42-45, 47]. The efficiencies obtained with these electrolytes are quite low at this stage due to the lower ionic conductivity of the electrolytes [53-55]. Also the interfacial contact and reaction between the TiO_2 film and the electrolyte is poorer for these quasi-solid-state/solid-state electrolytes. The meso- and macropore structure in the semiconductor film

becomes even more important to achieve effective penetration of such electrolytes.

2.2.3 Characterization of Dye Sensitized Solar Cells

Dye sensitized solar cells are characterized by a number of parameters. The most commonly used figure of merit is the power conversion efficiency of the cell, η, defined as

$$\eta = \frac{Pmax}{Pin*A} \text{ ----------(7)}$$

where P_{in} is the input power and P_{max} is the maximum power produced by the solar cell. Usually efficiency is normalized over the effective area, A of the solar cell. The efficiency of the solar cell is calculated from the current-voltage curve, produced by measuring photocurrent generated by the solar cell at different applied voltages. In the photovoltaic industry, an air mass coefficient is used to standardize the incident solar radiation. Usually it is refereed as "AM" and a number. For AM 1.5 solar spectrum, the intensity of illumination is taken as 1000 W/m^2.

The above equation for efficiency can also be expressed in terms of short circuit current and open circuit voltage parameters, which are more easily measurable parameters.

$$\eta = \frac{FF*Voc*Isc}{Pin*A} \text{ ----------(8)}$$

V_{oc} is the open circuit voltage and I_{sc} is the short circuit current. These parameters are very convenient to determine from the I-V curve, as shown in Figure 2.14. FF is fill factor which is the measure of squareness of the I-V characteristic curve. FF is always less than 1 [2]. The short circuit current, I_{sc}

depends on the solar cell structure, material properties and operating conditions [2]. For a dye sensitized solar cell, the amount of TiO_2 (which depends on the thickness of the coating and good interparticle connection of TiO_2 particles) affects the short circuit current. Better adsorption of dye molecules on the TiO_2 surface and higher conductivity of the electrolyte also improves I_{sc}. Open circuit voltage, V_{oc} changes along with I_{sc} and both vary inversely on the recombination rates within the cell [2]. The maximum voltage that can be obtained for DSSC is fixed for a TiO_2 electrode and I^-/I^-_3 redox mediator because the Fermi level of TiO_2 depends on the electrolyte component and their concentrations [2]. This is around 0.7-0.8 V. The fill factor depends on the sheet resistance of the transparent conductive layer (TCO) beneath the TiO_2 layer as well as on the I_{sc} and V_{oc}. Therefore, to obtain higher conversion efficiency of a dye sensitized solar cell, I_{sc} and, V_{oc} should be high and FF should be close to 1.

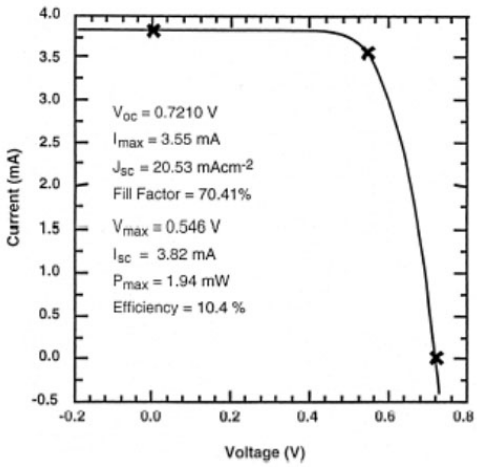

Figure 2.14 : Typical photocurrent–voltage curve obtained for a nanocrystalline TiO_2 solar cell [2]

2.3 Macroporous ceramic coatings

As mentioned in the earlier section, the photoanode of a typical dye sensitized solar cell consisting of the TiO_2 coating deposited onto the TCO coated substrate, needs to have a meso- as well as a macroporous microstructure with a continuous, interpenetrating network of pores. This provides better adsorption of the dye molecules on the TiO_2 surface and better permeation of the electrolyte throughout the TiO_2 structure.

In general, materials containing controlled macroporosity exhibit special properties and therefore find many technological applications. Porous ceramics show higher melting point, tailored electronic properties, high corrosion and wear resistance, controlled permeability, high surface area, low density, high specific strength, and low dielectric constant as compared to their dense counterparts [56]. These properties can be further tuned for specific applications by controlling pore size distribution, pore morphology and open/close porosity.

Different processing methods are employed to produce porous ceramics and they have a strong influence on the pore geometry, morphology and in turn on the above specified properties of the porous ceramic. The most commonly used method is partial sintering of porous powders which form necks at the connection points between pairs of particles and leave small pores without further compaction. This method usually gives lower porosity (<60%) and leaves smaller pores. Recently many novel techniques have been developed which allow more control on porosity, pore size distribution and morphology and which can be applied to ceramics with many different chemical compositions. Such techniques include sol-gel, templating

and solid freeform fabrication [56]. The applications where these techniques are commonly used include; electrodes and supports for batteries, solid oxide fuel cells, scaffolds for bone replacement and tissue engineering, heating elements, chemical sensors, catalytic materials, solar radiation conversion, etc. [57]. The most commonly used methods to produce macroporous ceramics are, replica, sacrificial templating and direct foaming methods [56]. Figure 2.15 illustrates these methods schematically and figure 2.16 outlines average pore sizes obtained by these methods. All three methods have been used before to produce macroporous TiO_2 structures. The direct foaming method produces larger pores on the order of a few hundred microns, therefore are not very suitable for producing titania for DSSCs. The optimum thickness of the titania coating for DSSC is around 10 to 20 micron, and therefore pore structures substantially smaller than 10 micron size are desired. The replica and sacrificial templating techniques will be discussed in further detail in the next section.

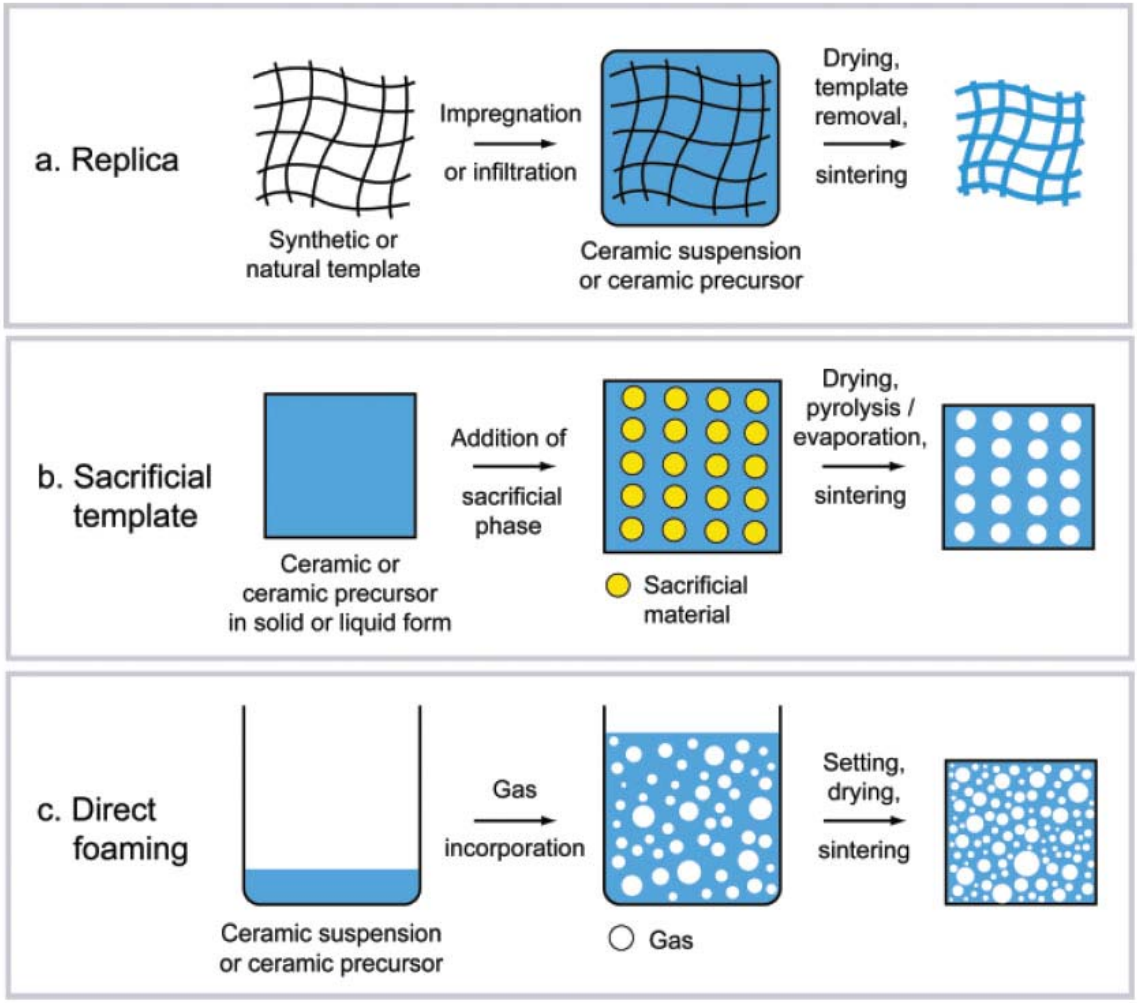

Figure 2.15 : Schematic illustration of replica, sacrificial templating and direct foaming methods to obtain macroporous ceramics [56]

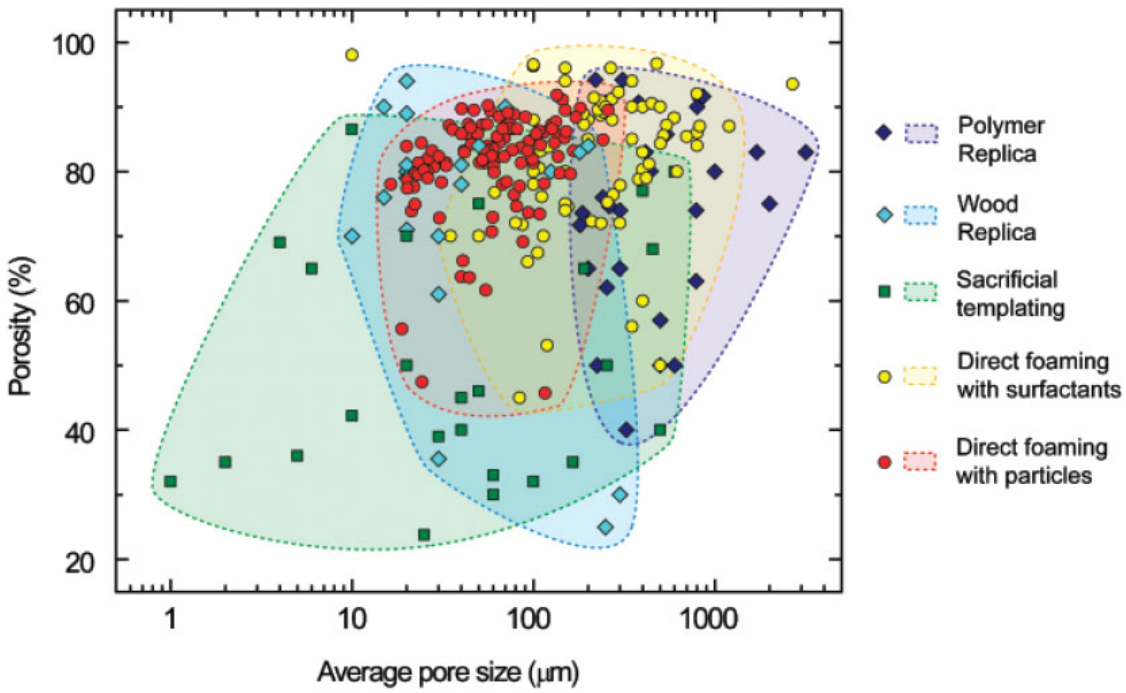

Figure 2.16 : Typical porosity and average pore size achieved by replica, sacrificial templating and direct foaming method [56]

2.3.1 Replica technique

In the replica method, the ceramic suspension is impregnated into a porous, cellular structure and it acquires the same porous morphology as the cellular structure. It is possible to obtain very high inter-pore connectivity by this method. The replica method usually produces an open porous structure, as the original cellular structure has to be accessible for the impregnation of the ceramic suspension. The ratio of open to closed pores in the final ceramic foam can be adjusted by controlling the viscosity and shear thinning behavior of the suspension [56]. The main drawback of this method is that the struts of the reticulated structure often crack during the heat treatment and this degrades the mechanical strength and electrical continuity of the product. Tsuge, et al. tried a layer-by-layer self assembly method using a spongy replica to fabricate titania films [58]. In this work, first a thick replica of poly(-allylamine hydrochloride)(PAH)/poly(acrylic acid) (PAA) films with high porosity was fabricated by a layer-by-layer method onto FTO coated glass substrate and then TiO_2 was deposited on the PAH/PAA films. The replica is removed by calcination. Pores with the length of 500 nm to 3 μm were obtained, but the thickness of the TiO_2 film was limited to 4 μm. The optimum thickness of the TiO_2 layer in the DSSC is known to be around 10-20 μm and it was difficult to fabricate thicker PAH/PAA replica by the proposed layer-by-layer method. Therefore this method seemed to be inconvenient for the dye solar cell application.

2.3.2 Sacrificial Templating Technique

Sacrificial templating is the most commonly used method to produce porous TiO_2 films for dye sensitized solar cell applications. Depending on the size of the template, the range of pore sizes obtained by this method varies from a couple of hundreds of nanometers to several millimeters. This can be very clearly observed in Figure 2.16. The sacrificial templating technique involves preparation of a two phase composite, consisting of a ceramic suspension or a precursor matrix phase and a dispersed, sacrificial phase. The sacrificial phase is first homogeneously mixed with the ceramic matrix and later extracted by heat or chemical treatment. Unlike the replica method, this method produces a porous ceramic displaying negative replica of the original template.

There is a wide variety of materials that have been used as pore formers to produce meso- or macroporous ceramics, such as natural and synthetic organics, salts, liquids, metals, ceramic compounds etc.[56] Natural and synthetic organic templates are most commonly removed by pyrolysis, involving long heat treatments at temperatures between 200 to 600 ^{0}C. In order to avoid cracking, the heat treatment rate has to be very slow, not more than 1 to 5^{0}C per min, typically. Templates consisting of salts or ceramic and metallic particles, are usually extracted by chemical etching. The extraction of salts can be easily achieved by repetitive washing the biphase composite with mild solvents, such as water. Ceramic and metallic particles or fibers require more aggressive agents and are in most cases removed by acidic leaching [59-60].

In all templating processes, it is very important to consolidate the continuous matrix phase before removal of the template, to avoid collapse of the porous structure during template extraction. Usually setting agents or binders are used to obtain a stiff porous network when the continuous phase is a suspension of particles. Sol-gel methods have also been used to consolidate the continuous phase [61-62].

The sacrificial template method is a very flexible method as it can be used with a variety of chemical compositions and can produce different pore structures. It also gives better mechanical strength to the final porous structure than the replica method because the continuous matrix phase remains intact and only the dispersed phase is extracted to generate the pores. Another advantage of this method is that it offers good control of the porosity, pore size distribution and pore morphology by using an appropriate templating material.

2.3.3 Sacrificial templating to produce porous titania films

Several sacrificial templating techniques have been used to produce porous titania coatings for the dye sensitized solar cell application [63-71]. Zhang, et al [72] used triblock copolymer Pluronic F127 as a template to produce highly ordered mesoporous TiO_2 thin films. They observed mesopores with a channel like structure and a preferential direction. Jiu [65] used copolymer F-127 (poly(ethylene oxide)$_{106}$-poly(propylene oxide)$_{70}$-poly(ethylene oxide)$_{106}$) and surfactant CTAB (cetyltrimethylammonium bromide) to obtain templated growth of porous TiO_2 films. A similar structure was obtained by Zukalová [68] using Pluronic P-123. Although high surface areas were achieved in these works, the

pore diameters obtained were quite small, in the range of 4 to 8 nm. Ito, et al.[73] used polyethylene glycol (M_w 20,000) and a cellulosic polymer template, acting as porosity controlling agent and thickener, respectively, in the TiO_2 paste. They coated this paste repetitively to obtain a thick, porous coating. The additives were later removed by calcination at 500^0C. The coating produced by this method was not uniform. Several cracks were observed on the surface of the 2, 3 and 4 times coated films. Five times coated films did not have any cracks but they were thicker than the optimum or desired thickness (10 to 20 μm) for the photoanode in the dye sensitized solar cells. The films made with up to 4 times repetitive coatings had mesopores but the five times coated film had some macro cavities. It was observed that the solar cell efficiency of the five times coated film was better than the four times coated film which was attributed to the increased diffusibility of the electrolyte into the porous TiO_2 electrode due to the macrocavities. TiO_2 films with structural channels consisting of pores of about 40 nm were produced by another group [74] where ZnO nanowires were used as the templates. The nanowires were packed into the TiO_2 films and subsequently etched by hydrochloric acid. The textural pore channels seemed to improve the DSSC performance by improving the penetration of quasi-solid/solid-state electrolyte.

2.3.4 Hierarchically meso-macroporous structured materials

As mentioned in the earlier section, the titania electrode in the dye sensitized solar cell needs to have dual porosity for peak performance. Sacrificial templating technique can be used to produce porous ceramics with a broad range of pore sizes and pore morphologies, with the use of appropriate templating

materials. Molecular, ionic or an assembly of organic templates can produce microporous (pore size below 2 nm), mesoporous(2-50nm) and macroporous(exceeding 50 nm) materials efficiently. Mesoporous materials offer very attractive structural features, such as highly ordered structures, ultrahigh surface area, narrow pore size distribution and tunable pore size/structure and therefore find applications in catalysis, adsorption, sensors and biotechnologies [75]. For applications where the diffusion of reactants and products is critical, mesoporous materials are required to have hierarchical pore structures at different length scales.

In the case of dye sensitized solar cells, the mesoporous, nanocrystalline TiO_2 coating has limited diffusibility to the electrolyte, therefore the introduction of larger, macropores is beneficial for the mass transport of the ionic species. Different templating materials have been tried to obtain bimodal porous structure in ceramics, for example dual surfactants and colloidal crystals. Self-assembled molecular aggregates or supramolecular assemblies are generally employed as the structure-directing agents of mesostructures and colloidal crystals, polymer foams, bio-celluloses, emulsions, vesicles, inorganic salt and ice crystals have been tried as templates to direct the creation of macroporous structures [75].

2.3.5 Emulsion Templating

Another interesting templating material used in the sacrificial templating technique is an emulsion. In the emulsion templating method, emulsions are used as templates to produce porous materials. Emulsions are dispersions of two immiscible liquids such as oil and water.

Usually emulsions are classified according to the nature of the external phase present: oil-in-water (o/w) and water-in-oil (w/o) emulsions [76]. Here any highly polar, hydrophilic liquid is considered as "water" and any non polar, hydrophobic liquid as "oil". Emulsions are also classified by the volume percentage of the internal, dispersed phase (internal phase ratio, IPR): emulsions with less than 30% IPR fall into first class; with 30 to 74% IPR form the second class; and above 74% form the third class. In low IPR systems (<30%), the physical properties of the whole system are determined by the external phase since there is not much interaction between the dispersed phase particles. As the IPR increases, droplets interfere and collide with each other giving rise to increase in the viscosity of the emulsion.

Emulsions are thermodynamically unstable. The dispersed phase particles can eventually coalesce to decrease the interfacial energy of the system. Therefore an emulsifying agent is often required to add to the emulsion to facilitate the emulsion production and slow down its destruction [76]. The commonly used emulsifiers are anionic/cationic/nonionic surfactants, finely divided solids, and proteins etc. In order to select suitable emulsifying agents to make a stable oil-in-water emulsion, the hydrophile-lipophile balance (HLB) method is employed [76]. By this method, emulsifying agents are assigned with a number according to their oil-soluble and

water-soluble nature. This HLB number is in the range of 1 to 20: 1 being hydrophobic nature and 20 being hydrophilic nature. In order to prepare an oil-in-water emulsion, the required HLB of the oil is matched with the candidate emulsifiers. Usually a mixture of emulsifiers works better than a single emulsifier.

The first reported use of emulsions as templates, was for the production of highly porous hydrophobic polymer called, polyHIPE [77]. In this work, a water-in-oil type of emulsion was used containing styrene and divinylbenzene as the external phase. The size of the cell in polyHIPE polymers was around 5 to 100 μm with the interconnecting pore size constituting around 20–50% of the cell diameter. Due to very large pore sizes, these polymers exhibited very low surface areas.

In order to produce an ordered porous structure in an inorganic oxide material by emulsion templating method, the structure of the dispersed droplets in the emulsion has to be maintained. This means the components of the emulsion and the inorganic precursor have to be compatible. Imhof and Pine used different emulsion formulations to produce various inorganic oxide porous materials [62, 78]. They prepared uniform dispersions of oil droplets and used sol-gel processing to grow a ceramic oxide at the exterior of the droplets. In the sol-gel process, a metal alkoxide is dissolved in a lower alcohol and hydrolyzed by the controlled addition of water. Here, the alcohol is used as a solvent because it can dissolve both, the apolar alkoxide and the polar water, due to its intermediate polarity. This reaction produces a solution (sol) of nanometer-sized particles of metal oxide. When this sol is further aged at a particular pH and temperature, aggregation and later gelation of the particle/system occurs. Further drying and

annealing removes the residual solvent and organic substances and leaves a porous solid metal oxide structure. Figure 2.17 illustrates the typical emulsion templating mechanism used by Imhof and Pine [78]. Using this procedure macroporous silica was produced with oil in formamide emulsion and a silicon tetramethoxide sol. The emulsion was first fractioned to produce a monodispersed, concentrated emulsion and then added to the silica sol. In this method, sometimes the emulsion droplets migrate and self assembles in local regions and this could affect the uniformity of the pore structure adversely. Figure 2.18 shows the microstructure of the silica produced by this method.

Zhang, et. al [79] employed polymers to produce macroporous silica with uniform mesopores by using oil in water emulsions. In this work, first polymer–silica composites were formed, by oil-in-water-in-oil sedimentation polymerization and then calcination of the organic polymer created a hierarchically porous silica structure with high porosity and surface area. Binks used another simple approach to prepare porous silica from emulsions stabilized by silica particles alone [80-81]. In his work, emulsions were stabilized entirely by silica nanoparticles having controlled wetability. Some excess silica particles were present in the continuous phase of the emulsion as well. By this method macroporous silica structures with pores in the range of 5-50 μm were produced successively after removal of the templates.

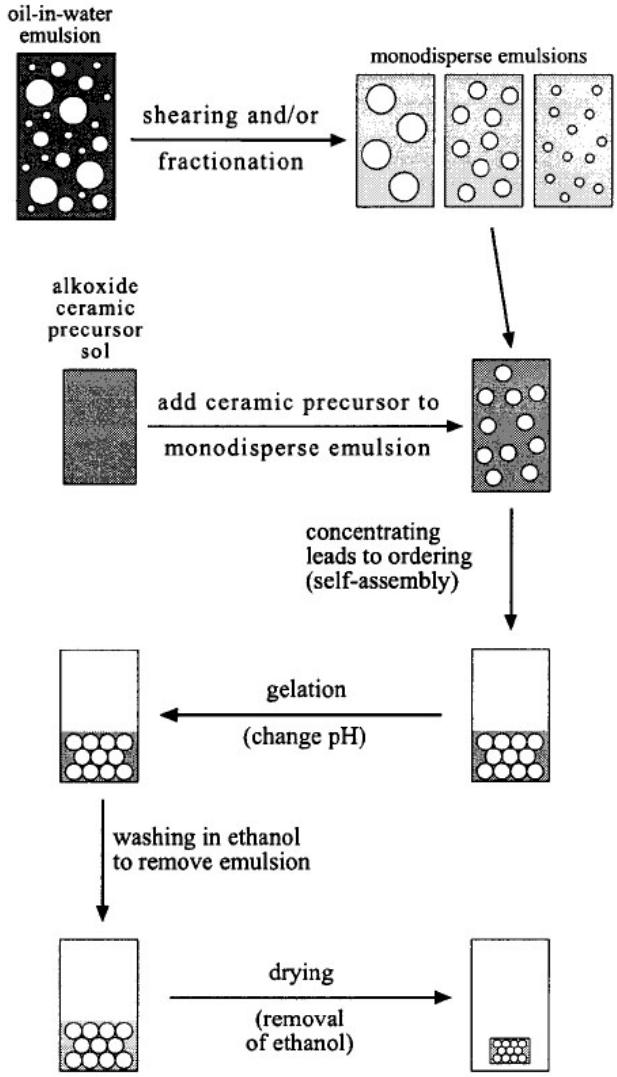

Figure 2.17: Schematic illustrating emulsion templating method [78]

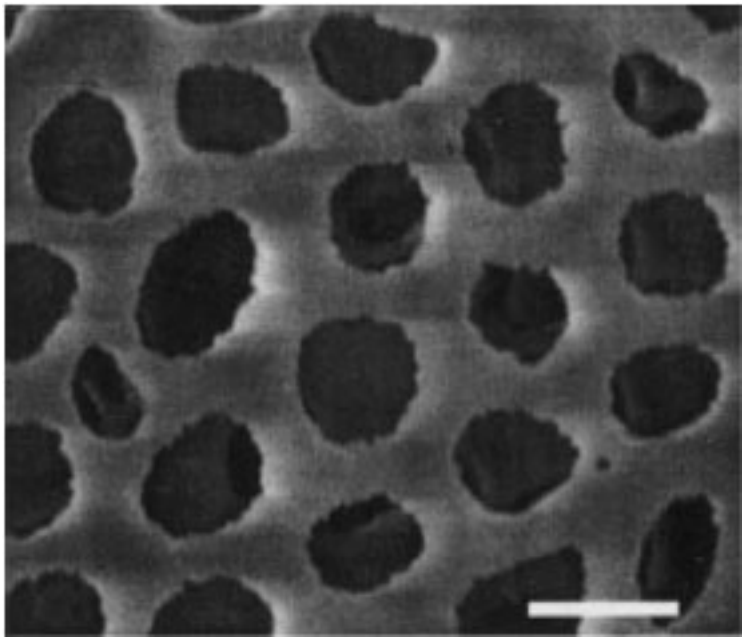

Figure 2.18: SEM micrograph of macroporous silica produced by emulsion templating . The scale bar equal 1 µm [78]

In general, many metal alkoxides are highly reactive to water and even to moisture in the air, which precludes the use of water based emulsions as templates. One approach to tackle this problem is to reduce the reactivity of the precursor by pre-treating it with another material. Imhof and Pine [62] pretreated titanium tetraisopropoxide with an equimolar amount of the chelating agent 2,4-pentanedione. They used isooctane-formamide emulsions as templates to produce porous titania structures. In another two-step method for producing meso/macroporous inorganic oxide monoliths, Chmelka et al.[82] used a sacrificial, preformed emulsion-templated scaffold to avoid direct contact of the inorganic precursors with the emulsion. In this method an inorganic precursor sol is infiltrated into the scaffold which at the end of the process is retrieved by calcination. Another way to handle the water-reactivity issue of the metal alkoxides is to use inorganic particles instead of molecular precursors. For example, alumina powders were used to produce porous alumina by polymerization and drying polymerizable water-in-oil emulsions and alumina powders [83]. To produce porous inorganic oxide materials from water-reactive precursors, non-aqueous emulsions can also be used. A variety of immiscible liquids are available, therefore finding a compatible emulsion is not a very difficult task.

Emulsion templating is a very flexible method to produce porous materials because by changing IPR, different pore structures can be obtained. With high IPR emulsions, pores in the range of 5 to 100 micron can be obtained with very high pore connectivity and with <50% IPR more closed pores can be obtained. The main

advantage of the emulsion templating method is that the oil droplets used as the templates are deformable and therefore they allow large shrinkages in the ceramic material during drying, preventing any cracking or structural degradation. This results in more uniform coatings of ceramic oxides. Another positive attribute of the oil template phase is that it can be removed very easily by evaporation, dissolution or heat treatment. Also, preparation of a stable emulsion is not an expensive process. Once a suitable formulation is obtained, just mixing and stirring the ingredients together can produce a stable emulsion without any need of high energy equipment. Since emulsion technology is extensively used in many commercial applications such as cosmetics and food products, there is an enormous amount of work done on formation and stabilization of emulsions using different liquids and surfactants. This helps in selecting suitable oil, water, and surfactant components, compatible to the corresponding sol-gel chemistry of the metal oxide. Furthermore, a wide range of volume fraction of templates can be accommodated in this method, which can even exceed the close packing limit of 74%. For more than 50% packing, ordered structures of pores can be easily obtained by emulsion templating.

In summary, from review of the literature it is apparent that emulsion templating method is a simple and effective method to produce meso/macroporous materials. However, the method had never been used to produce porous titania electrodes for dye sensitized solar cells. In the current research work, we therefore sought to achieve performance enhancement of the dye sensitized solar cells by incorporating interconnecting pore structures into the titania coatings using emulsion templating method.

References:

1. http://en.wikipedia.org/wiki/World_energy_resources_and_consumption.
2. Luque, A., Hegedus, S. *Handbook of Photovoltaic Science and Engineering*. 2003: John Wiley & Sons., p. 32-36.
3. Raugei, M., Frankl, P. *Life cycle impacts and costs of photovoltaic systems:Current state of the art and future outlooks.* Energy 2009, 34: p. 392-399.
4. Gratzel, M. *Photovoltaic and photoelectrochemical conversion of solar energy.* Philosophical Transactions of the Royal Society A 2007, 365: p. 993-1005.
5. Fritts, C. *New form of selinium cell, and some electrical discovories made by its use.* American Journal of Science 1883, 26: p. 465.
6. Chapin, D. M., Fuller, C. S., Pearson, G. L. *A New Silicon p-n Junction Photocell for Converting Solar Radiation into Electrical Power.* Journal of Applied Physics 1954, 6: p. 676-677.
7. http://content.answers.com/main/content/img/BritannicaConcise/image/72231.jpg.
8. http://ssd.phys.strath.ac.uk/images/8/81/CIGS_solar_cell.gif.
9. Kazmerski, L., NREL 2007.
10. O'Rourke, S., Kim, P., Polavarapu, H. *Solar Photovoltaics: Technology and Economics: Thin Films and Crystalline Silicon*, in *Deutche Bank - Globel Market Research Report*. 2007.
11. Goetzberger, A. *Applied Solar Energy*, in *World Climate & Energy Event*. 2002, Fraunhofer Institute for Solar Energy Systems ISE. p. 51-60.
12. O'Regan, B., Gratzel, M. *A low-cost, high-efficiency solar cell based on dye-sensitized colloidal TiO2 films.* Nature 1991, 353: p. 737-740.
13. Bedja, I., Hotchandani, S., Kamat, P.,V. *Preparation and Photoelectrochemical Characterization of Thin SnO2 Nanocrystalline Semiconductor Films and Their Sensitization with Bis(2,2'-bipyridine)(2,2'-bipyridine-4,4'-dicarboxylic acid)ruthenium(II) Complex.* Journal of Physical Chemistry 1994, 98: p. 4133-4140.
14. Rensmo, H., Keis, K., Lindstrom, H., Sodergren, S., Solbrand, A., Hagfeldt, A., Lindquist, S.E. *High Light to Energy Conversion Efficiencies for Solar Cells Based on Nanstructured ZnO Electrodes.* Journal of physical Chemistry B 1997, 101: p. 2598-2601.
15. Sayama, K., Sugihara, H., Arakawa, H. *Photoelectrochemical Properties of a Porous Nb2O5 Electrode Sensitized by a Ruthenium Dye.* Chemistry Of Materials 1998, 10: p. 3825-3832.
16. Fungo, F., Otero, L., Durantini, E. N., Silber, J. J., Sereno, L.E. *Photosensitization of Thin SnO2 Nanocrystalline Semiconductor Film Electrodes with Metallodiporphyrin.* Journal of Physical Chemistry B 2000, 104: p. 7644-7651.
17. http://rredc.nrel.gov/solar/spectra/am1.5/.
18. Nazeeruddin, M. K., Kay, A., Rodicio, I., Humphryabaker, R., Muller, E., Liska, P., Vlachopoulos, N., Gratzel,M. *Conversion of Light to Electricity by cis-X2Bis(2,2'-bipyridyl-4,4'-dicarboxylate)ruthenium(II) Charge-Transfer*

Sensitizers on Nanocrystalline TiO2 Electrodes. Journal of the American Chemical Society 1993, 115: p. 6382-6390.

19. Matson, R. *National solar technology roadmap: Sensitized solar cells*. 2008.
20. www. nature. com/nmat/journal/v2/n6/fig_tab/nmat914_f1.html.
21. Hagfeldt, A., Bjorksten, U., Lindquist, S. E. *Photoelectrochemical studies of colloidal TiO2 films: the charge separation process studied by means of action spectra in the UV region.* Solar Energy Materials And Solar Cells 1992, 27: p. 293-304.
22. DuPasquier, A. *An approach to laminated flexible Dye sensitized solar cells.* Electrochimica Acta 2007, 52: p. 7469-7474.
23. Kijitori, Y., Ikegami, M., Miyasaka, T. *Highly Efficient Plastic Dye-sensitized Photoelectrodes Prepared by Low-temperature Binder-free Coating of Mesoscopic Titania Pastes.* Chemistry Letters 2007, 36: p. 190-191.
24. Mandal, K., Choi, M., Noblitt, C., Rauh, R.D. *Progress in Producing Large Area Flexible Dye Sensitized Solar Cells.* Materials Research Society Symposium Proceedings 2005, 836: p. L1.2.1-L1.2.7.
25. Chittibabu, K.G. *Low temperature interconnection of nanoparticles. 2006, Konarka technologies.* B2, US 7094441,
26. Durr, M., Schmid, A., Obermaier, M., Rosselli, S., Yasuda, A., Nelles, G. *Low-temperature fabrication of dye-sensitizedsolar cellsby transfer of composite porous layers.* Nature Materials 2005, 4: p. 607-611.
27. lpi.epfl.ch/gif/scell99.gif.
28. Eastman, D. E. *Photoelectric work functions of transitin, rare earth and noble metals.* Physical Review B 1970, 2: p. 1-2.
29. Tsubomura, H., Matsumura, M., Nomura, Y., Amamiya,T. *Dye sensitised zinc oxide: aqueous electrolyte: platinum photocell.* Nature 1976, 261: p. 402-403.
30. Bjorksten, U., Moser, J. E., Gratzel, M. *Photoelectrochemical studies on nanocrystalline hematite films.* Chemistry Of Materials 1994, 6: p. 858-863.
31. Hodes, G., Howell, I. D., Peter, L.M. *Nanocrystalline Photoelectrochemical Cells: A New Concept in Photovoltaic Cells.* Journal of the Electrochemical Society 1992, 139: p. 3136-3140.
32. Vogel, R., Hoyer, P., Weller, H. *Quantum-Sized PbS, CdS, Ag2S, Sb2S3, and Bi2S3 Particles as Sensitizers for Various Nanoporous Wide-Bandgap Semiconductors.* Journal of Physical Chemistry 1994, 98: p. 3183-3188.
33. Bach, U., Lupo D., Comte P., Moser, J. E., Weissortel, F., Salbeck, J., Spreitzer, H., Gratzel, M. *Solid-state dye-sensitized mesoporous TiO[2] solar cells with high photon-to-electron conversion efficiencies.* Nature 1998, 395: p. 583-585.
34. Jiu, J., Wang, F., Sakamoto, M., Takao, J., Adachi, M. *Preparation of Nanocrystalline TiO2 with Mixed Template and Its Application for Dye-Sensitized Solar Cells.* Journal of Electrochemical Society 2004, 151: p. A1653-A1658.
35. Kopidakis, N., Benkstein, K. D., Lagemaat, J., Frank, A.J. *Transport-Limited Recombination of Photocarriers in Dye-Sensitized Nanocrystalline TiO2 Solar Cells*, in *Journal of Physical Chemistry B*. 2003. p. 11307-11315.
36. Gratzel, M. *Conversion of sunlight to electric power by nanocrystalline dye-sensitized solar cells.* Journal Of Photochemistry And Photobiology A-Chemistry. 2004, 168: p. 235-235.

37. Ferber, J., Luther, L. *Computer simulations of light scattering and absorption in dye-sensitized solar cells.* Solar Energy Materials and Solar Cells 1998, 54: p. 265-275.
38. Rothenberger, G., Comte, P.,Gratzel, M. *A contribution to the optical design of dye-sensitized nanocrystalline solar cells.* Solar Energy Materials & Solar Cells 1999, 58: p. 321-336.
39. Bach, U., Tachibana, Y., Moser, J.E., Haque, S. A., Durrant, J. R., Gratzel, M., Klug, D.R. *Charge Separation in Solid State Dye Sensitized Heterjunction Solar Cells.* Journal Of The American Chemical Society 1999, 121: p. 7445-7446.
40. Hagfeldt, A., Gratzel, M. *Light-Induced Redox Reactions in Nanocrystalline Systems.* Chemical Reviews 1995, 95: p. 49-68.
41. Pelet, S., Moser, J. E., Gratzel, M. *Cooperative effect of adsorbed cations and iodide on the interception of back electron transfer in the dye sensitization of nanocrystalline TiO2.* Journal Of Physical Chemistry B 2000, 1: p. 1791-1795.
42. Diebold, U. *The surface science of titanium dioxide.* Surface Science Reports 2003, 48: p. 53-229.
43. Fan, Q., McQuillinb, B., Bradleyc, D. D. C., Whiteleggd, S., Seddone, A.B. *A solid state solar cell using sol-gel processed material and a polymer.* Chemical Physics Letters 2001, 347: p. 325-330.
44. Li, Y., Hagen, J., Schaffrath, W., Otschik, P., Haarer, D. *Titanium dioxide films for photovoltaic cells derived from a sol-gel process*, in *Solar Energy Materials And Solar Cells*. 1999. p. 167-174.
45. Burnside, S. D., Shklover, V., Barbe, C., Comte, P., Arendse, F., Brooks, K., Gratzel, M. *Self-Organization of TiO2 Nanoparticles in Thin Films.* Chemistry Of Materials 1998, 10: p. 2419-2425.
46. Cao, F. *Electrical and optical properties of porous nanocrystalline TiO2 films.* Journal of physical chemistry 1995, 99: p. 11974-11980.
47. Fredin, K., Nissfolk, J., Hagfeldt, A. *Brownian dynamics simulations of electrons and ions in mesoporous films.* Solar Energy Materials & Solar Cells 2005, 86: p. 283â€“297.
48. Ni, M., Leung, M. K. H., Leung, D. Y. C., Sumathy, K. *An analytical study of the porosity effect on dye-sensitized solar cell performance.* Solar Energy Materials & Solar Cells 2006, 90: p. 1331-1344.
49. Benkstein, K. D., Kopidakis, N., Lagemaat, J. V. D., Frank, A.J. *Influence of the Percolation Network Geometry on Electron Transport in Dye-Sensitized Titanium Dioxide Solar Cells.* Journal of Physical Chemistry B 2003, 107: p. 7759-7767.
50. Vlachopoulos, N., Liska, P., Augustynski, J., Gratzel, M. *Very efficient visible light energy harvesting adn conversion by spectral sensitization of high surface area polycrystalline titanium dioxide films.* Journal Of The American Chemical Society 1988, 110: p. 1216-1220.
51. Renouard, T., Fallahpour, R. A. Nazeeruddin, M. K., Baker, R., Lever, A. B. P. Gratzel, M. *Novel Ruthenium Sensitizers Containing Functionalized Hybrid Tetradentate Ligands: Synthesis, Characterization and INDO/S Analysis.* Inorganic Chemistry 2002, 41: p. 367-278.

52. Saito, Y., Kambe, S., Kitamura, T., Wada, Y., Yanagida, S. *Morphology control of mesoporous TiO2 nanocrystalline films for performance of dye-sensitized solar cells.* Solar Energy Materials & Solar Cells 2004, 83: p. 1â€“13.
53. Cao, F. Oskam, G., Peter, C. *A Solid State, Dye Sensitized Photoelectrochemical Cell.* Journal of Physical Chemistry 1995, 99: p. 17071-17073.
54. Matsumoto, M., Miyazaki, H., Matsuhiro, K., Kumashiro, Y., Takaoka, Y. *A dye sensitized TiO2 photoelectrochemical cell constructed with polymer solid electrolyte.* Solid State Ionics 1996, 89: p. 263-267.
55. Nogueira, A. F., De, P., Marco, A., Montanari, I., Monkhouse, R., Nelson, J. *Electron Transfer Dynamics in Dye Sensitized Nanocrystalline Solar Cells Using a Polymer Electrolyte.* Journal Of Physical Chemistry B 2001, 105: p. 7517-7524.
56. Studart, A. R., Gonzenbach, U. T, Tervoort, E., Gauckler, L.J. *Processing Routes to Macroporous Ceramics: A Review.* Journal of American Ceramic Society 2006, 89: p. 1771-1789.
57. Rice, R.W. *Porosity of Ceramics*. 1998, New York: Marcel Dekker Inc, p. 539.
58. Tsuge, Y., Inokuchi, K., Onozuka, K., Shingo, O., Sugi, S., Yoshikawa, M., Shiratori, S. *Fabrication of porous TiO2 films using a spongy replica prepared by layerby-layer self-assembly method: Application to dye-sensitized solar cells.* Thin Solid Films 2006, 499: p. 396-401.
59. Miyagawa, M., Shinohara, N. *Fabrication of Porous Alumina Ceramics with Uni-Directionally-Arranged Continuous Pores Using a Magnetic Field.* Journal of Ceramic Society Japan 1999, 107: p. 637-644.
60. Wang, H., Sung, I. Y., Li, X. D., Kim, D. *Fabrication of Porous SiCCeramics with Special Morphologies by Sacrificing Template Method.* Journal of Porous Materials 2004, 11: p. 265-271.
61. Imhof, A., Pine, D. J. *Preparation of Titania Foams.* Adv.Mater. 1999, 11: p. 311-314.
62. Imhof, A., Pine, D. J. *Ordered Macroporous Materials by Emulsion Templating.* Nature 1997, 389: p. 948-951.
63. Holland, B. T., Blanford, C. F., Stein, A. *Synthesis of Highly Ordered Three-Dimensional Mineral Honeycombs with Macropores*, Science. 1998. p. 538-540.
64. Jiang, P., Cizeron, J., Bertone, J. F., Colvin, V. L. *Preparation of Macroporous Metal Films from Colloidal Crystals*, Journal of American Chemical Society. 1999. p. 7957-7958.
65. Jiu, J., Wang, F., Sakamoto, M., Takao, J., Adachi, M. *Performance of dye-sensitized solar cell based on nanocrystals TiO2 film prepared with mixed template method*, Solar Energy Materials and Solar Cells 2005. p. 77-86.
66. Ni, P.,Cheng, B.,Zhang, D. Applied Physics Letters 2002, 80: p. 1879-1881.
67. Wijnhoven, J., Vos, W. L. *Preparation of Photonic Crystals Made of Air Spheres in Titania.* Science. 1998. p. 802-804.
68. Zukalova, M., Zukal, A., Kavan, L., Nazeeruddin, M. K., Liska, P., Gratzel, M. *Organized Mesoporous TiO2 Films Exhibiting Greatly Enhanced Performance in Dye-Sensitized Solar Cells.* Nano Letters 2005, 5: p. 1789-1792.
69. Abdelsalam, M. E., Bartlett, P. N., Baumberg, J. J., Coyle, S. *Preparation of Arrays of Isolated Spherical Cavities by Self Assembly of Polystyrene Spheres on*

Self Assembled Pre-patterned Macroporoud Films. Advanced Materials 2004, 16: p. 90-93.

70. Zhong, Z., Yin, Y., Gates, B., Xia,Y. *Preparation of Mesoscale Hollow Spheres of TiO2 and SnO2 by Templating Against Crystalline Arrays of Polystyrene Beads.* Advnced Materials 2000, 12: p. 206-209.
71. Zhou, Z., Zhao, X. S. *Opal and Inverse Opal Fabricated with a Flow-Controlled Vertical Deposition Method.* Langmuir 2005, 21: p. 4717-4723.
72. Zhang, Y., Wang, J., Li, J. *Mesophase configurations and optical properties of mesoporous TiO2 thin films.* journal of electroceramics 2006, 16: p. 499-502.
73. Ito, S., Kitamura, T., Wada, Y., Yanagida, S. *Facile fabrication of mesoporous TiO2 electrodes for dye solar cells: chemical modification and repetitive coating.* Solar Energy Materials & Solar Cells 2003, 76: p. 3-13.
74. Chena, Z., Tang, Y., Yang, H., Xia, Y., Li, F., Yia, T., Huanga, C. *Nanocrystalline TiO2 film with textural channels: Exhibiting enhanced performance in quasi-solid/solid-state dye-sensitized solar cells.* Journal of Power Sources 2007, 171: p. 990-998.
75. Yuan, Z., Su, B. *Insights into hierarchically mesoâ€"macroporous structured materials.* Journal of Materials Chemistry 2006, 16: p. 663-677.
76. Lissant, K. *Emulsions and Emulsion Technology. Surfacatnt Science. Vol. 6.* 1974: Marcel Dekker,INC.
77. Barby, D., Haq, Z. European Paten 60138
78. Imhof, A., Pine, D. J. *Uniform Macroporous Ceramics and Plastics by Emulsion Templating.* Chemical Enginerring Tehcnology 1998, 21: p. 682-685.
79. Zhang, H., Hardy, G. C., Rosseinsky, M. J., Cooper, A.I. *Uniform Emulsion-Templated Silica Beads with High Pore Volume and Hierarchical Porosity.* Advanced Materials 2003, 15: p. 78-81.
80. Binks, B. P., Lumsdon, S.O. *Stability of oil-in-water emulsions stabilised by silica particles.* Physical chemistry chemical physics 1999, 1: p. 3007-3016.
81. Binks, B.P.. *Macroporous Silica From Solid Stabilized Emulsion Templates.* Advanced Materials 2002, 14: p. 1824-1827.
82. Maekawa, H., Esquena, J., Bishop, S., Solans, C., Chmelka, B.F. *Meso/Macroporous Inorganic Oxide Monoliths from Polymer Foams.* Advanced Materials 2003, 15: p. 591-596.
83. Otoishi, S., Tange, Y., Matsuda, H. *Preparation of porous alumina bodies by W/O-type emulsion method.* Journal of Ceramic Society Japan 2000, 108: p. 487-491.

CHAPTER 3: SYSTEM OF APPROACH

The objective of this research was to produce porous titania coatings with interconnected pore networks using templating methods and to apply these porous coatings to dye sensitized solar cells. Such pore networks are believed to facilitate the permeation of the electrolyte into the titania coating during device fabrication and enhance the ion conduction during device operation. Enhanced conduction is anticipated to increase the dye regeneration rate and therefore the photocurrent during the operation of these dye sensitized solar cells. In the effort to meet this objective, the research work was organized into four primary tasks which are described below. All the experimentation performed under this research belongs to one of the following tasks.

1. Identification of suitable sacrificial templating materials.

This task involved finding a templating material which is compatible with the titania and which can create pores of the order of a few hundred nanometers in size. During the initial part of the research, commercial aqueous suspensions of latex polystyrene were used as the template materials. Although this material was not very economical for the intended application, it was easily available and was convenient to prove the concept. Once all the ground work was done, oil-in-water emulsions were selected as the primary templating process for the rest of the research work. The emulsion templating method proved to be very effective at improving the conductivity of the end-product devices and was a simpler way of templating the titania coatings compared to the use of polystyrene latex precursors. All the characterization and the performance evaluation of the dye sensitized solar cells, was

performed on the emulsion templated solar cells (as developed under the tasks below).

2. **Production of templated titania coatings.**

Producing uniform and crack-free templated titania coatings was very important to analyze the effect of templating on the solar cell performance and assess the feasibility of the templating method to be used commercially. Various mainstream deposition methods such as blade coating, spin coating and roll-to-roll coating were explored to understand the coating characteristics and manufacturing issues while handling the emulsion and titania dispersion to give a good quality coating.

3. **Characterization of templated titania coatings.**

   a. **Microstructure:** The porous titania coatings, templated with polystyrene latex particles as well as with oil in water emulsions, were characterized using scanning electron microscope to study the microstructure. The polystyrene templated titania coatings were characterized in more detail to understand the interaction between template particles and template-titania particles. Under this study a theoretical model was built to further understand how the template particles (or pores) formed different structures with respect to varying template concentration and how the drying rate of the coating influenced the microstructure of the coating. For this study spin coating, blade coating and roll to roll coating methods were investigated.

   b. **Pore structure:** The pore structure and surface area analysis was performed on the templated as well as nontemplated coatings using mercury porosimetry and BET specific surface area measurements.

c. **Electrochemical impedance spectroscopy (EIS):** EIS was employed to quantitatively study the effect of the additional porosity on the titania/electrolyte interface. Impedance spectroscopy proved to be a very useful diagnostic tool to study the changes in the kinetics of the electrochemical processes in the dye sensitized solar cell with the more open, porous structure.

4. Testing the performance of the templated dye sensitized solar cells.

The templated titania coatings were assembled into the dye sensitized solar cells and the solar cell performance was compared against the nontemplated solar cells. Different cell parameters and testing conditions were compared to understand the effect of templating in more detail.

CHAPTER 4: EXPERIMENTAL PROCEDURES

All the materials, experimental procedures, and characterization techniques used in the research, are presented in this chapter. The organization of the chapter follows the organization given before in chapter 3, which gave the overall research approach to this dissertation.

4.1 Production of titania dispersion with sacrificial templates

4.1.1 Titania dispersion

Titanium dioxide nanoparticles were purchased from Evonik-Degussa (product name- Aeroxide P25). An aqueous dispersion of 40 wt% TiO_2 was prepared in the lab which was used for the blade coating experiments. First 0.25 mL of acetylacetone and 7 mL of distilled deionized water (DIW) were mixed together, then 6 g of P25 powder and 7 mL of DIW were slowly added to this mixture until a uniform slurry was obtained. The mixing was done using a stirring rod in a vial. After the titania was well dispersed in the solution, 0.1 mL of the Triton X-100 surfactant was added to the dispersion to improve the wetability of the dispersion and reduce the surface tension effects. This recipe is a modified version of one given by Nazeruddin, et al. [1] The recipe was tailored slightly to produce TiO_2 films with different thicknesses. This titania dispersion has been referred as the “nontemplated titania” in the thesis.

For spin coating and roll coating experiments, a pre-synthesized aqueous titania dispersion (product name – Aeroxide P40), obtained from Evonik-Degussa, was used. This was also a 40 wt% dispersion of titania with primary particle size of 40-50 nm

4.1.2 Latex polystyrene templates

Aqueous suspensions of monodispersed, polystyrene particles were purchased from Thermo Scientific. The desired concentration of polystyrene suspension was added directly to the titania dispersion (Aeroxide P25 or P40) and stirred to make a uniform mixture. A small amount of Tritan X-100 was also added to lower the surface tension and improve the wetability of the dispersion. The coating was obtained by blade coating, spin coating or roll coating method. The coating was air-dried for 10 minutes and then heat treated in the furnace at 500 ^{0}C for 30 minutes with a ramp rate of 2 ^{0}C/min. During the heating process, the polystyrene templates were removed and titania nanoparticles were partially sintered together providing better connection between particles. The coatings obtained with this method were very uniform and crack-free.

4.1.3 Oil-in-water emulsion templates

In this method emulsions were used as the templating material. The titania dispersion was made using Aeroxide-P25 powder as described in section 4.1.1. Because these titania nanoparticles were hydrophilic in nature, water had to be present as the external phase in the emulsion. Therefore the oil-in-water emulsion type was chosen for the templating phase. The most important parameters to consider while obtaining the desired type of emulsion (in this case oil-in-water) are: phase volume ratio, choice of emulsifiers and method of manufacture. In the present work, the concentration of the oil in the emulsion was kept to less than 50 wt%. At higher concentrations of oil, the emulsion was not stable. For all the characterization experiments, 20 and 40 wt% oil in water emulsions were used.

The recipes for the same are given in table 4.1. They represented two distinct cases of emulsions with very different oil droplet sizes (~200 nm and ~4000 nm, respectively) and therefore having potential to produce different pore structures in the titania coating. The emulsions were added to the titania dispersion (prepared as per described in section 4.1.1) and stirred for 10 to 15 minutes to prepare the "emulsion templated titania" samples for further characterization. While selecting suitable candidates for the emulsifying agents, hydrophile-lipophile balance (HLB) method [2] was employed. In this method, the emulsifying agents are assigned a number according to the balance between their oil-soluble and water-soluble nature fractions. This HLB number can be in the range of 1 to 20: 1 being most hydrophobic in nature and 20 being most hydrophilic in nature. In order to prepare an oil-in-water emulsion, the required HLB of the oil is matched with the candidate emulsifiers. Often a mixture of emulsifiers (one having affinity towards water and another having affinity towards oil) works better than a single emulsifier by itself. After trying different oils and surfactants finally paraffin oil and Tween 80 (polyoxyethylene sorbitan monoleate)/Span 80 (sorbitan monooleate) emulsifier blend was chosen to formulate the oil-in-water emulsion for our templating studies. The structure and composition of the emulsifiers is given on the following page. The combined HLB of this emulsifier blend was set at around 11. After fine tuning the emulsion formulation, a stable emulsion was produced by mixing the ingredients and would be stable within just 10-15 minutes. Therefore the method of preparing the emulsion proved to be very simple and convenient.

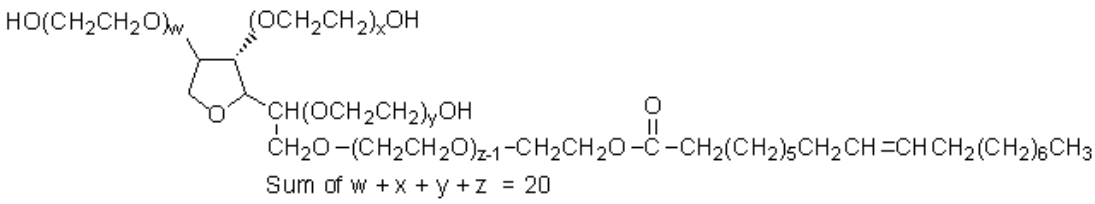

Figure 4.1: Structure of Tween 80 (source: Sigma Aldrich)

Table 4.1: Properties of Tween 80 emulsifier

grade	Sigma Ultra
form	viscous liquid
mol wt	micellar avg mol wt 79,000
composition	Oleic acid, ~70% (balance primarily linoleic, palmitic, and stearic acids)
total impurities	<0.005% Phosphorus (P)
CMC	0.012 mM(20-25°C)
anion traces	chloride (Cl^-): <0.05%
	sulfate (SO_4^{2-}): <0.05%
cation traces	Al: <0.0005%
	Ca: <0.0005%
	Cu: <0.0005%
	Fe: <0.0005%
	K: <0.005%
	Mg: <0.0005%
	NH_4^+: <0.05%
	Na: <0.05%
	Pb: <0.001%
	Zn: <0.0005%
HLB	15

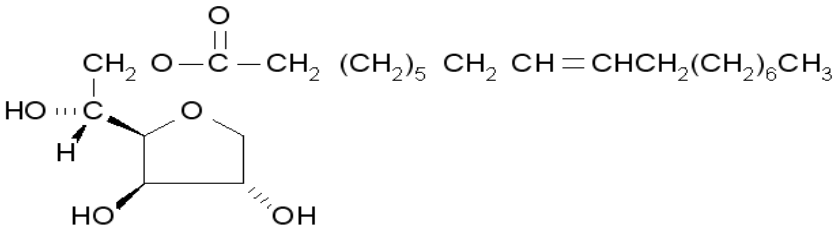

Figure 4.2: Structure of Span 80 emulsifier

Table 4.2: Properies of Span 80 emulsifier

refractive	*n*20/D 1.48(lit.)
viscosity	1200-2000 mPa.s (20 °C)
HLB	4.3±1.0
density	0.99 g/mL at 20 °C

4.2 Production of templated titania coatings

4.2.1 Blade coating

Blade coating was the primary deposition technique used to produce the titania coatings in this research. In this technique, two rectangular pieces of scotch tape were put in the middle of the FTO coated glass piece. They defined the boundaries of the coating deposition area and created a height barrier for the coating to be deposited. More layers of the tape were used to increase the thickness of the coating that was deposited between them. One layer of the scotch tape produced approximately 10 to 15 microns thick film depending upon the viscosity of the dispersion. Figure 4.3 represents the schematic of the typical blade coating deposition method. About 0.5 ml of titania dispersion was dispensed on one end of the deposition area, which is immediately spread out (or wiped off) using a thin metal strip, blade or a microscope slide in the downward direction. The wiping action evened out the titania ink in the deposition area set by the scotch tape and removed the excess ink. This method produced very uniform and defect free coatings with high reproducibility.

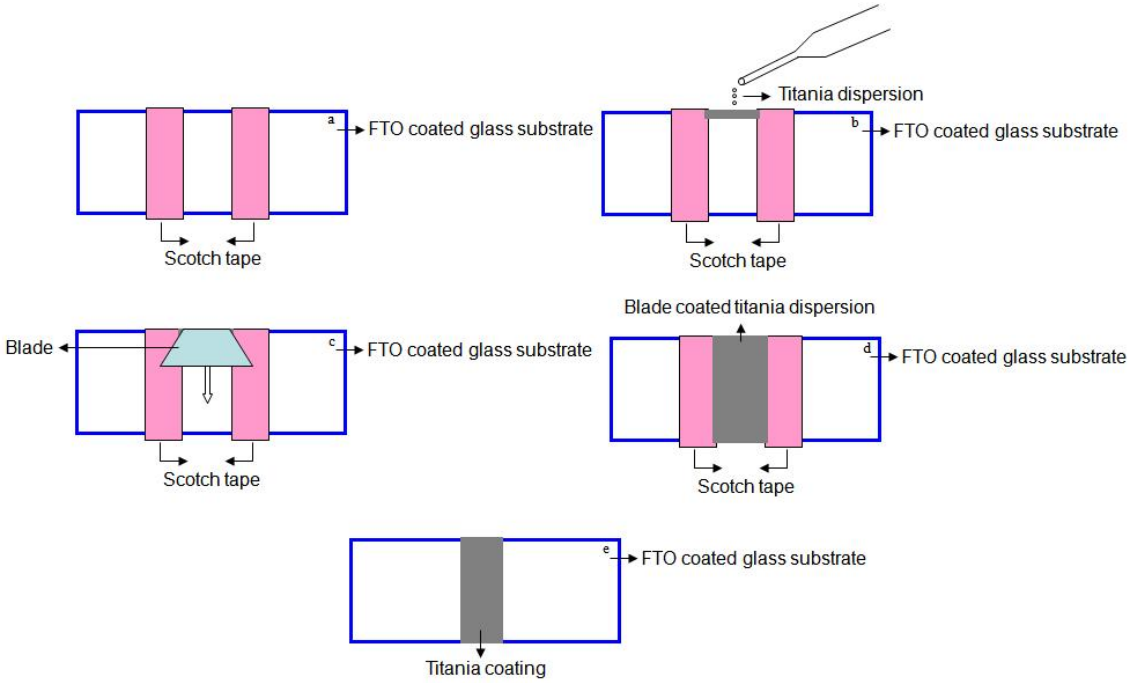

Figure 4.3: Schematic illustrating blade coating method

Table 4.3: Recipe to prepare 20 gm of the emulsions

Emulsion	Paraffin Oil (gm)	Water (gm)	Span 80 (gm) (HLB 4.4)	Tween 80 (gm) (HLB 14.8)
20 wt% oil in water	4	15	0.34	0.66
40 wt% oil in water	8	11	0.34	0.66

4.2.2 Spin Coating

Spin coating method was used to produce very thin coatings of templated titania. A mixture of the pre-synthesized aqueous suspension of TiO_2 nanoparticles from Evonik-Degussa (40-50 nm, 40 wt%) and aqueous suspension of polystyrene mono-sized particles (1 μm, 10 vol%) from Thermo Scientific, was spun on the FTO coated glass substrate at 2000 rpm for 1 min. Most of the solvent was evaporated during this time. To remove the polystyrene templates from the coating and allow sintering of TiO_2 nanoparticles, the spin-coated samples were heated at 500 ^{0}C in air for 30 minutes.

4.2.3 Roll coating

Roll-to-roll coating method was used to produce flexible titania coatings. ITO coated PET (polyethylene terephthalate) films were used as substrates. The equipment used for roll coating experiment was a Mini-Labo™ test coater made by Yasui Seiki, Co. (USA). This roll coater utilized the "reverse micro gravure™" coating method [3]. This method used an engraved metal cylinder (roll) to apply only specific volume of the solution on the substrate [3]. The substrate/film was fed between the engraved roll and the backing roll, both rotating in opposite directions. If the direction of the two is the same, the coating may not adhere well. This condition is referred to as "film splitting" and it can be a source of coating defects. In the *reverse* gravure process, the coating is applied in a shearing manner, therefore a smooth coating is obtained. Figure 4.4 illustrates the roll coating mechanism.

The surface of the roll in the "micro gravure™" coater contained regularly spaced texturing of the surface. These cells held a well defined volume of the solution to be deposited. The geometry, number, spacing and depth of these cells were a factor in determining the thickness of the coatings produced. The reverse gravure coating method produced very uniform and highly reproducible coatings.

The ink formulation used for the roll coating experiment was based on the pre-synthesized aqueous suspension of TiO_2 nanoparticles (Aeroxide P40, 40-50 nm, 40 wt%) and aqueous suspension of polystyrene mono-sized particles (1 μm, 10 vol%). Samples with different concentrations (1, 2, 5, 6, 7, 8 and 10%) of polystyrene were prepared. Triton X-100 surfactant was added at a 0.1 % concentration level to improve the wetting properties of the ink. Figure 4.5 shows a picture of the roll coated film. Since the PET films, used as substrates, lose their dimensional stability if heated above 150 ^{0}C , the titania films were heat treated only up to 150 ^{0}C for an hour. To remove the polystyrene templates, the samples were immersed in toluene for 15 minutes and then again heated at 100 ^{0}C for 20 minutes. To characterize the thickness and microstructure of roll coated films, profilometry and SEM were used respectively. Image analysis of the SEM data was performed using Matlab and Fovea Pro (with Photoshop CS2) software.

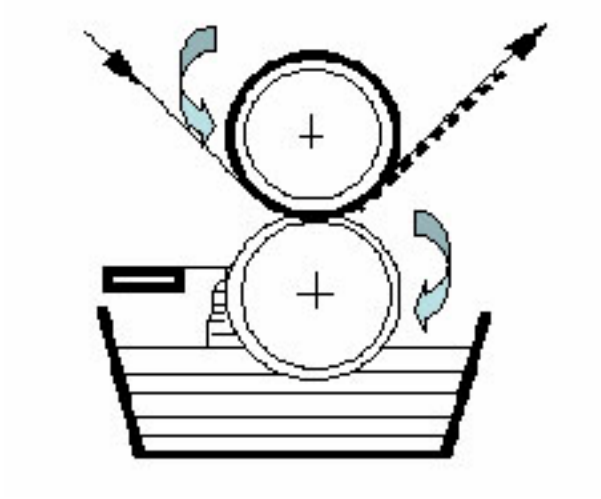

Figure 4.4: Reverse Micro Gravure™ Coating. Source : Yasui Seiki Co., USA [3]

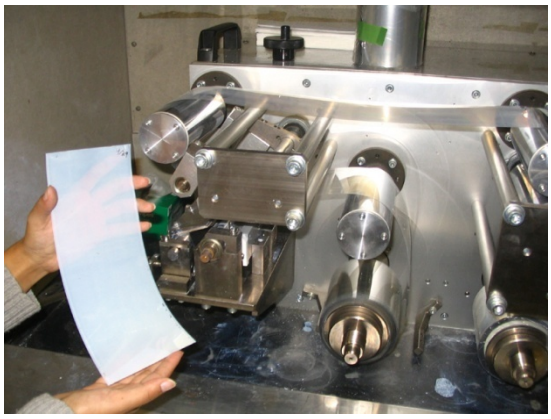

Figure 4.5: Roll coated titania film on PET substrate

4.3 Characterizing the templated titania coatings

4.3.1 Thickness

Profilometry (Tencor, Alpha-step 200) was used to measure the thickness and uniformity of the titania coatings. In this method, a small needle runs across the coating, and measures the height of the step of the coating from the substrate. The flatness of the step quantifies the uniformity of the coating.

4.3.2 Microstructure

Scanning electron microscopy (SEM) was used to examine the microstructure of the templated and nontemplated titania films. In SEM, a high energy, focused beam of electrons is used to scan the surface of the sample in a raster pattern. The interaction of the incident electrons with the sample generates signals in the form of secondary electrons, backscattered electrons, characteristic x-rays, specimen current and transmitted electrons. Specialized detectors are used to catch these signals. Secondary electron imaging (SEI) was used in this research as it can produce very high resolution images of the sample surface topography. Up to 10 nm of resolution is very common for SEI. In the present work such a high resolution was required to see mesopores (2-50 nm sized pores). To analyze if the templated coatings had interpenetrating pores, good depth of field was required. Therefore working distance was set between 10 to 15 mm. The input voltage was set to 5 kV.

The equipment used for SEM was Zeiss (DSM 982 Gemini) microscope at Rutgers University. The sample preparation involved cutting small pieces of titania coating, sticking them on a stub with a double-sided, black conductive

carbon tape and then sputtering gold on the top of the sample to avoid surface charging. The titania samples were kept in the desiccators for at least 24 hours before taking images to get rid of any adsorbed moisture from the sample surface.

In order to study the particle interaction between template particles and template/titania particles, Fovea Pro image analysis program and Matlab program was used. The Fovea Pro program works as a plug-in with the Adobe Photoshop CS2 software.

4.3.3 Mercury Porosimetry

As the present research mainly involved incorporation of meso and macroporous structures into the titania films, characterization of pore size, volume, distribution and other porosity related parameters was crucial. Mercury porosimetry technique was employed for this purpose. In this technique a non wetting material (typically mercury) is intruded into the pores in the sample under pressure. Micromeritics' Autopore 9400 porosimeter was used for these experiments. This instrument can characterize pores in the range of 0.003 to 360 micron. To prepare the samples for porosimetry experiments, a thick coating of titania dispersion (templated or nontemplated) was drop-cast into a glass Petri dish and air dried for 2 hours. Later it was heated in the oven at 500 ^{0}C for 30 minutes with a ramping rate of 2 ^{0}C/minute. Flakes of the coating were carefully collected to prevent disturbing the internal structure. The sample was dried in the nitrogen at 200 ^{0}C for 24 hours before doing porosimetry, to remove any adsorbed moisture.

4.3.4 BET Specific Surface Area

BET (Brunauer, Emmett and Teller) surface area technique was used to measure the specific surface area of the templated and nontemplated titania coatings. The Micromeritics Gemini 2375 equipment was used for these measurements.

This surface area analyzer utilizes two gas reservoirs connected to the sample and to an empty balance tube. Both are filled with equal volumes of the adsorptive (usually nitrogen) gas. A transducer on the sample side monitors the target pressure as the sample adsorbs the gas. This method of dosing and accounting for the volume of gas uptake is very sensitive and accurate.

4.3.5 Electrochemical Impedance Spectroscopy (EIS)

Electrochemical impedance spectroscopy was used as a diagnostic tool to study the effect of emulsion templating on the internal resistances and electron motion and recombination kinetics within the dye sensitized solar cells.

EIS is a steady state method used to obtain the electrical response of an electrochemical cell to an applied AC potential over a range of frequencies[4]. Electrochemical impedance is usually measured with a very small input signal, which does not perturb the system much. The data is represented as the Nyquist plot or Bode plot and analyzed by fitting to an equivalent electrical circuit model, based on the physical electrochemistry of the system under study.

EIS data for emulsion templated and nontemplated cells were compared by applying an appropriate equivalent circuit and by analyzing the circuit parameters

extracted through data fitting. The electrochemical impedance spectroscopy was performed using an impedance analyzer (Solartron analytical, 1255B) connected to a potentiostat (Solartron Analytical, 1287). The EIS spectra were measured over a frequency range of 10^{-1}–10^{6} Hz at 298 K under open circuit condition with 10 mV amplitude. The electrical impedance spectra were characterized using the Z-View software (Solartron Analytical).

4.4 Testing the performance of the templated dye sensitized solar cells

4.4.1 Materials

4.4.1.1 TCO coated glass/film substrate

The glass substrates used to deposit the templated and nontemplated titania coatings, were purchased from Hartford Glass, IN, USA. They were pre-coated with fluorine doped tin oxide (FTO) resulting in 15-30 Ω/□ sheet resistance. The typical thickness of the substrate was 2.3 mm. The substrates were cleaned before use by sonicating in DI water for 15 minutes. To produce the photoanodes, the cleaned FTO slides were deposited with TiO_2 paste, and to produce the photocathodes, they were sputtered with platinum. Although the conductivity of the FTO beneath Pt was not necessary, it showed improved adhesion for Pt compared to deposition directly onto glass. The platinum was sputtered for 2 minutes under 100 watt power.

For the roll to roll coating deposition, flexible PET (polyethylene terephthalate) films were used (Sheldahl Inc, USA). The PET substrates were pre-coated with indium tin oxide with 100 Ω/□ sheet resistance. They could not withstand ultrasonic cleaning, therefore they were cleaned simply by wiping with ethanol.

4.4.1.2 Dye

The sensitizer dye was purchased from Solaronix (product name – Ru-535). To produce the dye solution, 25 mg of the Ru-535 dye was dissolved in 100 ml of anhydrous ethanol by stirring for 2-3 hours. The prepared dye solution was always stored in a tightly sealed plastic bottle to avoid

degradation by exposure to moisture in the air. The dye solution was reused after the TiO_2 coated substrates were soaked in it, until the original purple color faded significantly (usually within 2 to 3 weeks).

4.4.1.3 Electrolyte

Several ionic liquid based electrolytes were prepared in the lab in line with recipes in the literature. The preparation of these electrolytes involved simple mixing and stirring of the appropriate amounts of the chosen chemicals. Most electrolytes used an imidazolium iodide (Ionic Liquids Technologies GmbH & Co. KG) mixed with 4-tert-butylpyridine. The electrolyte used for the most of the research work was based on 3-methoxypropionitrile (MPN) solvent with a recipe of 0.3 M 1-Hexyl 3-Methyl Imidazolium Iodide, 0.5 M 4-tertbutylpyridine, 0.05 M Iodine and 0.01 M Lithium Iodide [5].

4.4.2 Assembly of dye sensitized solar cell

The dye sensitized solar cells were assembled by sandwiching the electrolyte between the photocathode and photoanode. The photoanode was made up of a 1 cm * 2 cm FTO coated microscope glass piece, on which a 0.5 cm * 1 cm strip of TiO_2 coating was blade coated (as described above in section 4.2.1). Figure 4.6 describes the steps in assembling a typical dye sensitized solar cell used for this research. Usually the 10-20 micron thick layer of titania is white in color, but after soaking it in the dye solution for 12 to 15 hours, it turns purplish in color. After removal of the titania coating from the dye solution, it was washed with ethanol and dried in air for 5 minutes. A separator membrane of 1.25 cm * 1 cm size was cut and dipped into the electrolyte solution and put on the photoanode as shown in the figure 4.4, covering the titania coating and one side of the exposed FTO coated glass substrate. It prevented the direct contact of the platinum with the FTO glass. On the top of this assembly the platinum coated FTO glass electrode was placed in such a way that some bare FTO substrate was exposed for making external electrical connections. In the end, a mask with 0.25 cm^2 area hole was placed on the back side of the photoanode and the whole assembly was held together using two binder clips.

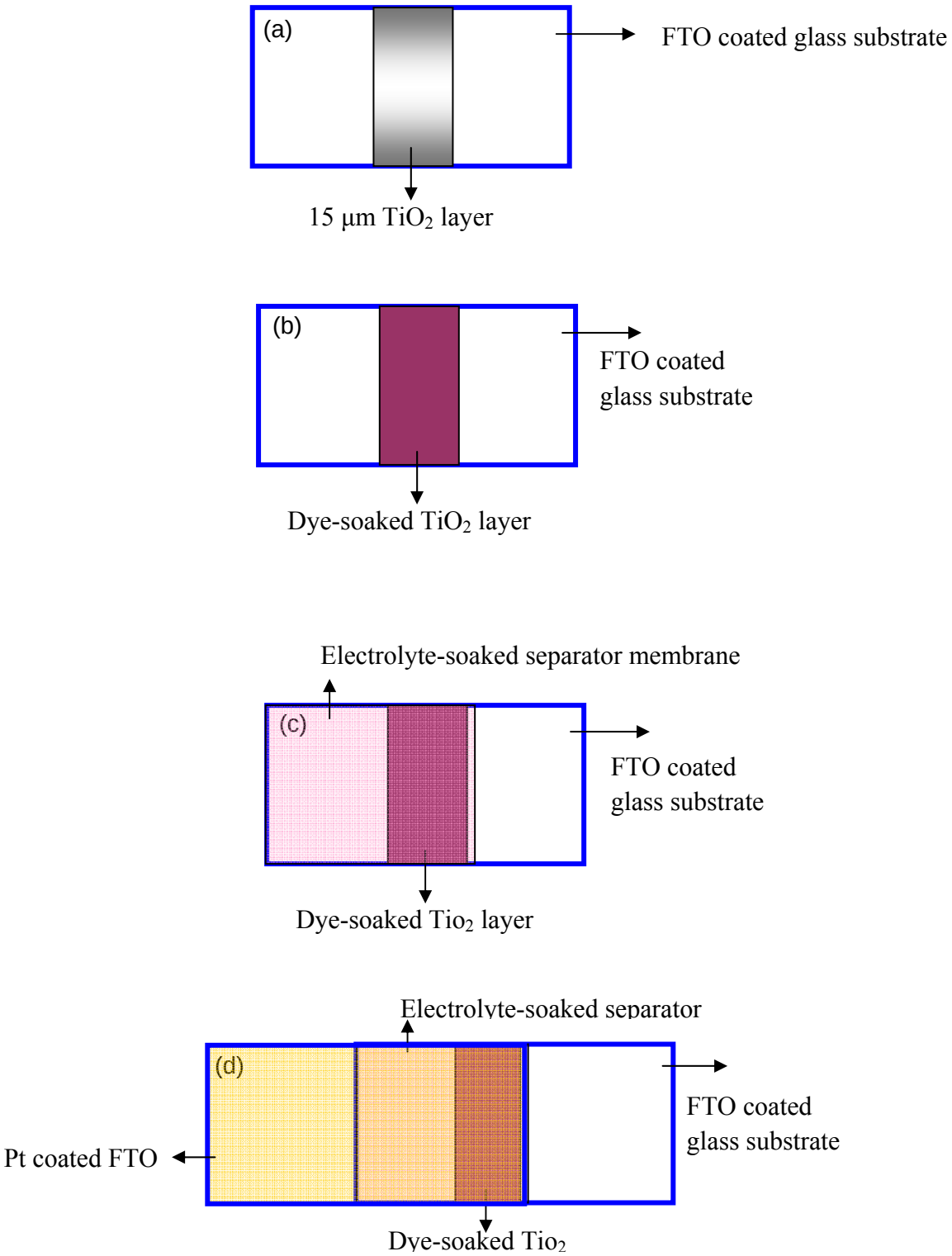
(a)
FTO coated glass substrate
15 µm TiO_2 layer
(b)
FTO coated
glass substrate
Dye-soaked TiO_2 layer
Electrolyte-soaked separator membrane
(c)
FTO coated
glass substrate
Dye-soaked Tio_2 layer
Electrolyte-soaked separator
(d)
FTO coated
glass substrate
Pt coated FTO
Dye-soaked Tio_2

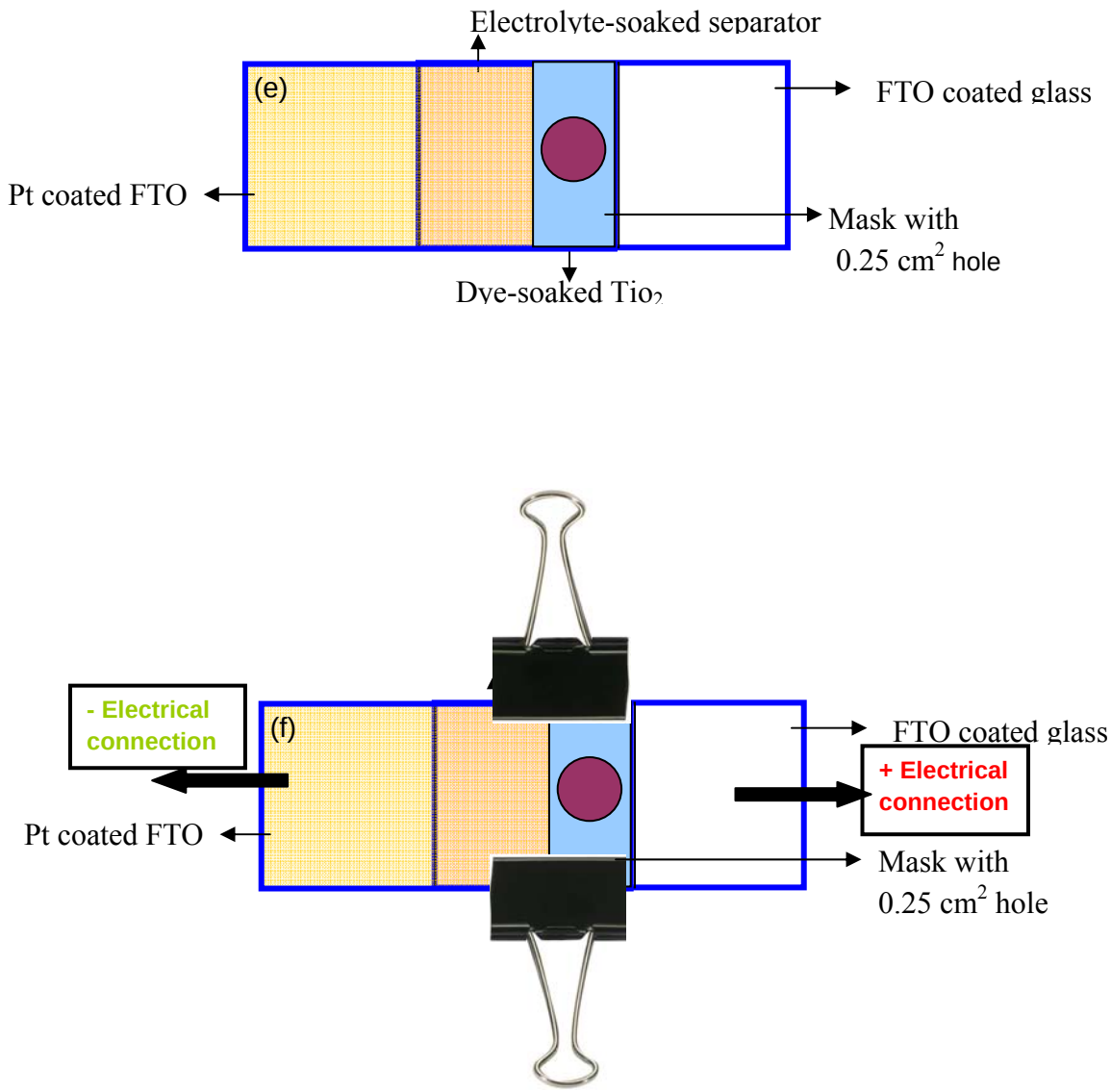

Figure 4.6: Schematic representing steps of dye sensitized solar cell assembly

4.4.3 Solar Cell Characterization

The performance of the dye sensitized solar cells was characterized by plotting the current-voltage curve under simulated solar illumination. Since the cells were not completely sealed, but just held together using the binder clips, they were assembled in the solar simulator lab just before measuring the current-voltage characteristics. This was done to avoid any effect of electrolyte evaporation on the solar cell performance. The assembled solar cells were placed on a table at a fixed height in such a way that the light output from the 300 W Xenon solar simulator (Newport, Oriel 91160A) on the cell was 90 W/m^2 measured by an irradiance meter (Daystar, Solaqua) as shown in Figure 4.7. The light was passed through the 0.25 cm^2 mask on the photoanode. Alligator clips were used to make the electrical connections. They were connected on the other side to a voltage source (HP 4140B pA meter/voltage source). A Labview program was used on the solar simulator as well as on the electrical characterization equipment through which -0.3 to 1 volts were fed to the solar cell with a step size of 10 mV. The photo current was collected in the dark and under 90 W/m^2 illumination. The output was represented in two formats: current vs. voltage data points and calculated solar cell characteristics such as efficiency, fill factor, short circuit current, and open circuit voltage.

Figure 4.7: Images of a) Newport solar simulator and computer, and b) the voltage supply.

References:

1. Nazeeruddin, M., K., Kay, A., Rodicio, I., Humphryabaker, R., Muller, E., Liska, P., Vlachopoulos, N., Gratzel, M. *Conversion of Light to Electricity by cis-X2Bis(2,2'-bipyridyl-4,4'-dicarboxylate)ruthenium(II) Charge-Transfer Sensitizers on Nanocrystalline TiO2 Electrodes.* Journal of the American Chemical Society 1993, 115: p. 6382-6390.
2. Lissant, K. *Emulsions and Emulsion Technology. Surfacatnt Science. Vol. 6*.1974: Marcel Dekker, INC.
3. http://www.yasui.com//microgravure.htm.
4. Ross, M. J., William, K. R. *Impedance Spectroscopy: Emphasizing Solid Materials and Systems*.1987, New York: John Wiley & Sons.
5. Ma, T., Akiyama, M., Abe, E., Mimai, I. *High-Efficiency Dye-Sensitized Solar Cell Based on a Nitrogen-Doped Nanostructured Titania Electrode.* Nano Letters 2005, 5: p. 2543-2547.

CHAPTER 5: RESULTS AND DISCUSSION

This chapter presents the results of this research. All the experiments discussed in this chapter compare the performance of emulsion templated titania coatings with respect to nontemplated coatings.

The chapter starts with a discussion on the microstructural analysis of the polystyrene-templated coatings deposited using the blade coating, spin coating and roll coating methods. Blade coating proved to be the most suitable method for the intended application; hence this method was selected as the method of deposition for comparing the effect of emulsion templated devices. The rest of the chapter focuses on the characterization of emulsion templated coatings produced using the blade coating method. Analysis of the microstructure, pore size distribution, surface area, impedance spectroscopy and I-V characterization has been discussed in detail.

As described in chapter 3 - System of Approach, all the experiments of the research were categorized into following four main tasks.

1. Identification/production of suitable sacrificial templating material,
2. Production of templated titania coatings
3. Characterization of the templated titania coatings
4. Testing of the templated dye sensitized solar cells

This chapter briefly discusses the results of the first two tasks. The rest of the chapter concentrates on the third and fourth tasks.

5.1 Identification/production of suitable sacrificial templating material

As illustrated in the literature review, there is a wide range of materials that can be used as sacrificial templates to produce a porous ceramic coating (in this case titania). In chapter 4 the two template materials used in this research, latex polystyrene suspension and oil in water emulsions, were described in detail. The method of producing the titania dispersions with these templates was also explained. This section describes the properties of the two templating materials.

5.1.1 Polystyrene templates

A monodispersed, aqueous suspension of the latex polystyrene particles (10 wt%), purchased from Thermo Scientific, was used as the sacrificial templates in the initial phase of this research. This suspension mixed easily with the P25 titania nanoparticles and the resulting dispersion was very stable. The mean diameter of the template particles was 1 μm as per specification. Further characterization of the original latex suspension was not performed.

The initial microstructural analysis and the solar cell testing performed on the polystyrene-templated titania coatings helped substantiate the hypothesis that having a network of open pore channels would benefit the solar cell performance. However, the polystyrene templates would have proven to be prohibitively expensive for large area application. Dye sensitized solar cell technology is mainly being developed as a low cost PV technology that can be easily commercialized. The use of a specialized, expensive product such as the monodispersed latex polystyrene suspension did not seem to be commercially viable for this application. Therefore, a major aspect of the present research was

to investigate an alternative templating material, one that would be more economically feasible. However, the easy commercial availability of the polystyrene templates helped lay the groundwork for the present research.

5.1.2 Emulsion templates

Oil in water emulsions were selected as the primary templating materials for this research as it satisfied all the constraints encountered by the polystyrene templates. A wide range of oils and surfactants/emulsifiers are available in the market with which a variety of emulsion formulations can be easily prepared at a very low cost. Additionally, the particle size of the oil droplets dispersed in water could be easily controlled by changing the oil and the emulsifier concentration.

5.1.2.1 Emulsion formulation

Different types of oils such as silicone oil, octane, decane and paraffin oil were used to form emulsions with water. Paraffin oil with the Span 80/Tween 80 blend of emulsifier formed a stable emulsion easily. Therefore this was selected as the system for templating. The hydrophilic-lypophilic balance (HLB) of the emulsion was set at 11.26. The formulations used for most of the characterization experiments contained 20 wt% or 40wt % oil and 1 wt% emulsifier blend dispersed in DI water. The exact recipe of the formulations is given in chapter 4.

5.1.2.2 Characterization of the emulsion:

- Particle size measurement:

Emulsion appearance and stability can be controlled to a great extent by the droplet size of the dispersed phase. For particle sizes above 100 nm, the emulsion is milky white. Dynamic light scattering method (ZetaPALS) was used to measure the oil droplet sizes in the emulsions. If the droplet size is too large, it results in interference between light waves scattered from the same particle, giving erroneous data. Therefore optical microscopy was also performed to verify the results. Table 5.1 lists the mean diameter of the oil droplets in the emulsions prepared with different oil phase concentrations. The amount and HLB value of the surfactant mixture was kept the same for all the formulations. Emulsions with 10 to 20 wt% oil produced stable emulsions with particle sizes around 100-300 nm. Emulsion with 30 and 40% oil had larger oil particles and they started to sediment after 10 to 15 minutes.

- Optical microscopy:

Optical microscopy was used to confirm the dynamic light scattering data of the particle size analysis. 20 and 40 wt% emulsions were primarily used for all the characterization experiments, optical micrographs of which are shown in

Figure 5.1. They clearly show the difference in the oil droplet sizes. Both micrographs show that there were some big oil droplets in the range of 1 to 50 μm. But the number of the bigger droplets in the 20 wt% emulsion seems to be lower than the 40 wt% emulsion. The volume fraction of these bigger droplets

must be very low therefore the mean diameter obtained by the ZetaPALS was substantiated. This was confirmed later with the microstructural analysis and the pore size distribution analysis performed on the emulsion templated titania coatings.

- Stability:

Generally, an emulsion with a sharply defined distribution containing a maximum fraction of small diameter droplets is more stable. Deterioration of the rheological properties of the emulsion occurs mainly due to the change in the particle size distribution. A time study was performed on the 20 wt% emulsion, in which the oil droplet size distribution was characterized every day for two weeks. Figure 5.2 shows this plot. It was observed that the 20 wt% emulsion had good stability over this period. On the other hand, the emulsion with 40 wt% oil started to phase separate only after 10 to 15 minutes. This was due to the bigger oil droplets (4 to 5 microns), which caused flocculation and sedimentation.

Table 5.1: Dynamic light scattering particle size analysis

Oil Concentration (%)	Mean Diameter – Volume Averaged (nm)
10	107
20	165
30	3900
40	5650

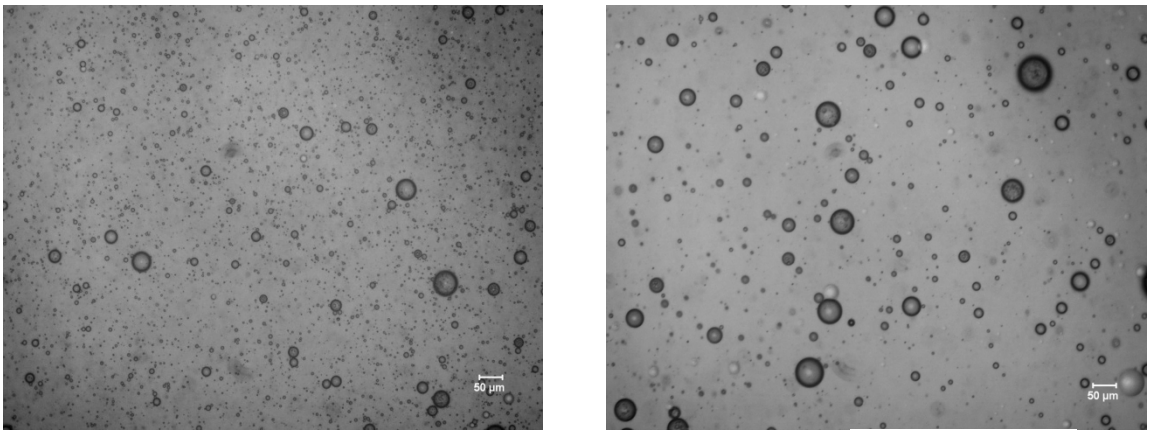

(a) (b)

Figure 5.1: Optical micrograph of (a) 20 wt% and (b) 40 wt% oil in water emulsion (scale bar: 50micron)

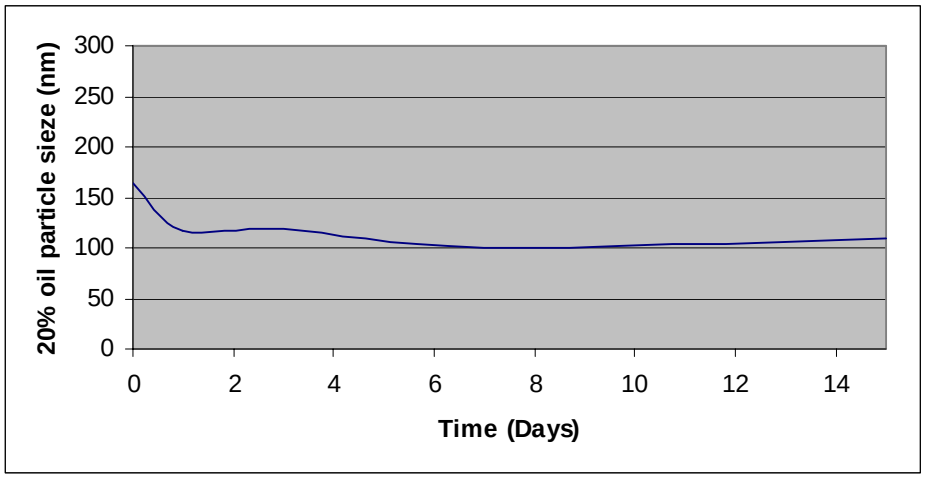

Figure 5.2: Change in the mean oil droplet diameter with respect to time, in the 20% oil in water emulsion

- Thermogravimetric Analysis (TGA)

Thermogravimetry is a technique in which the weight change of the sample is monitored with respect to the temperature. It is a useful technique to determine the temperature of decomposition of the constituents of a sample. In the present work it was useful to know at what temperature the sacrificial paraffin oil template is burned off from the emulsion templated titania coating.

Three samples were analyzed with TGA: 1) Nontemplated titania, which was a dispersion of titania nanoparticles in DI water (with some Tritan X-100 and acetyl acetone acting as stabilizers) 2) 20 % emulsion templated titania, in which the titania nanoparticles were dispersed in the 20 wt% oil-in-water emulsion, 3) 40 % emulsion templated titania, in which the titania nanoparticles were dispersed in the 40 wt% oil-in-water emulsion. The heating program used for the TGA experiment was same as the one used for the post deposition treatment of the titania coatings (setpoint- 500 ^{0}C, dwell time – 30 min, ramp- 2 ^{0}C/min).Figure 5.3 plots the TGA data of the three samples as described above. The first weight loss is observed at around 200^{0}C and it continues up to 300^{0}C. Since this curve is common among all the three samples, it must be due to the decomposition of the carboxyl gourps associated with the surfactant Triton X-100 and chelating agent acetyl acetone. The second weight loss curve is seen only in the emulsion templated samples, therefore it is due to the decomposition of the paraffin oil in the emulsion. The oil started to burn at 340^{0}C and was fully removed when the sample was heated above 400^{0}C.

The 20 wt% emulsion templated sample stabilized at around 60% of the original sample weight. The 40% emulsion templated sample stabilized at around 49% of the original sample weight. Both runs show good emulsion removal by 400^0C.

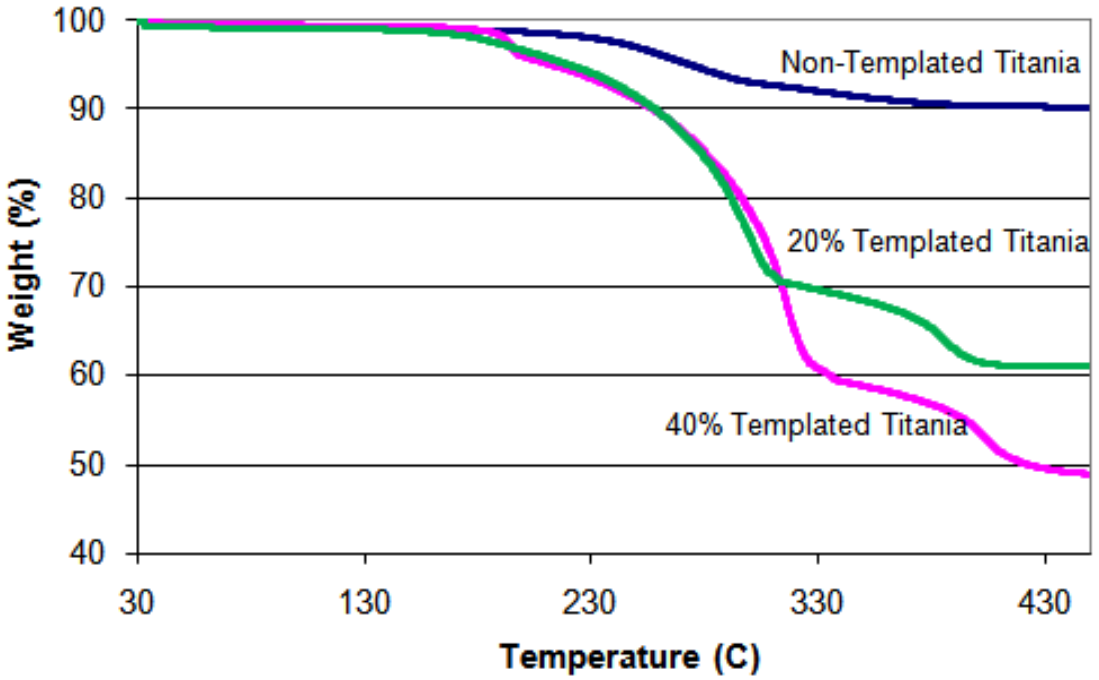

Figure 5.3: TGA data of the nontemplated, 20% emulsion templated and 40% emulsion templated samples

5.2 Production of ttemplated titania coatings

The microstructure as well as the overall quality of the titania coating is influenced by the coating deposition method. The quality of the coating plays an important role in the performance of the dye sensitized solar cell. Cracks or crevices in the coating affect the electron transport through the titania nanoparticles adversely. They can also bring the electrolyte directly in contact with the FTO coated substrate and increase the recombination current. Therefore it is very important to obtain a uniform, crack-free titania coating.

Different commercial deposition methods such as blade coating, spin coating, and roll coating were tried in this research. Spin coating and roll coating methods were tried only with the polystyrene-templated titania suspensions. Spin-coated films were very thin, of the order of 500-600 nm thickness and had only a monolayer of template particles. Roll coated films were deposited on the flexible PET substrates and produced thicker coatings of around 1 to 2 micron, depending on the viscosity of the suspension. Roll coated films could not be heat treated above 150 ^{0}C, therefore were washed with toluene to remove the polystyrene templates. Both of these thinner coating methods were used in the early phase of research to understand more about how template particles interact during the key early coating drying stage.

Blade coating was used as the primary deposition method for further studies as it produced uniform coating with high reproducibility and which were suitable for good solar cell fabrication.

Table 5.2 lists the typical thicknesses of the blade coated films with different formulations of the emulsion/dispersion. The thickness was mainly determined by the scotch tape put on the substrate to define the coating area, and by the viscosity of the dispersion mixture.

For all the three deposition methods, the coating parameters or the technique had to be fine tuned to obtain uniform and defect-free coatings. In case of the blade coated and roll coated films, the heating rate was also influential on the development of cracks in the coating. A slower heating rate was used for the emulsion templated coatings to avoid cracks. In general, it was observed that the templated coatings were more uniform than the nontemplated ones. This could be mainly due to the higher viscosity of the templated inks which slowed down the drying rate and reduced the crack formation.

Sample	**Average Thickness (µm)**
Non-templated titania	12
40 wt% P25 + 10 wt% polystyrene	15
40 wt% P25 + 10 wt % O/W emulsion	15
40 wt% P25 + 20 wt % O/W emulsion	20
40 wt% P25 + 30 wt % O/W emulsion	25
40 wt% P25 + 40 wt % O/W emulsion	38

Table 5.2: Average thickness of blade coated films with different formulations of templates

5.3 Characterization of templated titania coatings

5.3.1 Microstructure

5.3.1.1 Polystyrene templates

- Blade coated films

The polystyrene-templated titania dispersion was prepared as per the procedure described in chapter 4. The microstructure of the blade coated, templated titania film is shown in Figure 5.4. Figure 5.5 shows the same microstructure at a higher magnification. In the SEM micrographs, the dark pockets are pores created by the removal of the polystyrene templates by heat treatment. The white particles are the titania nanoparticles. The size of the pores was determined by the size of the templates. In the presented work, 1 micron sized polystyrene templates were used. It can be seen from the micrographs that the pores are of micron size and are interconnected. This interconnection is a desirable characteristic of the titania coatings in order to achieve good penetration of electrolyte throughout the titania structure. It can be observed from the higher magnification micrograph that the smaller titania particles are sintered to each other at the necks, creating mesopores of the size of 30-50 nm. These pores are the main microstructural feature of the high specific surface area titania nanoparticle coatings (whether templated or not).

Since blade coating is a slow drying process the polystyrene template particles often have enough time to self assemble into a close-packed honeycomb like structure. The smaller titania particles get packed into the voids between the bigger polystyrene particles. Therefore, upon removal of

the polystyrene particles, titania particles remain interconnected producing macroporous channels that penetrate into the mesopore network of TiO_2 nanoparticles. From the micrographs, it can be seen that the pores are all spatially aligned and interconnected with an average size slightly smaller than the template size of the polystyrene particles. This is due to the shrinkage of the pores upon heat treatment. The pore size can be controlled by using different sized polystyrene templates. Polystyrene particle dispersions in the range of 300 nm to 3 microns were available at Thermo Scientific. Therefore a variety of pore sizes can be obtained in the TiO_2 coating. From the cross-sectional view of the coating (Figure 5.6), it can be seen that the pores in the upper layers of the coating are self assembled into face-centered-cubic structures. In the lower layers they have lower regularity, which can be attributed to a substrate confinement effect.

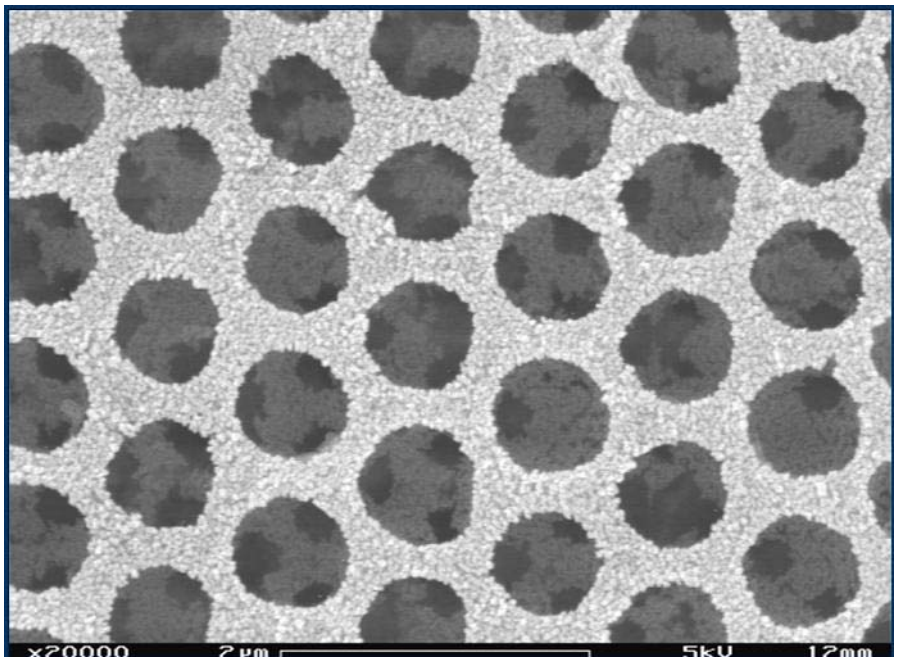

Figure 5.4: Blade coated titania coating templated with the polystyrene particles. Dark colored holes are pores and white colored particles are of titania

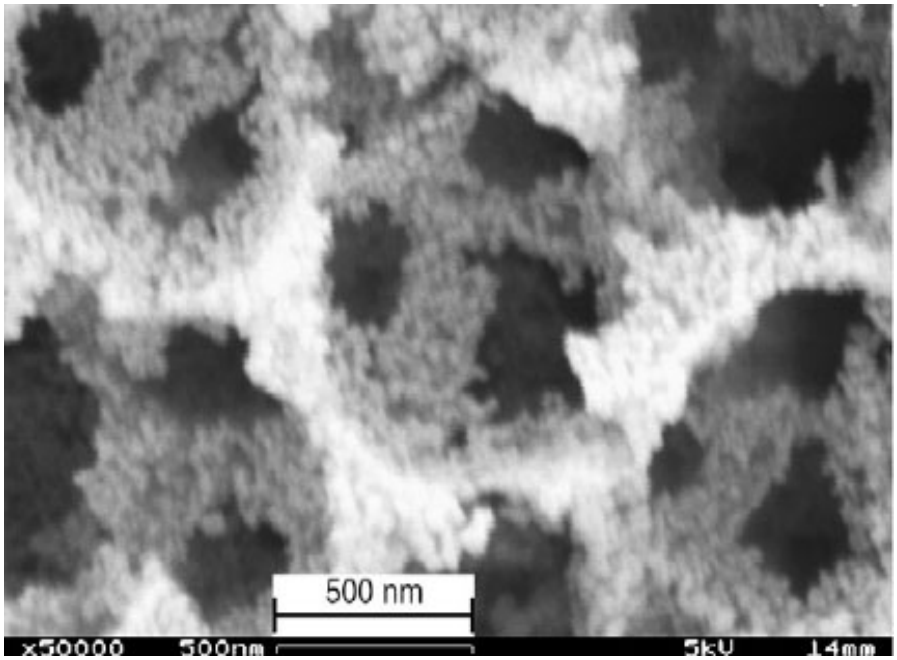

Figure 5.5: Magnified view of blade coated titania coating templated with polystyrene particles

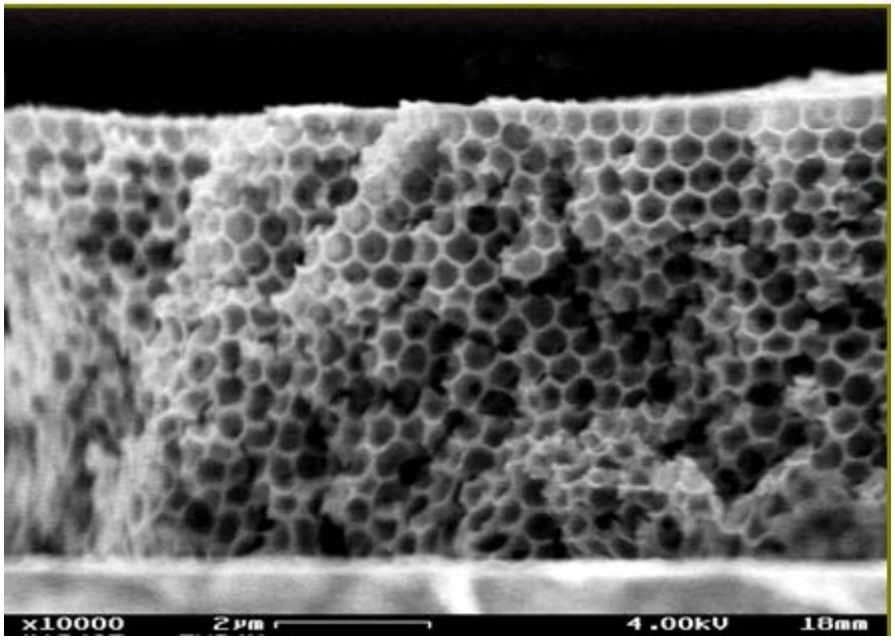

Figure 5.6: Cross-sectional view of the blade coated template TiO_2 coating

- Spin coated films

To study and compare the microstructure of the titania coating produced using a fast drying process, the spin coating method was used. Very thin titania coatings were deposited having only one layer of template particles using spin coating technique and particle interactions between the template polystyrene particles and polystyrene-titania particles were studied.

Effect of spinning on polystyrene templates: When the polystyrene-titania dispersion was dispensed on the substrate, initially the particles had a random association with each other as they mixed continuously through natural Brownian motion. The thickness of the film at this stage was around 250 μm, which was very large as compared to the size of the polystyrene particles (1μm).

The hydrodynamics involved in the spin coating process have been investigated by various authors [1-4]. During the initial stages of spinning, the thinning is mainly due to the viscous effects. The centrifugal outflow is more dominant and since the particles are immersed in the solvent, they move around in response to the convective outflow. At a stage in the spin coating process, the convective effect and the simultaneous solvent evaporation are approximately equal in magnitude. This occurs at fluid depths on the order of only a few microns. Beyond this point more thinning occurs by solvent evaporation than by viscous outflow. As the solvent evaporates, the concentration of the particles rises forcing more interparticle interactions to take place. When the thickness of the film is approximately equal to the

polystyrene particle diameter, each individual spherical particle touches the substrate and causes a local upward bump in the fluid interface. The deformation in the fluid interface depends upon the wetting properties of the particle interface, i.e. position of the contact line and magnitude of the contact angle. If two such particles are close enough, there is an overlap of the menisci around the two particles which causes fluid level in the inner region to be higher than in the outer region. Figure 5.8 illustrates this condition schematically [5-7]. It can be observed from Figure 5.8 that due to the slope of the liquid interface with respect to the horizontal, the X component of the surface tension force σ varies along the contact line. The X component of the surface tension can be calculated as

$$F_X = \frac{2\pi\sigma r_c^2 (\sin\Psi)^2}{L} \quad \text{----------(1)}$$

where σ is the surface tension, r_c is radius of the three phase contact line at the particle surface, Ψ is angle of the meniscus slope at the contact line and L is the separation distance. This force is termed as "Lateral Capillary Force" which could be attractive or repulsive depending upon the nature of the overlapping menisci. If both are concave or convex (i.e. of the same type), forces are attractive, otherwise repulsive. For micrometer sized particles with $r_c << L << (\sigma/\Delta\rho)g)1/2$, Fx is very strong (attractive) for larger deformations. Here Δρ is the difference between mass densities of the liquid and gas phase and g is gravitational acceleration. The attractive lateral capillary forces cause two dimensional aggregations particles.

The vertical component Fy of the lateral capillary force acts in downward direction pressing the particles against the substrate and further reducing their mobility. This also forces the removal of the small TiO_2 particles which might be caught below the larger polystyrene particles. As the fluid film becomes more and more thin due to evaporation, deformation at the fluid interface increases, which in turn increases the lateral capillary force and causes attraction in particles separated by distance L.

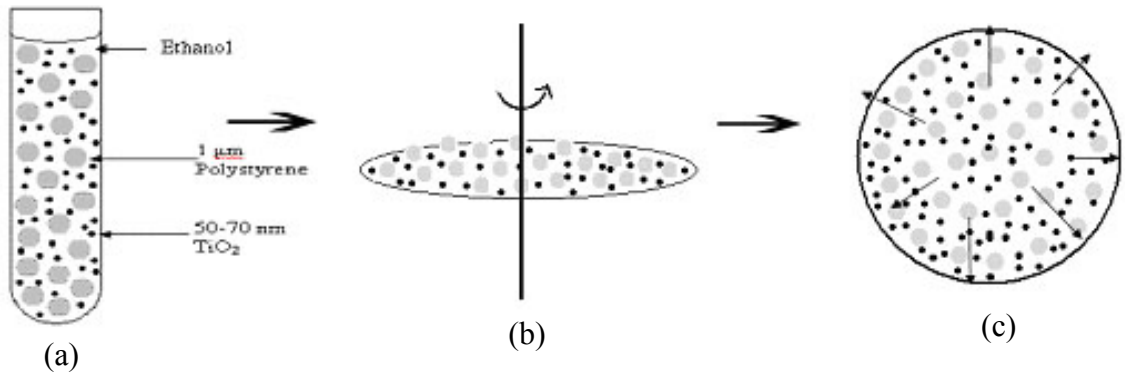

Figure 5.7: (a)Solution to be spin coated- particles move with brownian motion. (b)After dispensing, particles are confined in 2D, immersed in fluid. (c)During initial stages of spinning outflow moves the particles.

Figure 5.8: Theoretical model showing agglomeration of polystyrene particles and effect of lateral capillary forces on TiO_2 particles

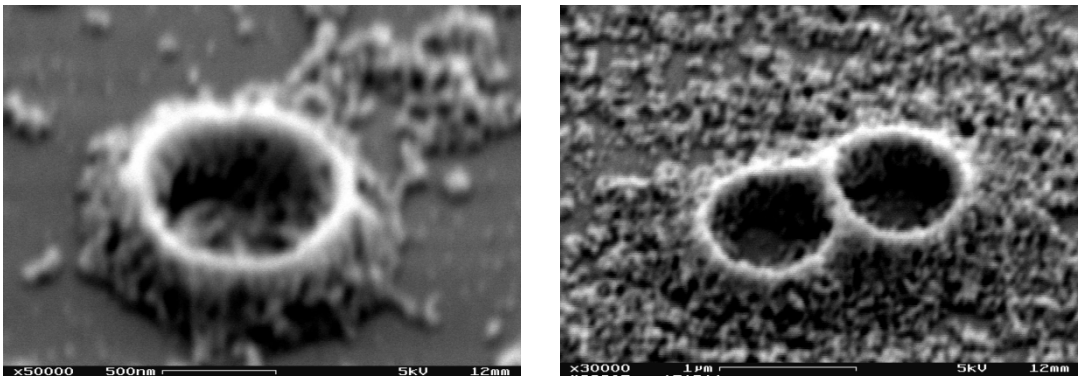

Figure 5.9: Effect of lateral capillary forces on TiO_2 particles: agglomeration around polystyrene particles. The volcano shapes are places where polystyrene spheres had been, but have been burned out to leave behind the surrounding TiO_2 nanoparticles.

Effect on TiO_2 nanoparticles: When the thickness of the film is in the range of diameter of the polystyrene particles and lateral capillary forces start acting on polystyrene particles, smaller TiO_2 nanoparticles still move in the liquid layer. These nanoparticles get carried towards the big particles by convective flow as depicted in Figure 5.8 and Figure 5.9. Some of the TiO_2 particles may also get pulled on the top of the polystyrene particles along with the fluid and as the evaporation at the top of the template particle would be faster, the particles may stay there forming a network around the polystyrene.

Effect of polystyrene concentration on the microstructure: At lower concentrations, the polystyrene template particles are well dispersed and less likely to be within the $r \ll L \ll (\sigma/\Delta\rho)g)^{1/2}$ distance from each other. With increasing concentration more and more particles are influenced by these capillary forces, resulting in different patterns of agglomeration.

An experiment was carried out with systematically increasing the polystyrene concentration in the titania dispersion to be spun, while keeping TiO_2 concentration fixed at 1 wt %. Figure 5.10 shows the SEM micrograph of the coating spin coated with 1 wt% polystyrene, 1 wt% TiO_2 and mixed in equal ratio. To quantitatively analyze the distribution of particles in the image, the Fovea Pro image analysis toolkit and a Matlab program was used. Histograms for the average nearest neighbor distances in the image and the coordination number for each particle were generated with these programs. The histograms were plotted for only smaller distances because for larger distances the particle-particle interaction becomes insignificant.

It can be seen from the micrograph shown in Figure 5.10 as well as from the coordination histogram shown in Figure 5.11 and Figure 5.12 that at 1 wt % concentration, the template polystyrene particles are well-dispersed in the coating with very few occurrences of pairs. TiO_2 is also very uniformly spread on the substrate except around the polystyrene particles where they form a close network. The topographic contrast is very obvious at the edges of the pores. When the polystyrene concentration is increased up to 5 wt%, template particles are still well-dispersed with some occurrences of pair and triplet structures (Figure 5.13 and Figure 5.14). With further increase in the polystyrene concentration to 7%, 8% and 10%, different patterns of the particles are observed. As seen in Figure 5.15 and Figure 5.16, 8% polystyrene gives rise to many, small and long chain-like structures. A closer look at these chains in

Figure 5.19 shows how TiO_2 nanoparticles get collected around the polystyrene particles. At 10 wt%, polystyrene particles start getting agglomerated to larger extent forming hexagonally close packed regions. It can also be observed that at this stage more and more TiO_2 particles get agglomerated near the polystyrene particles therefore exposing the substrate.

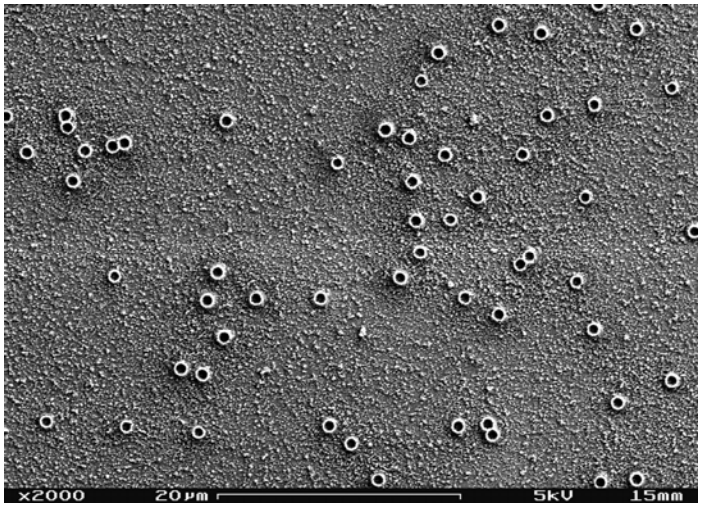

Figure 5.10: SEM image of 1 wt% TiO2, 1 wt% polystyrene dispersion, no of particles: 57

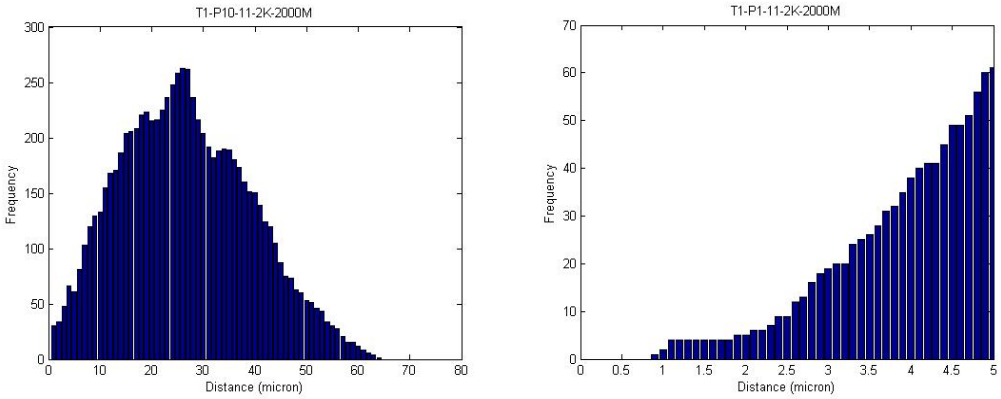

Figure 5.11: Histogram for 1 wt% TiO2, 1 wt% polystyrene , no of particles: 57

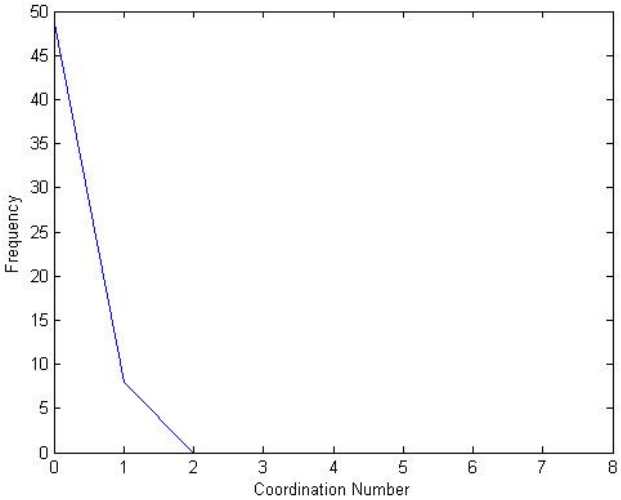

Figure 5.12: Coordination histogram for 1 wt% TiO2, 1 wt% polystyrene, no of particles: 57

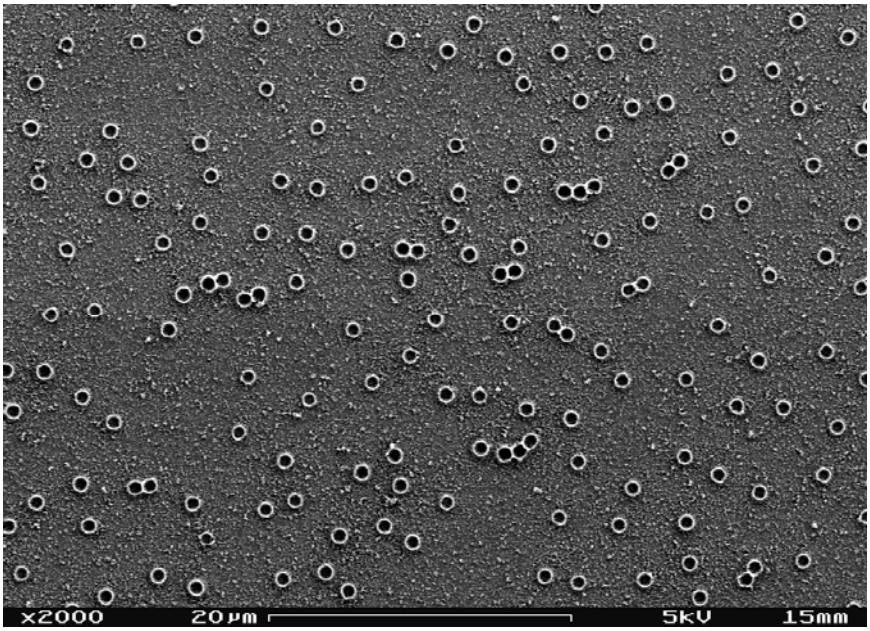

Figure 5.13: 5 wt% TiO2, 1 wt% polystyrene, no of particles:125

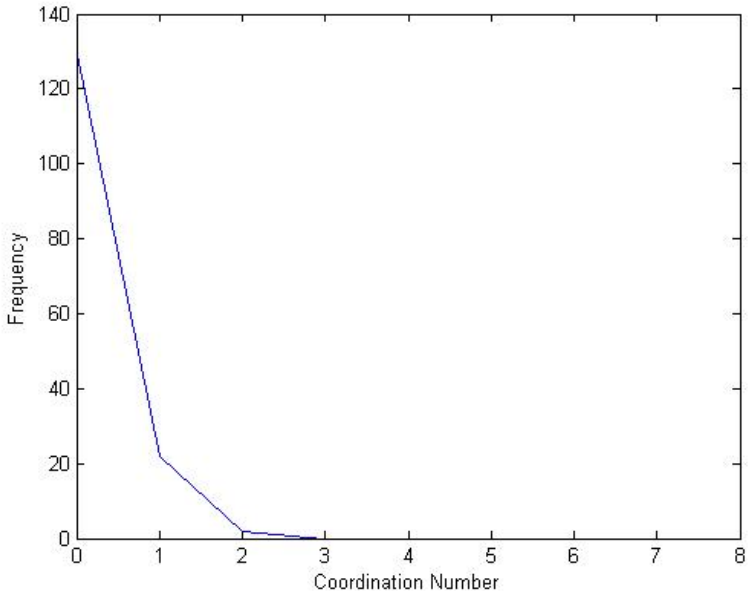

Figure 5.14: Coordination histograms for 5 wt% TiO2, 1 wt% polystyrene

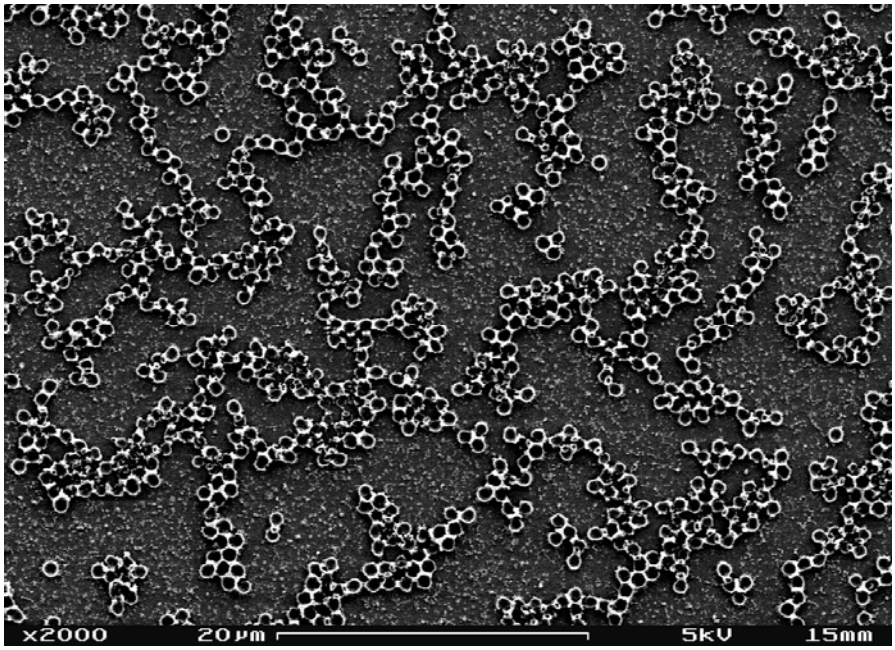

Figure 5.15: 8 wt% TiO2, 1 wt% polystyrene, no of particles:494

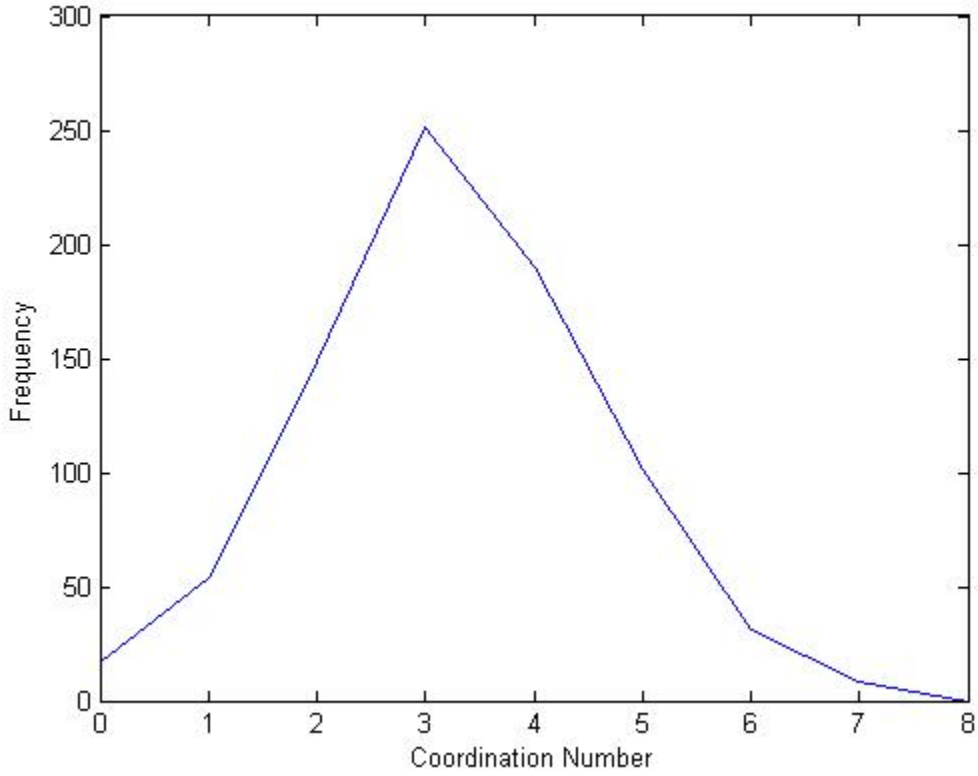

Figure 5.16: Coordination histogram of 8 wt% TiO2, 1 wt% polystyrene, no of particles:494

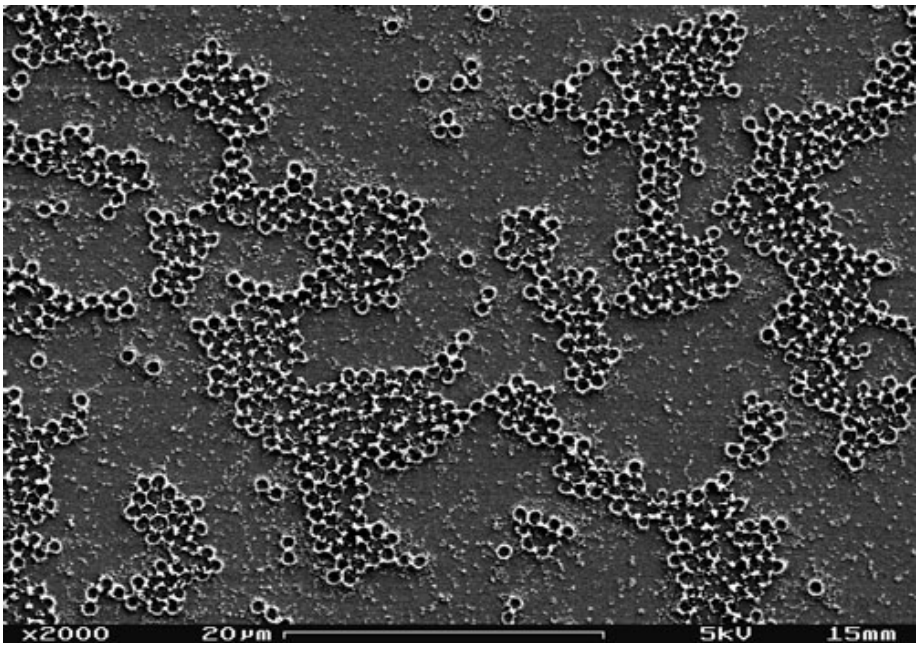

Figure 5.17: 10 wt% TiO2, 1 wt% polystyrene, no of particles:663

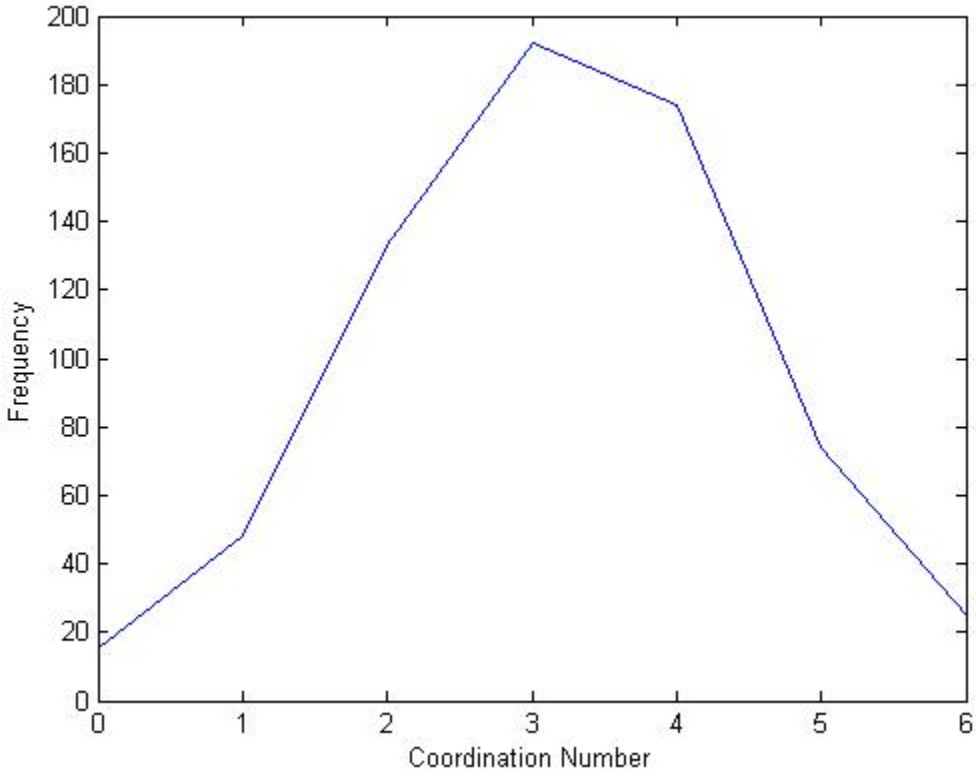

Figure 5.18: Coordination Histogram of 10 wt% TiO2, 1 wt% polystyrene, no of particles:663

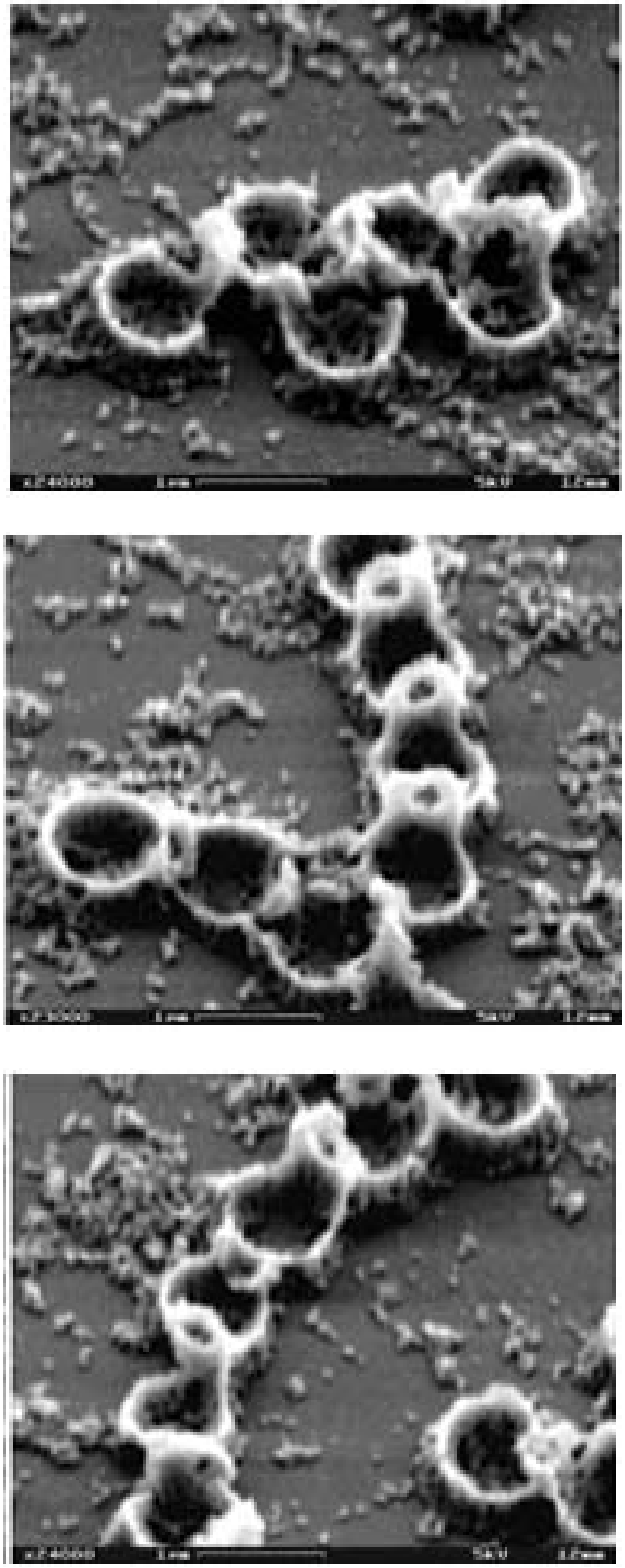

Figure 5.19: Chain-like structures in 7 wt% polystyrene, 1 wt% TiO_2 coating

- Roll coated titania films

The study of microstructure to understand the template and titania particle interactions was further extended to roll coated titania coatings. Single and multiple layers of templated titania were deposited by roll coating onto ITO coated PET (polyethylene terephthalate) substrates. A microstructural study was performed similar to that on the spin coated films.

Quantification of a characteristic aggregation distance: In order to make it easier to study the microstructure of the roll coated templated films, very dilute solutions of template particles were roll coated onto the PET substrates. Figure 5.20 shows a micrograph of such coating deposited with templated titania dispersion containing 1wt% polystyrene and 10 wt% titania. The corresponding coordination number histogram shows that most of the template particles in this micrograph are dispersed with no directly touching neighbor particle. There are few pairs and triplets but a hexagonal packing pattern is not observed.

The coordination number histogram has been plotted by first calculating the distances between all the particles in the micrograph and then counting the number of particles present within the radius of 1.3 μm of each particle. Figure 5.21 and Figure 5.22 show micrographs of roll coated templated titania with the same formulation of the dispersion but with two and three layers of deposition, respectively. Their corresponding histograms are also plotted alongside. As the number of layers was increased from 1 to 2 and 3, the

particle arrangements were changed which are reflected in the respective histograms.

In order to further understand how particles take up a particular pattern, a theoretical model was developed. The model consisted of images generated with the same number of template particles as in the SEM micrographs (with random X and Y coordinates). These particles were randomly dispersed in the model images using a Matlab program. The minimum separation between the centers of these simulated particles was set at 1 micron. This ensured that the simulated particles were consistent with the polystyrene template particles. For a particle, the nearest neighbors were defined as particles whose centers that lie within a certain threshold distance from the reference particle. Using threshold distances between 0.1 to 3 μm, nearest neighbor histograms were generated for the simulated images. These histograms were compared with the experimental histogram using a curve fitting algorithm to determine the threshold distance for which the simulated and the actual histogram matched closely. Figure 5.23 shows one such comparison between experimental and the simulated histograms. Figure 5.24 is the plot of curve fitting parameter χ^2 vs. threshold distance, where

$$\chi^2 = \text{sum (experimental value} - \text{theoretical value)}^2 \text{----------} \quad (2)$$

The plot of χ^2 vs. threshold distance indicates that, in general, at 1 wt% concentration, the template particles were initially placed randomly on the substrate. But due to the capillary forces and surface tension, the particles moved by approximately 0.6 μm before the solvent was completely

evaporated. This model for assessing particle motion was also applied to the experimental images with two and three layers of coating (Figure 5.21 and Figure 5.22). The average aggregation distance numbers for the two and three layer coatings were slightly smaller compared to single layer (1.45 and 1.35 μm respectively). This was mainly due to the higher density of the particles in these images.

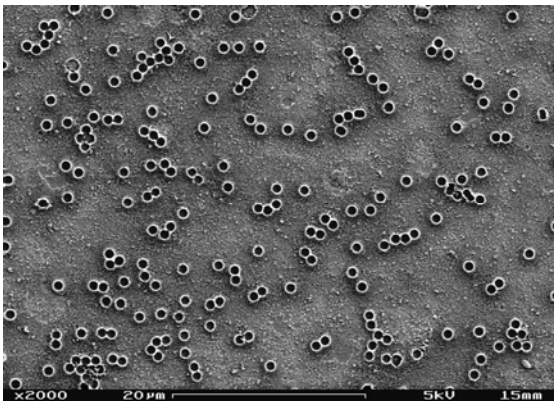

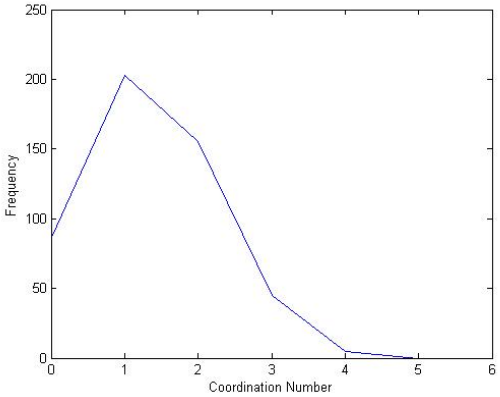

Figure 5.20: 1 wt% polystyrene , 10wt% titania, 1 layer of roll coating

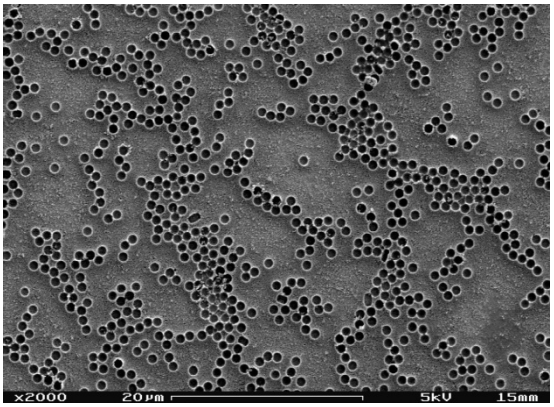

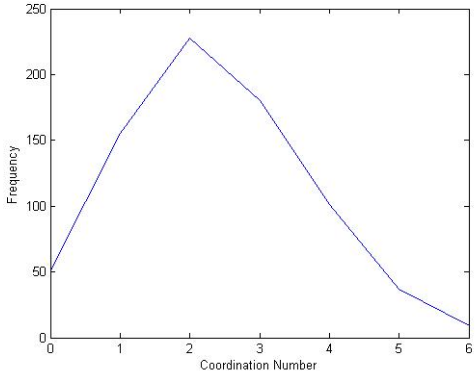

Figure 5.21: : 1 wt% polystyrene , 10wt% titania, 2 layers of roll coating

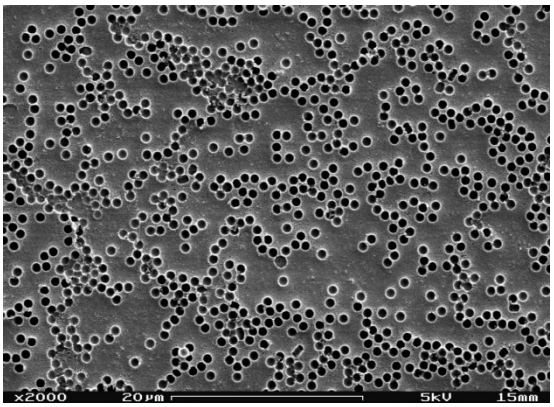

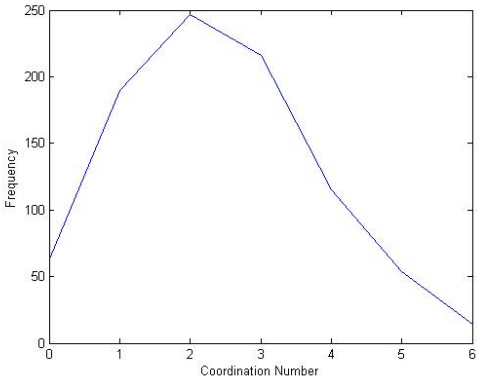

Figure 5.22: : 1 wt% polystyrene , 10wt% titania, 3 layers of roll coating

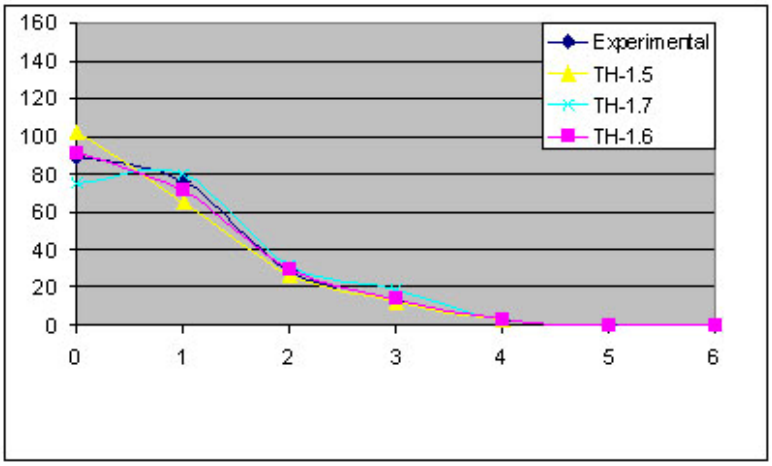

Figure 5.23: Theoretical histogram for threshold distance 1.6 matches closely with the experimental histogram.

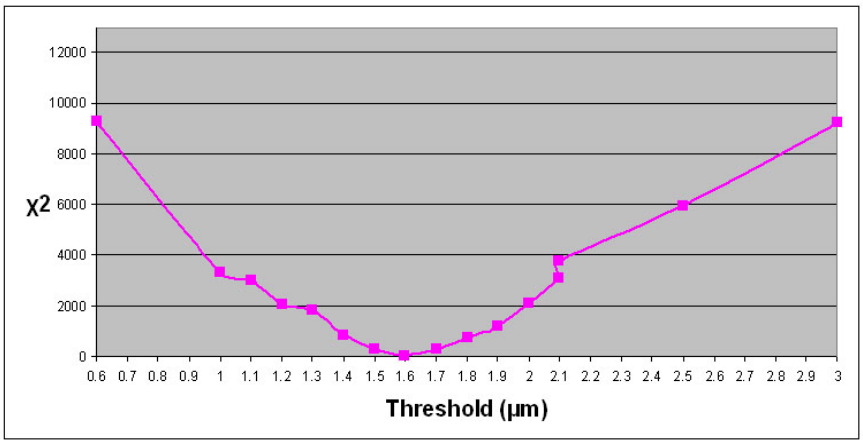

Figure 5.24: Curve fitting parameter is lowest for threshold distance 1.6 µm

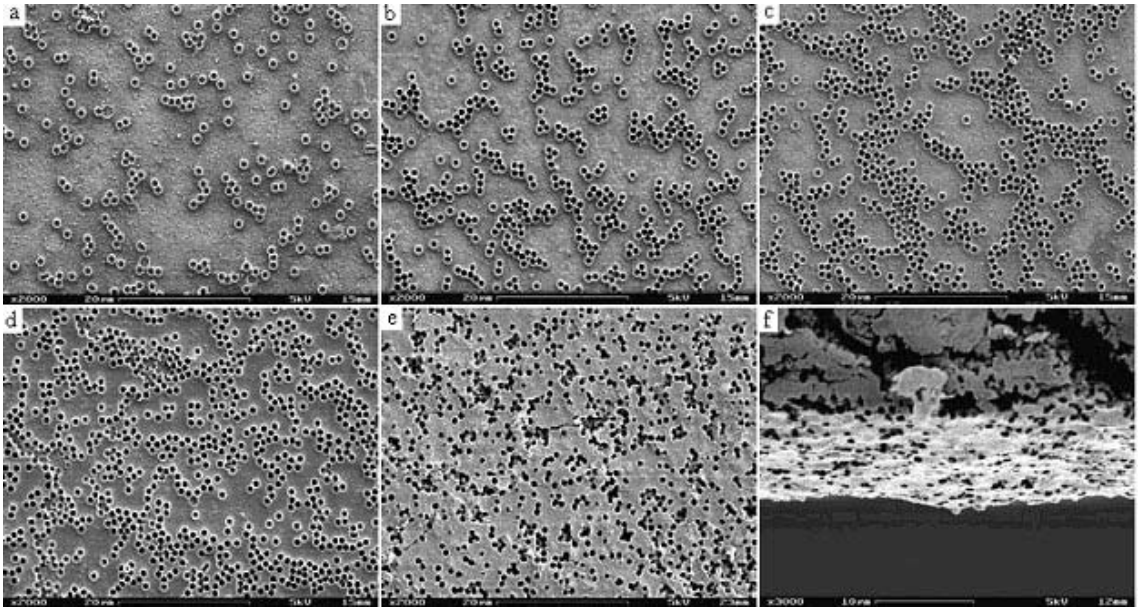

Figure 5.25: : a) 1 wt% TiO2, 1 wt% polystyrene on PET b) 2 wt% TiO2, 2 wt% polystyrene- one layer c) 2 wt% TiO2, 2 wt% polystyrene - two layer d) 2 wt% TiO2, 2 wt% polystyrene -three layer e) 5 wt% TiO2, 2 wt% polystyrene -ten layer f) cross section view of 5 wt% TiO2, 2 wt% Polystyrene

5.3.1.2 Motivation to find an alternate template material:

As mentioned at the beginning of this chapter, blade coating was used as the coating method for the continuation of this research. These coatings were assembled into solar cells and tested as described in Chapter 4. From the initial characterization and the solar cell testing with the blade coated polystyrene templated titania coatings, the following observations were made (refer to Figure 5.26 and Figure 5.27).

- The overall efficiency of the solar cells improved with the use of templated, porous titania electrodes. This substantiated the hypothesis of this research.
- The change in the template particle concentration influenced the porosity levels as well as the microstructure of the titania coating. For low template concentrations, the pores created by the template particles were randomly arranged while at higher concentrations the pores created a more close packed, honeycomb-like structure.
- The efficiency of the solar cells went through an optimum as porosity increased. After a certain porosity value, the efficiency of the cells showed a drop. Figure 5.26 and Figure 5.27 show the I-V plots and corresponding microstructures of the tested cells. The highest efficiency was obtained for the cells having random pore structure in titania. The close packed, honeycomb-like pore structure showed lower efficiencies than the nontemplated solar cells. This result indicated that monodispersed template particles (which can give more perfect, close packed pore

structures) were not necessary for the titania electrode to achieve an interconnected and random pore structure.

- As mentioned earlier, the readymade suspensions of latex polystyrene particles purchased from Thermo Scientific were expensive. Therefore it was decided to use a different lower cost templating material system for the further research.

Based on the above observations and a thorough literature review, emulsion templates were selected over polystyrene templates. At this stage of the research I had already deposited the polystyrene-templated coatings using blade coating, spin coating and roll coating method and was trying to explore the inkjet printing techniques for the same. Several formulations of the ink with different solvent systems were tried but the polystyrene template particles were found to clog the nozzle of the inkjet cartridge. Because any alternative templating material should be compatible with inkjet printing technique as well, emulsions (which are deformable) were selected for further study. It is expected that the emulsion droplets could be easily pinched through the inkjet nozzle without clogging. Oil-in-water emulsion templating system seemed to satisfy all the constraints posed by the polystyrene templates. In the following sections, a detailed discussion on the characterization of the emulsion templated coatings is presented.

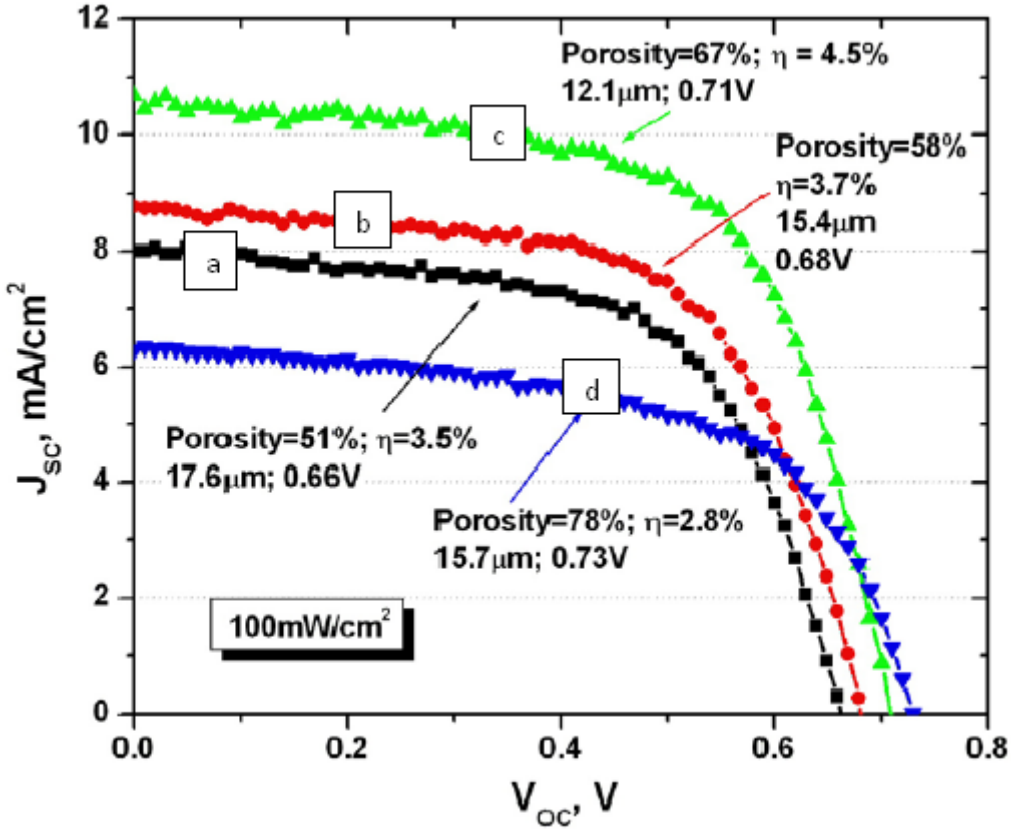

Figure 5.26: I-V characteristics of the dye sensitized solar cells templated with polystyrene particles. Four plots show I-V curves for cells having different loading of templates

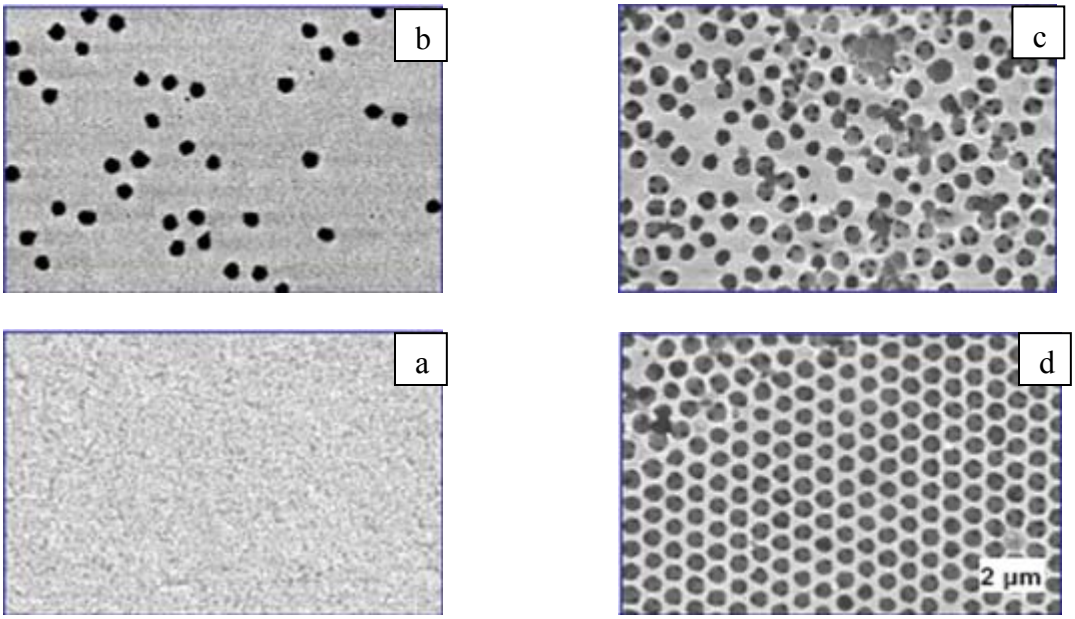

Figure 5.27: SEM micrographs of templated titania coatings with increasing concentration of templates from a to d

5.3.1.3 Emulsion templates

Two types of emulsions with 20 wt% and 40 wt% concentration of oil in water were selected for coating and device characterization. As discussed in the initial part of this chapter, the 20 wt% emulsion contained oil particles with mean diameter in the range of 100 to 300 nm, therefore had a very good stability. The mean diameter of the oil particles in the 40 wt% emulsion was around 3-5 µm. On the other hand, it remained stable for only 15-20 minutes. Each emulsion was then mixed with the P25 titania nanopowder. These samples are referred to as "20% emulsion templated titania" and "40% emulsion templated titania" samples respectively. A third sample, prepared with only aqueous titania dispersion (no emulsion), is named as the "nontemplated titania" sample. These three samples are used for all the characterization experiments discussed hereafter.

The emulsion templated and nontemplated dispersions were blade coated onto the FTO coated glass as described in Chapter 4. The microstructures of these three samples were studied using scanning electron microscopy. Figure 5.28, Figure 5.30 and Figure 5.34 show the SEM micrographs of the three samples. Figure 5.29, Figure 5.31 and Figure 5.35 are the respective higher magnification pictures.

The nontemplated titania coating as shown in Figure 5.28 and Figure 5.29 seems to be very dense. From the high magnification micrograph, though, the small pores can be observed. These pores were created when

the TiO_2 nanopowder started sintering and formed necks between the particles when they were heat treated to 500^0 C. From the micrograph, these pore sizes were of the order of 30 to 100 nm.

The microstructure of the 20% emulsion templated titania coating as shown in Figure 5.30 and Figure 5.31, contain larger pores of the order of 1 to 2 micron as well as the small pores. The large pores are created by the removal of the oil droplets in the emulsion templated titania coating by heat treatment. The small pores are due to the partial sintering of titania nanoparticles. To confirm that the bigger pores are present in the bulk of the sample and not only on the surface, a cross sectional SEM was performed. The cross-sectional micrographs in Figure 5.32 and Figure 5.33 show the presence of the pores throughout the depth of the sample. The pores also seem to be interconnected which agrees with the mercury porosimetry data presented below.

The 40% emulsion templated titania coatings contain even bigger pores than the 20% sample. In the lower magnification micrograph in Figure 5.34 pores of the order of 1 to 5 micron are seen. In all cases, the bigger pores (created by the oil droplet templates) push the titania particles close together during drying. Then during annealing they can sinter together in the same manner that is found in the non-templated structures.

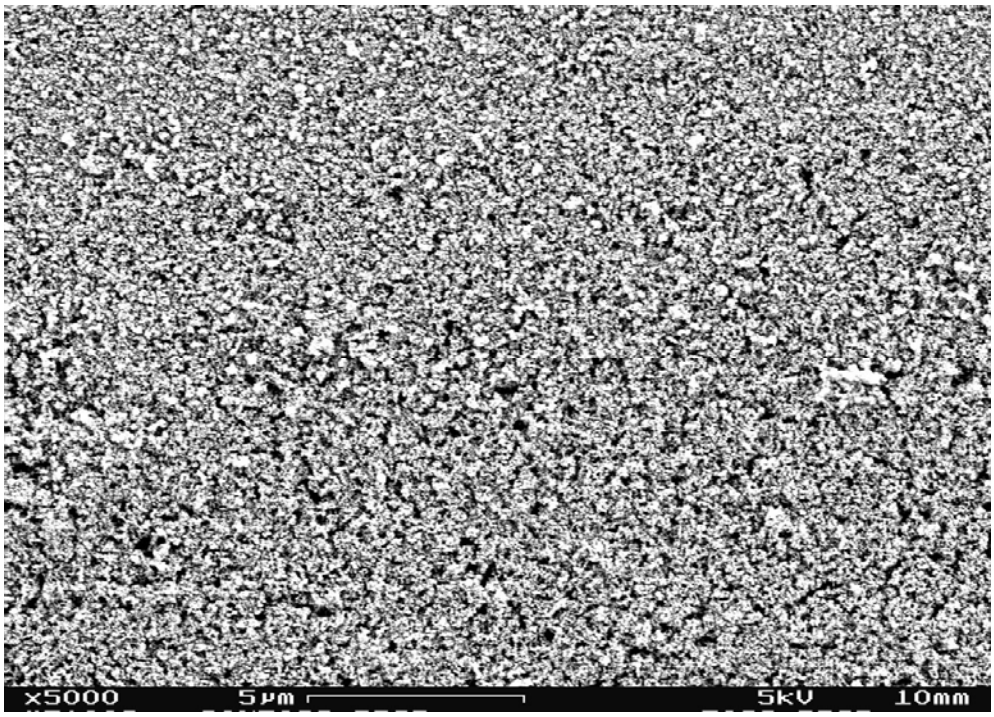

Figure 5.28: Nontemplated titania coating

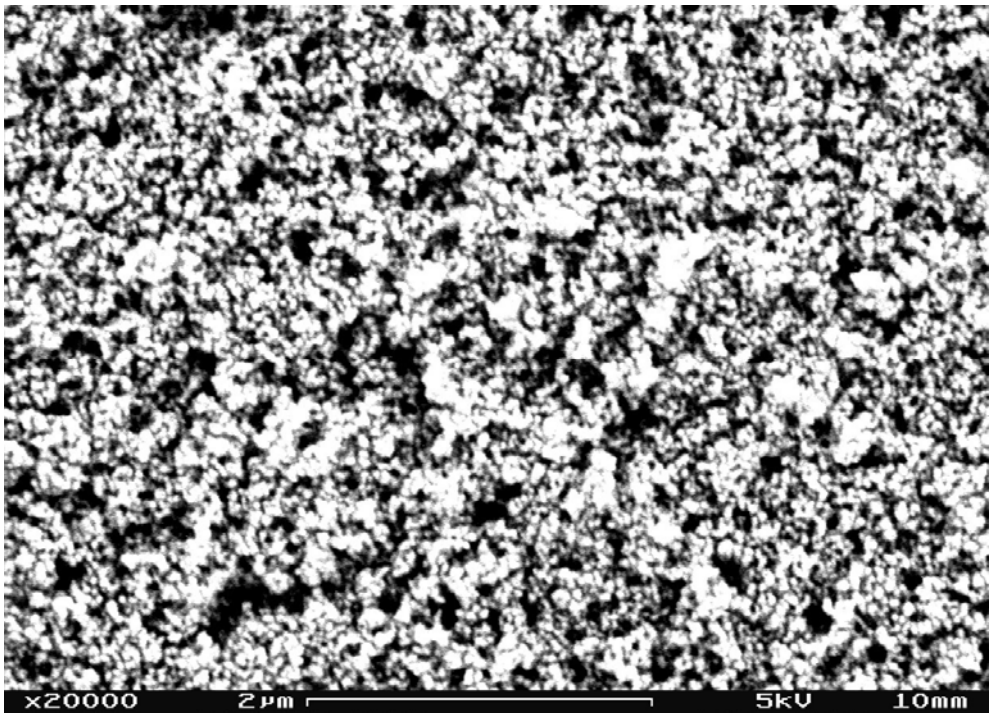

Figure 5.29: Nontemplated titania coating high magnification

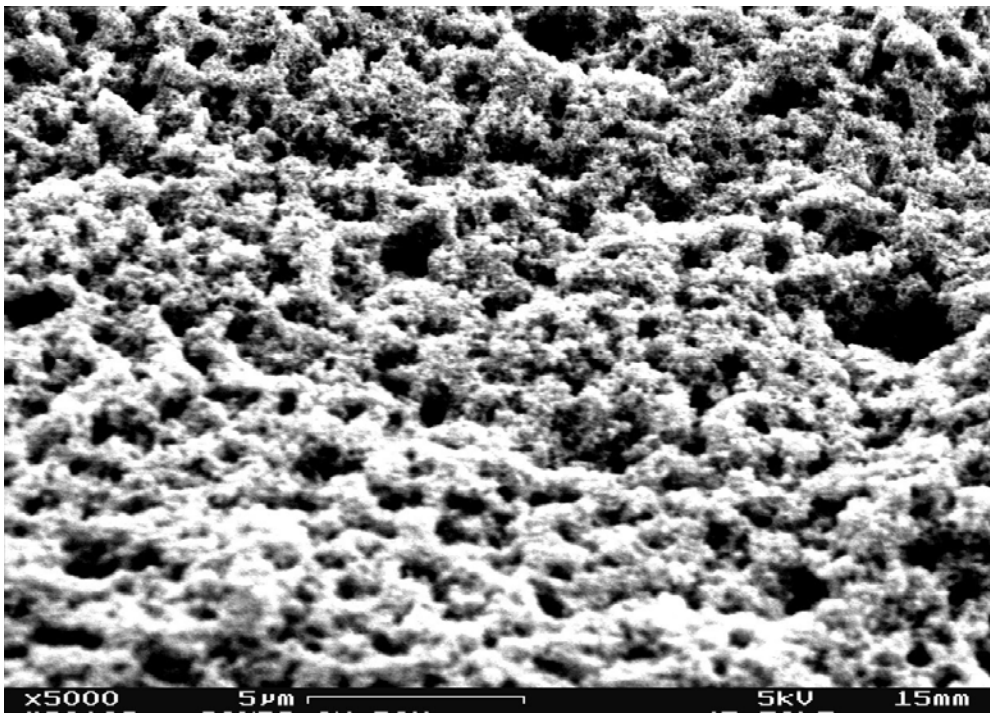

Figure 5.30: 20% Emulsion templated titania coating

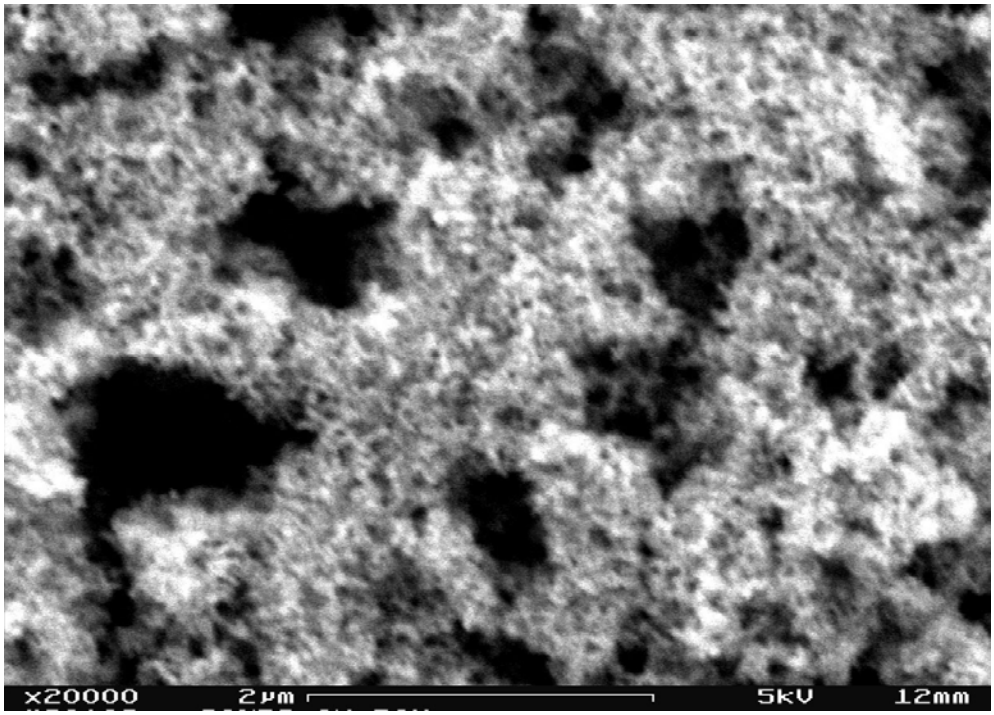

Figure 5.31: 20% Emulsion templated titania coating- high magnification

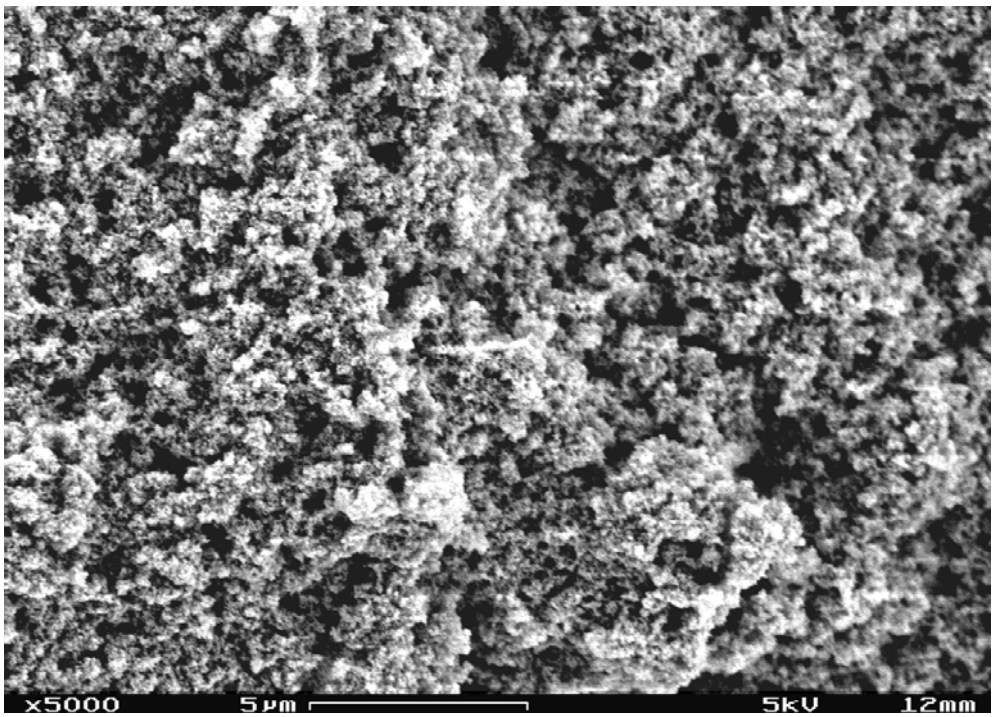

Figure 5.32: Cross-sectional micrograph of 20% emulsion templated titania coating

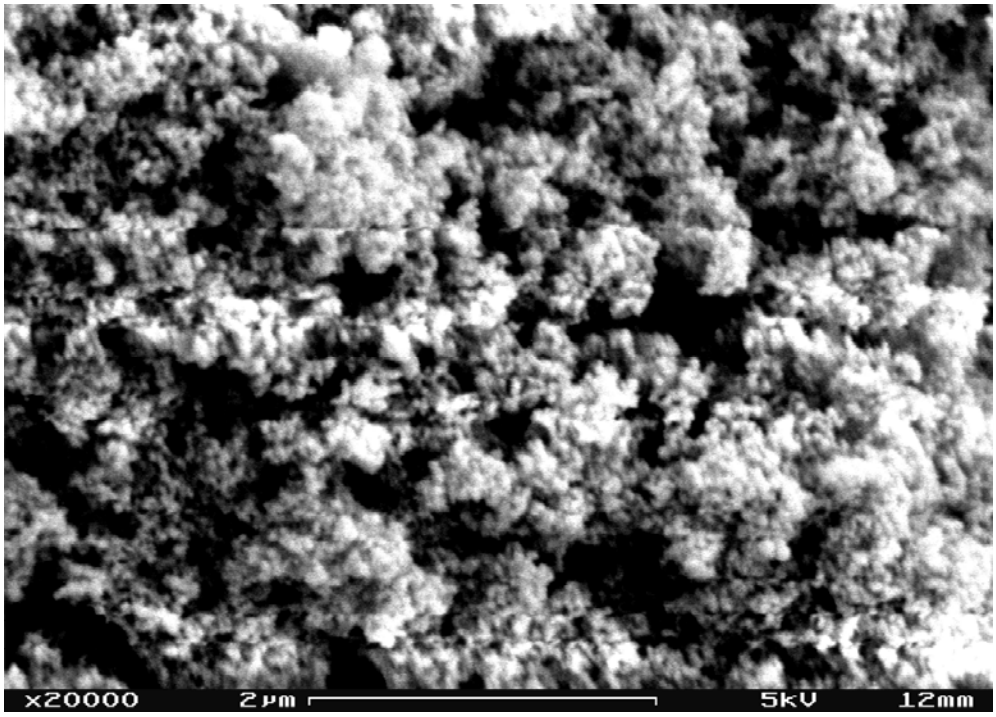

Figure 5.33: Cross-sectional micrograph of 20% emulsion templated titania coating- High magnification

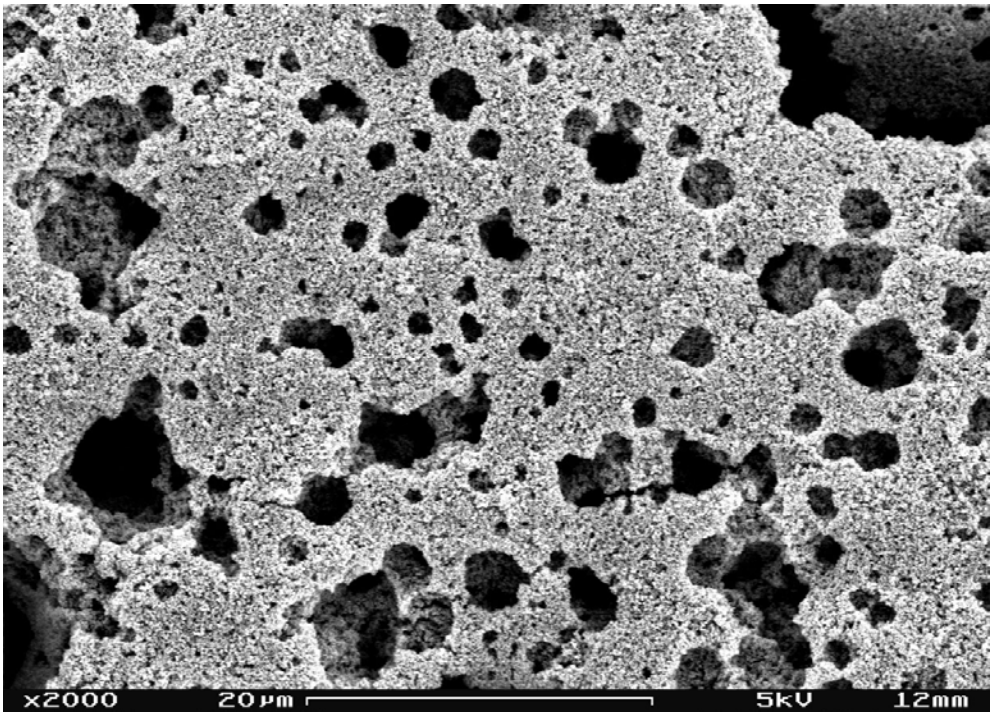

Figure 5.34: 40% Emulsion templated titania coating

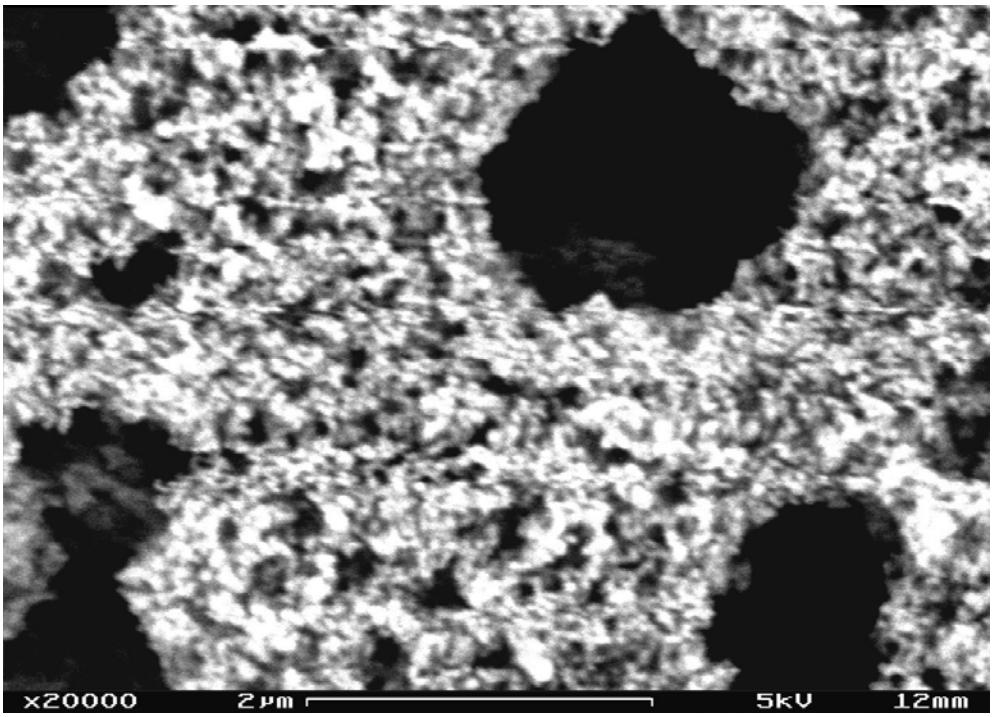

Figure 5.35: 40% Emulsion templated titania coating-High magnification

5.3.2 Pore structure analysis

To support the information obtained from the electron microscopy analysis about the pore structure of the templated and non-templated titania coatings, mercury porosimetry was performed on the same three samples. For mercury porosimetry, first thick coatings were produced by drop casting the three samples of titania dispersion and emulsion in three Petri dishes. The coatings were then heat treated using the same heating cycle as described before. Because of the greater thickness, the coatings formed big cracks. The Petri dishes were put upside down on a paper and were gently tapped. The flakes of the coating were then collected gently trying not to disturb the internal structure. Mercury porosimetry allowed us to study the pore size distribution and determine the percent porosity of these samples.

In porosimetry, the characterization of the pore structure is performed by intruding mercury into the pores by applying pressure to the surrounding mercury phase, therefore only interconnected and open pores can be sensed. Figure 5.36 plots the incremental intrusion of the mercury with respect to the pore diameter in the emulsion templated and nontemplated titania samples. The porosimetry results agree completely with the microscopy results discussed above. All three samples show a distinct peak at around 60 nm corresponding to the mesoporosity in the films arising from the nanocrystalline structure of the titania particles. Also, the amplitude of the 60 nm peak shown by the nontemplated sample was somewhat higher than the templated samples. This indicates that the templated

samples might have somewhat lower surface area than the nontemplated sample. This was confirmed in the next section in the BET surface area measurements.

The 20% emulsion templated sample showed two additional peaks at around 100 nm and 500 nm. The 40% emulsion templated sample showed a broader peak covering 70 nm to 1 micron range, suggesting that this sample was more polydispersed than the 20% sample. The presence of the extra peaks is thought to be a result of partial coalescence of oil droplets during the coating drying stage and is consistent with the view provided by SEM (Figure 5.31,Figure 5.35). The volume fraction of pores in the emulsion templated and nontemplated samples is shown in the Table 5.3. The %porosity level increases from 53% in the non-templated material to 69% and 82% in the 20 wt% and 40 wt% emulsion templated titania samples, respectively.

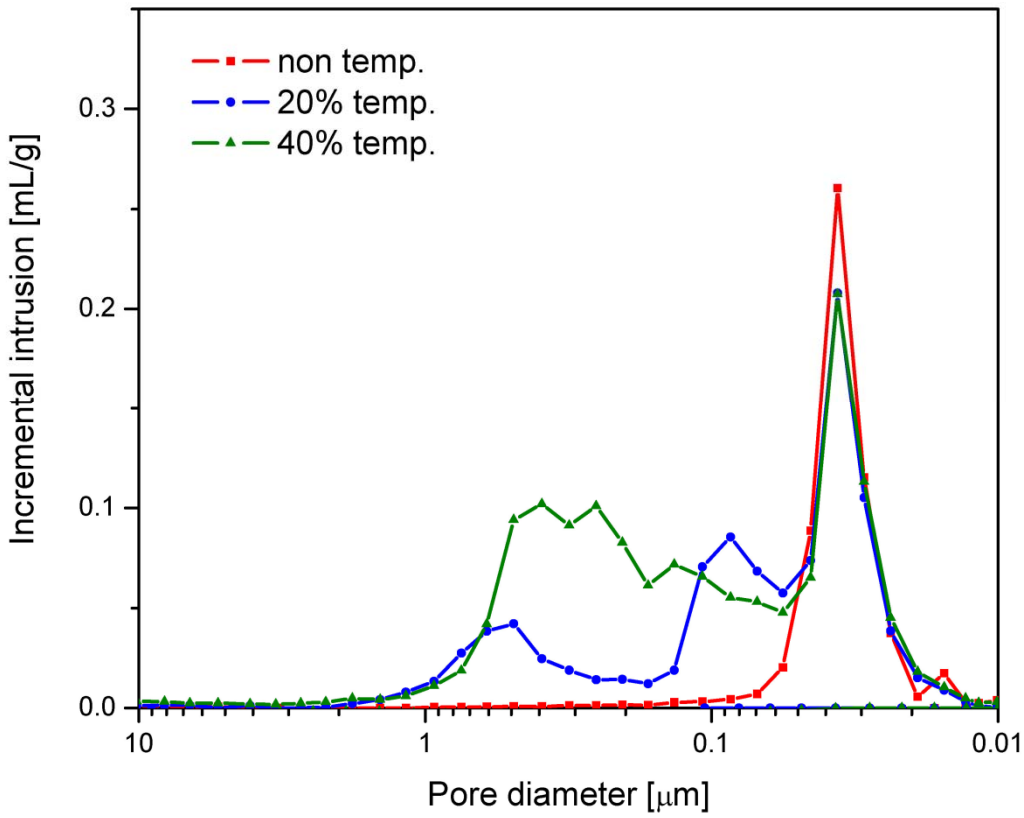

Figure 5.36: Porosimetry data

Table 5.3: % Porosity levels of emulsion templated and nontemplated samples

Sample	% Porosity
Non templated titania	53%
20% Emulsion templated titania	69%
40% Emulsion templated titania	82%

5.3.3 Specific surface area

For the BET surface area measurement, the samples were prepared by the same procedure as for the mercury porosimetry experiment. Table 5.4 lists the measured BET specific surface area values of the templated and nontemplated coatings. The specific surface area is mainly decided by the size of the TiO_2 particles which in turn is related to the mesoporosity of the titania coatings. As seen in the mercury porosimetry data, emulsion templating process did not alter the mesoporosity of the titania films much. All the three samples showed a peak at 60 nm. The smaller amplitude of the peak of the template samples suggested that their surface area might be little bit lower. In line with this observation, the templated coatings showed 10 to 20% reduction in surface area compared to the nontemplated coatings. This might be due to residue from the oil or other inorganic impurities from the Tween80 (polyoxyethylene sorbitan monoleate) or Span80 (sorbitan monooleate) emulsifiers. The oil that reached to the mesopores in the titania conceivably left some internal residue during the heat treatment. The structure and composition of Tween 80 and Span 80 was given in Chapter 4. They contain some anion (chloride, sulfate) and cation (Na, Al, Mg, NH_4^+ etc.) traces which can get bonded to titania, therefore decreasing the number of available sites for dye molecules to bond.

Table 5.4: BET specific surface area comparison of non-templated and emulsion templated samples

Sample	Specific surface area (m^2/g)
Non-templated titania	50
20% Emulsion template titania	42
40% Emulsion templated titania	41
60% Emulsion templated titania	43

5.3.4 Association of microstructure with an electrical model

From the electron microscopy and porosimetry study, it was observed that the 20 wt% emulsion templated titania coatings had a good potential to improve the permeation of the electrolyte through the coating. The 20 % templated coatings had uniformly dispersed pores of the size of around 200 nm to couple of microns.

In this section, an electrical model of the dye sensitized solar cell [8] has been studied. The electron and ion motion during the operation of the dye sensitized solar cell has been coupled with the microstructure of the titania coating. This comparison is useful to understand what kind of microstructure will improve the charge transport in the titania coating. First the charge transport though a mesoscopic titania coating is studied. Figure 5.38 shows a schematic of such a mesoscopic titania coating. In the electrical circuit schematic model shown in Figure 5.37, each titania nanoparticle has been considered as a separate resistive element. An infinite transmission line model has been used to represent all the electron transfer processes[8]. Resistances to electron flow through the titania nanoparticles are represented on the top line. Charge transfer resistance across titania/electrolyte interface is represented with a parallel RC circuit and resistance to electrolyte conduction in the spaces between titania particles is represented in the bottom line. The series resistance effects that can occur because of the long distances of conduction through the tiny pores between the nanoparticles, are important to note.

By introducing macropore channels into the titania coating (see Figure 5.40), the resistances to electrolyte resistance can be decreased or even eliminated if the percolation threshold is reached. The modified electrical circuit schematic model is shown in Figure 5.39. Although the electrolyte will still face some resistance while penetrating through the local mesopore channels while accessing the inner titania nanoparticles (represented by the single small resistance value addressing each local region), the overall charge transfer across the titania/electrolyte interface will definitely be faster. In Figure 5.39, each such local region is given a single series resistance that relates to electrolyte conduction through a short distance of tiny pores, but once into the template-generated large-sized interconnected porosity then rapid conduction is anticipated and no resistance values are drawn in.

As seen in the earlier sections, the oil in water emulsion templating method can incorporate such macropore channels into the titania coatings. For coatings using commercial P25 nanoparticles (70% anatase, spherical nanoparticles with average aggregate size of around 300 nm), the microstructure with around 60 to 70 % porosity and interconnected pores of the order of 200 nm to 2 to 3 microns, is favorable. Further electrical conduction studies and solar cell testing results, presented in following sections, have confirmed this conclusion.

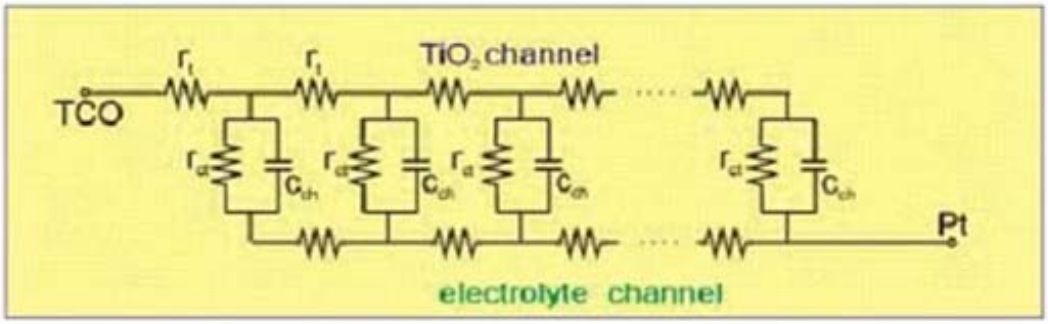

Figure 5.37: Electrical model describing electron transfer processes in dye solar cell containing mesoscopic titania film[adapted from [8]].

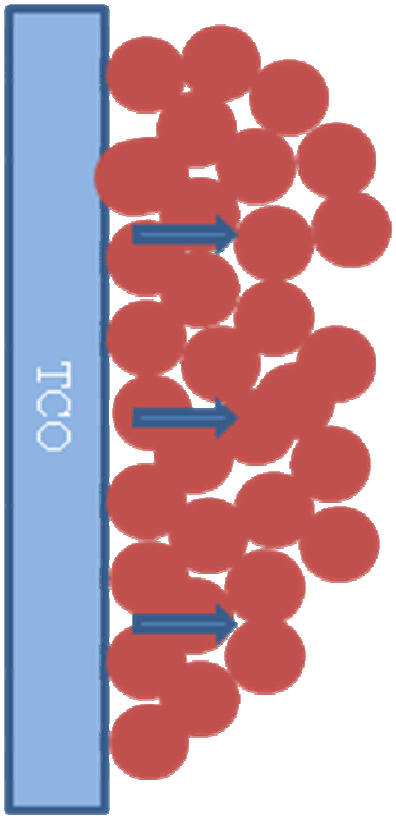

Figure 5.38: Schematic of mesoscopic titania film (also showing electrolyte flow though the coating). Conduction in the electrolyte must happen in the tiny pores between the 50nm sized titania particles.

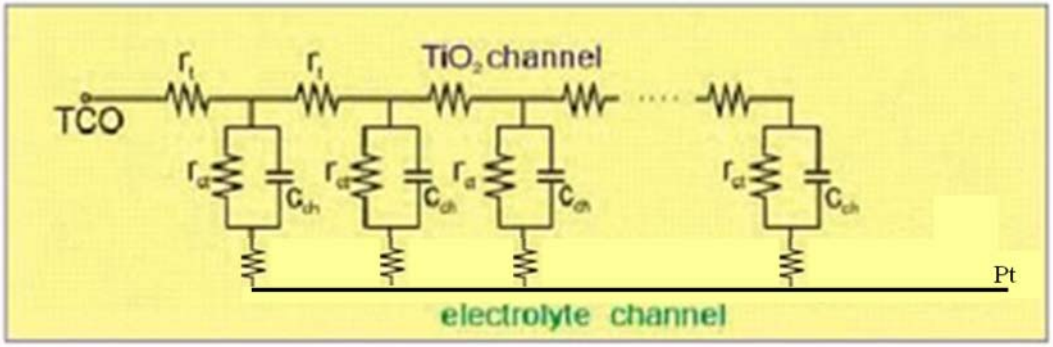

Figure 5.39: Electrical model describing electron transfer processes in dye solar cell containing meso-, macroporous titania film

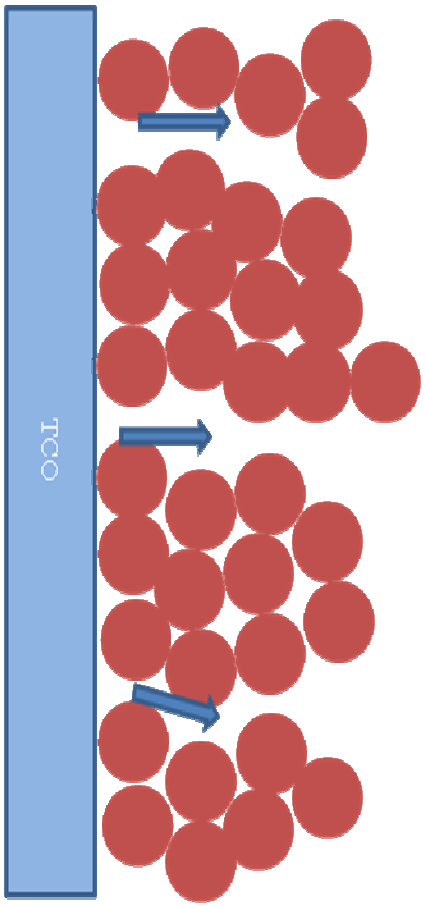

Figure 5.40: Schematic of macroporous titania film (easier electrolyte flow through the coating). Longer distances of conduction can then happen in the channels left behind by the template particles, though short distances must still be passed through the tiny nano-channels between the sintered titania particles.

In related earlier studies, it has been shown that high aspect ratio (rods, tubes, wires etc.) titania nanoparticles [9] could allow faster electron transport than spherical particles, due to their lower percolation threshold. But to achieve this it is important to achieve appropriate alignment of the nanoparticles in the coating. The schematic in Figure 5.42 shows an ideal arrangement of titania nanorods. This kind of alignment could provide high surface area for dye adsorption as well as open pore channels for effective penetration of the electrolyte. But in reality Figure 5.42), the nanorods or wires get entangled and form more dense structure. It is possible that oil templates of the order of few hundred nanometers could also be helpful in separating such nanorods and helping them align vertically to improve the electron transport, which would be an interesting topic for future work.

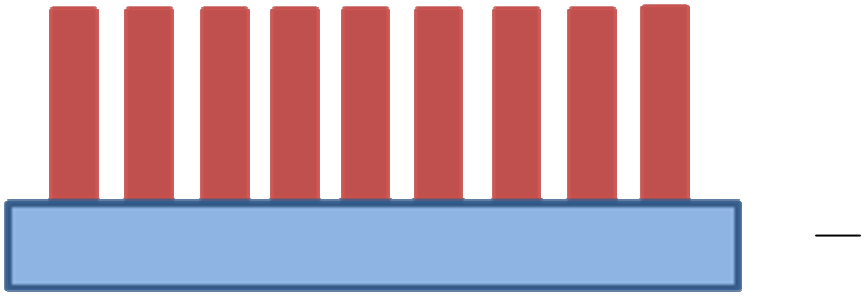

Figure 5.41: Schematic of titania coating made with nanorods

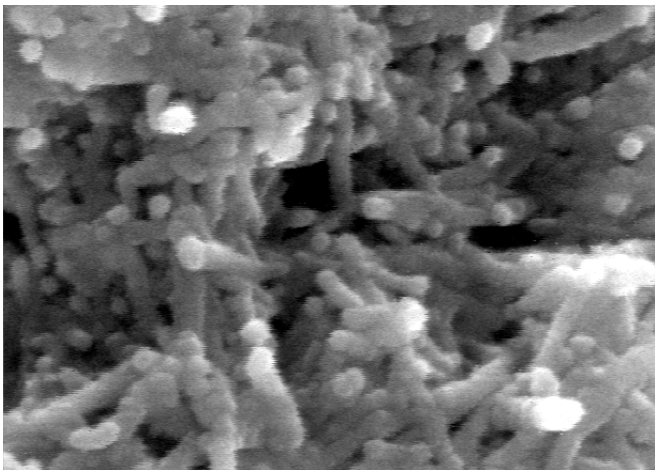

Figure 5.42:SEM image of hydrothermally grown titania nanorods (data from J. Sorge)

5.3.5 Electrochemical impedance spectroscopy (EIS)

In order to study the effect of emulsion templating on the internal resistances and electron transfer kinetics of the dye sensitized solar cell, electrochemical impedance spectroscopy (EIS) was employed. The basic working mechanism of this method has been discussed in Chapter 4. EIS data of the templated as well as nontemplated solar cells were analyzed and compared. EIS data are usually represented in the form of either a Nyquist plot or a Bode plot. In the present work, Nyquist plot representations are primarily used. Typically the Nyquist plot of a dye sensitized solar cell shows three semicircles, corresponding to the three main photoelectrochemical processes occurring during the cell operation: Nernst diffusion of iodine/iodide species through the electrolyte and titania coating, electron transfer at the titania/dye/electrolyte interface and electron transfer at the counter electrode [10-13]. The semicircle associated with the Nernst diffusion process is usually seen at frequencies between 0.01 to 0.1 Hz and therefore requires a long recording time. The cells tested in the present research were not completely sealed; therefore the EIS data acquisition time was limited to a couple of minutes per cell. Otherwise the gradual evaporation of the volatile electrolyte could influence the results. Also, it was more important to observe the semicircle associated with the titania/dye/electrolyte interface and study the changes in it with respect to the added porosity of the titania electrode. Therefore the frequency range selected for the EIS data acquisition was from 0.1 Hz to 10^6 Hz, which means, only two semicircles associated with the Pt electrode interface and the TiO_2/dye/electrolyte interface were observed. Figure 5.43 shows the Nyquist

plot of the 20% emulsion templated dye sensitized solar cell. It clearly shows two semicircles. The smaller semicircle is seen from frequencies 316 Hz to 63 KHz and the larger semicircle is seen in the frequency range of 0.1 Hz to 316 Hz.

A simplified electrical circuit model was used which represented the electrochemical processes taking place in a dye sensitized solar cell and is consistent with EIS models of DSSC's used in the literature. Figure 5.45 shows this equivalent RC circuit. The EIS data generated by this circuit was fitted with the experimental data shown in Figure 5.43 and the results are presented in Figure 5.44. The data fitting was done over the frequency range of 0.1 Hz to 50 KHz.

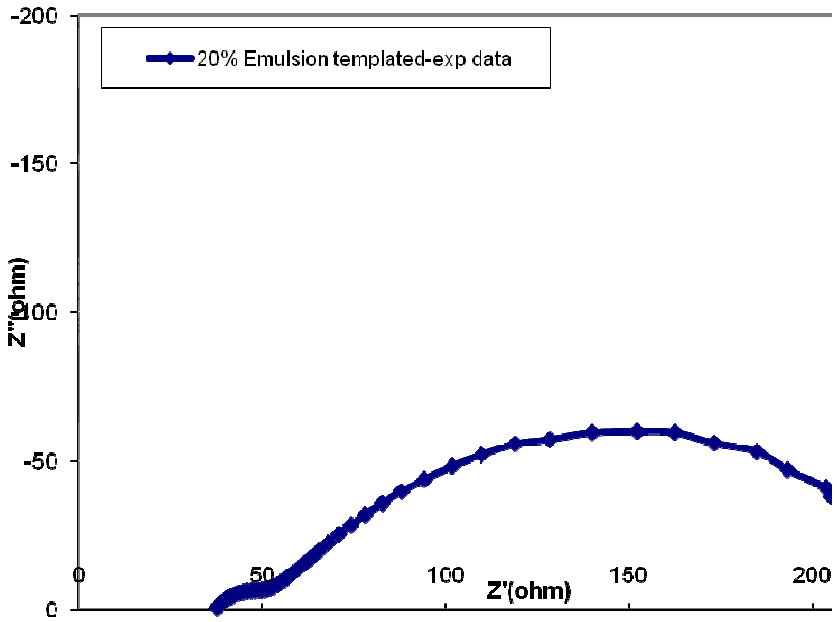

Figure 5.43: Nyquist plot of 20% emulsion templated dye solar cell

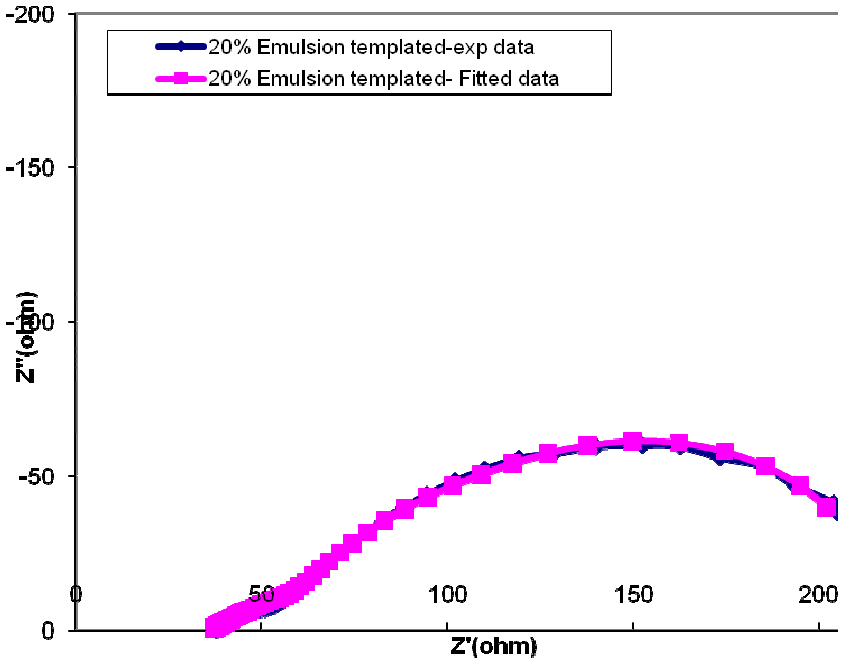

Figure 5.44: Nyquist plot of 20% emulsion templated dye solar cell with the fitted plot

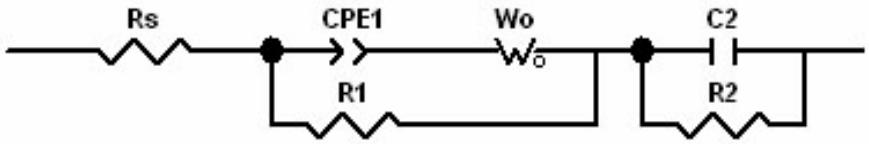

Figure 5.45: Equivalent circuit used for fitting impedance data

The equivalent circuit used for fitting the EIS experimental data contains elements that represent the key physical processes occurring during the operation of the dye sensitized solar cell. The series resistance Rs includes components from the sheet resistance of the FTO and the series resistances of the TiO_2 and electrolyte. The electron charge transfer at the Pt/electrolyte and TiO_2/dye/electrolyte interface is represented by the RC circuits with parameters R_1, C_1 and R_2, C_2 respectively. Although the semicircle associated with the Nernst diffusion through titania coating was not observed up to 0.1 Hz frequency, the interaction of the ionic species within the pore structures related to the recombination process happening at the TiO_2/dye/electrolyte interface is seen in the medium frequency range. The Warburg diffusion impedance model (Wo) is used in the equivalent circuit to take into account this diffusion process. Wo is defined as,

$$Wo = \sigma\omega^{-\frac{1}{2}}(1-j)\tanh\left(\delta\sqrt{j\omega/D}\right) \text{ ---------- } (3)$$

where σ is the Warburg coefficient, ω is the radial frequency, δ is the Nernst diffusion layer thickness and D is the average diffusion coefficient of the diffusing species.

In the R1/C1 circuit which represents the Pt/electrolyte interface, a constant phase element (CPE) has been used instead of a capacitor. The constant phase element is defined as

$$CPE = 1/\ T(jw)^P \text{ ---------- } (4)$$

CPE is defined by two values, T and P. If P equals 1, then the equation is identical to that of a capacitor. Often a CPE is used in a model in place of a

capacitor to compensate for non-homogeneity due to distribution of time constants in the porous electrodes.

In order to confirm the association of the two semicircles with the interfaces in the dye solar cell, impedance spectroscopy was performed under different conditions.

5.3.5.1 EIS under different illumination:

Figure 5.46 shows the impedance spectra collected for the 20% emulsion templated dye solar cell under different levels of illumination. The green, blue and red plots were recorded for incident illumination of 150 W/m^2, 100 W/m^2 and 50 W/m^2 respectively. The blue plot was recorded without illumination. It can be easily seen that only the bigger, lower frequency range semicircle showed a dependence on the illumination intensity. In the dye solar cell, the TiO_2/dye/electrolyte interface primarily responds to the illumination intensity. As illumination gets stronger, more photons irradiate the dye, causing more charge carriers to get injected into the TiO_2 conduction band. And, because this is an effective "open-circuit" measurement then we are pumping the titania with charges until these charges recombine with the dye somewhere internal to the system. This reduces the impedance of the TiO_2/dye/electrolyte response and enables a limited current through the local electrolyte regions as well, to satisfy the current boundary conditions. The same effect was observed in the bigger semicircle of the EIS plot in Figure 5.46. The plot recorded without illumination had very high impedance as compared to the other plots recorded with illumination. This confirmed the association of the TiO_2/dye/electrolyte interface with the bigger semicircle. There was not much difference in the high frequency (smaller) semicircle impedance of the four plots. The X-intercept of the plots is associated with the series resistance Rs in the equivalent model. This series resistance also did not seem to change with the illumination intensity.

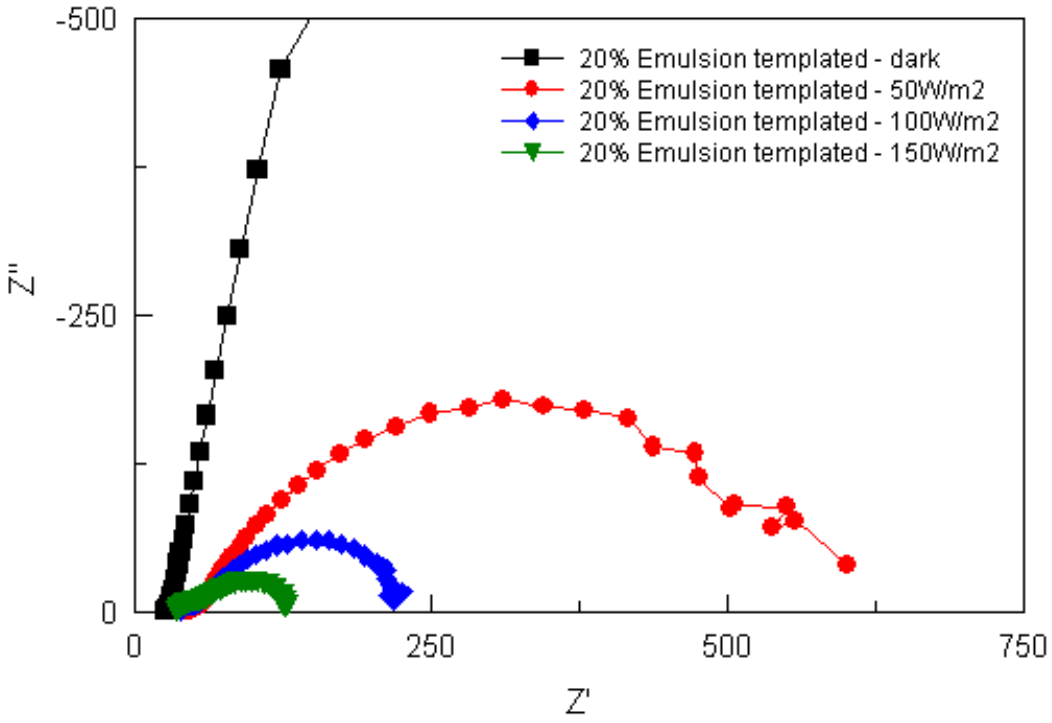

Figure 5.46: Impedance spectra of 20% emulsion templated DSSC under different illumination intensities

5.3.5.2 EIS with different number of separator membranes:

In order to avoid short circuit in the dye solar cell, a separator membrane had been inserted in between the titania electrode and the counter electrode. Impedance data of two 20% emulsion templated solar cells were collected using single and multiple layers of the membranes in between the electrodes. Figure 5.47 compares the impedance data of those two cells. It was observed that with multiple layers of membranes, the impedance spectra showed only a lateral shift toward the right hand side. The additional layers of membranes effectively increase the thickness of the solar cell which got reflected in the impedance spectra in terms of the shift in the series resistance Rs of the cell. There was no other difference in the cell configuration of these two samples. This experiment confirmed the association of Rs in the equivalent circuit model with the series resistance of the electrolyte.

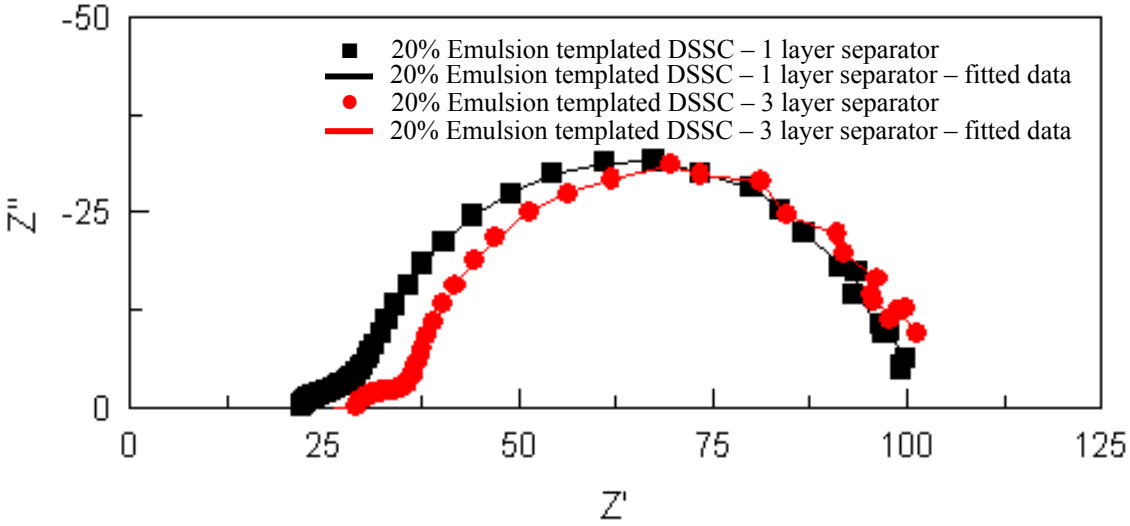

Figure 5.47: : Impedance spectra of 20% emulsion templated DSSC with different number of membrane separators. Solid line indicates the fitted data

5.3.5.3 EIS on templated and nontemplated cells:

Once the association of the bigger semicircle was confirmed with the TiO_2/dye/electrolyte interface, the EIS data for templated and nontemplated cells were compared. Figure 5.48 plots the impedance data for the nontemplated, 20% emulsion templated and 40% emulsion templated cells. It was observed that the emulsion templated solar cells had lower impedance for this interface as compared to the nontemplated cells. The Pt electrode/electrolyte interface impedances were not much different than each other. The R_2 and C_2 parameters associated with the bigger semicircle were extracted after curve fitting the EIS data with the equivalent circuit. The changes in the R_2 and C_2 parameters have been plotted in Figure 5.49 with respect to the oil concentration (% porosity) of each sample. Four cells of each type were tested and the average of R_2 and C_2 parameters have been plotted with the error bars in Figure 5.49.

The resistance R_2 was observed to decrease with the increase in the oil (template phase) concentration, i.e. with the addition of larger-sized porosity. We associate this reduction in resistance with the greater ease of conduction in the electrolyte phase to connect with the recombination process that is taking place. The capacitance C_2 value increased with the porosity. The capacitance arises due to charge separation as modeled by a simple capacitor with a spacing, d, between electrolyte ions and TiO_2 and high (typically 40 to 50 m^2/g) specific surface area (SSA) of TiO_2 electrodes according to:

$$C = \frac{\varepsilon A}{d} \quad \text{----------(5)}$$

where A is the electrode surface area accessible to electrolyte ions, and ε is the electrolyte dielectric constant. The BET surface area measurements had shown that SSA of templated coatings was not much different from the non-templated ones, but the separation between the electrolyte and titania in the templated coating would definitely be smaller by having better channels through the bigger sized pore structure, which resulted in an increase in the capacitance. Conversely, the ionic conductivity σ of a porous electrode is linked to its porosity P, tortuosity T and the ionic conductivity of the pure electrolyte σ_0 by the relation:

$$\sigma = \sigma_o * \frac{P}{T^2} \text{ ----------(6)}$$

The macroporosity caused by the emulsion results in higher overall porosity and lower tortuosity, which causes the increase in ionic conductivity σ of the TiO_2 electrode. This result indicated that the diffusion of redox ionic species through the electrolyte was faster in the emulsion templated solar cells. This would improve the dye regeneration process and in turn would improve the photocurrents of the solar cell as will be seen in section 5.4.

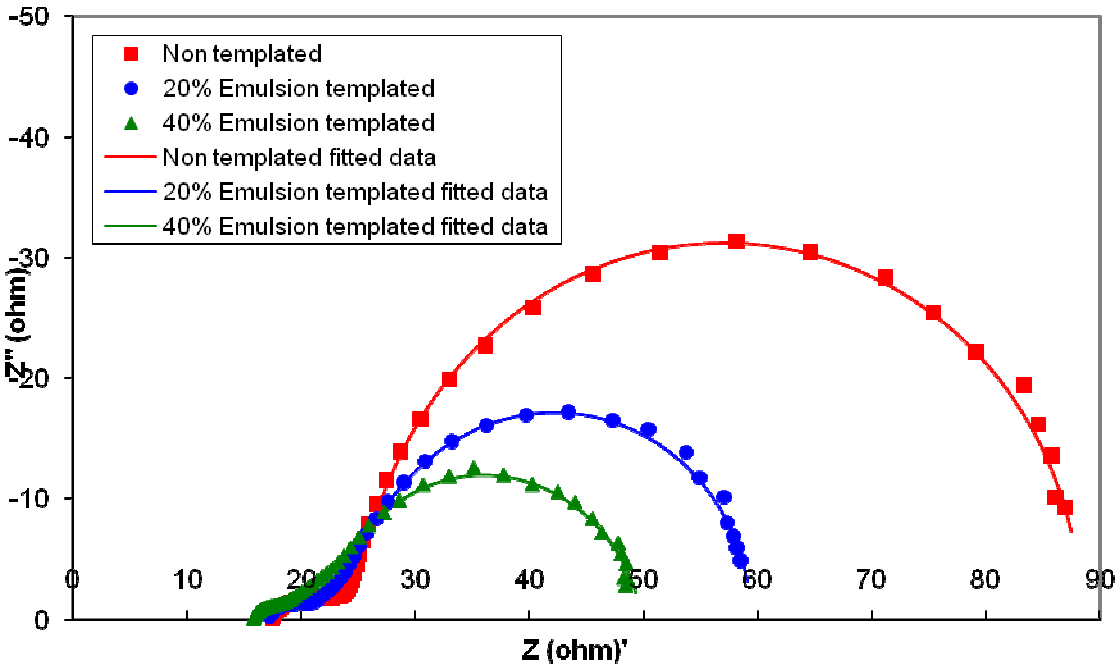

Figure 5.48: Impedance spectra of nontemplated (■), 20% (●) and 40% (▲) emulsion templated DSSC. Solid line indicates the fitted data

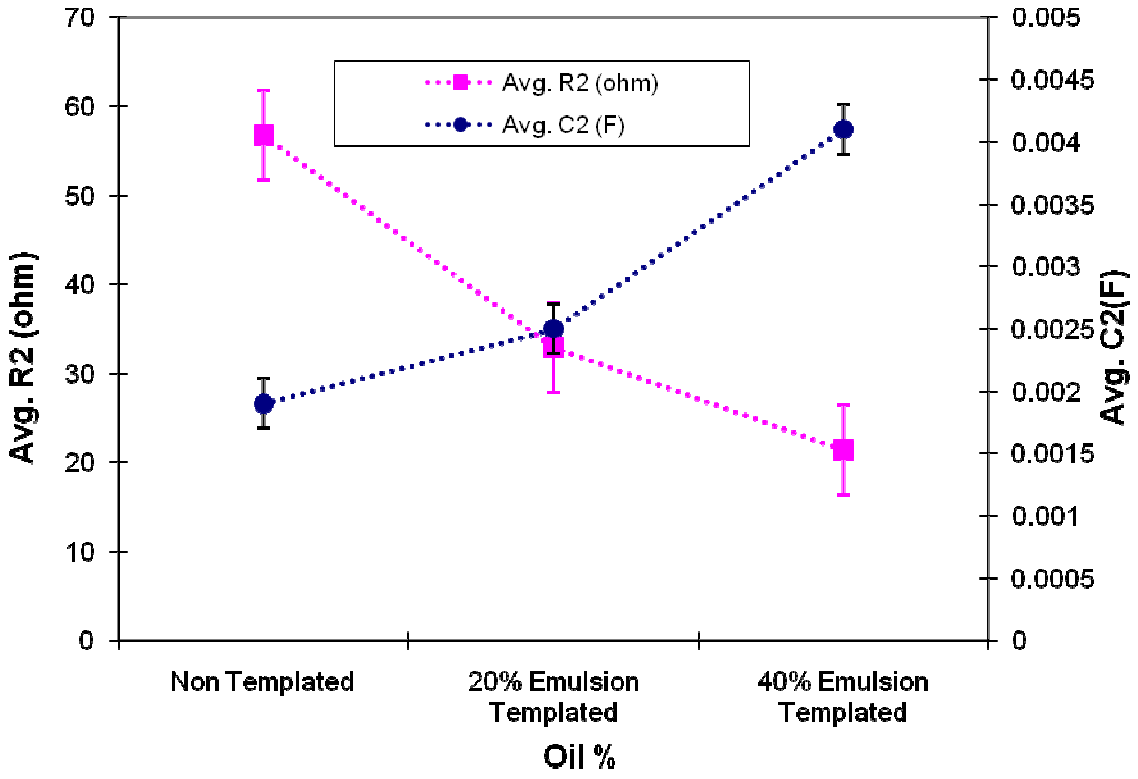

Figure 5.49: Plot of charge transfer resistance (R_2) and chemical capacitance (C_2) of the TiO_2/dye/electrolyte interface (average values of 4 samples have been plotted along with standard error bars)

5.3.5.4 EIS with liquid and quasi-solid electrolytes:

The main purpose of employing emulsion templating method was to create a network of interpenetrating pores in the bulk of titania coating so that the electrolyte can easily penetrate through it and help regenerate the dye faster. This is even more important when a quasi-solid, polymer gel electrolyte is used in the dye solar cell because we anticipate that conduction through this phase will be slower than with the liquid electrolytes. There has been an increasing trend in use of polymer gel electrolytes instead of liquid electrolytes in the dye solar cell system to avoid electrolyte leakage and corrosion in the cell. But the polymer gel electrolytes have lower ionic conductivity as compared to the solvent based electrolytes, which degrades the overall system performance. The interpenetrating pore structure created by the oil templates are designed to provide better pathways for the electrolyte to flow through the titania therefore it is interesting to compare the impedance data of polymer gel electrolyte and a solvent based liquid electrolyte in the nontemplated and emulsion templated cells.

The liquid electrolyte we used for this experiment was prepared in the lab as per the recipe given in Table 5.5.[14] To make the quasi-solid electrolyte 30wt% PVDF-HFP (poly(vinylidenefluoride-co-hexafluoropropylene, Solvay, Belgium) was added to this liquid electrolyte. The electrolyte obtained was quite viscous. The ionic conductivities of the liquid and quasi-solid electrolytes were 11 mS/cm and 2.47 mS/cm, respectively. The ionic conductivity of the gel electrolyte was almost 4 times lower than the liquid electrolyte.

Ingredient	Molecular weight (gm/mol)	Density (gm/ml)	Weight (gm)	Volume (ml)
Acetonitrile	41.05	0.782	3.91	5
Methoxypropionitrile	85.11	0.939	4.695	5
4-tertbutylpyridine	135.21	0.923	0.06	0.07
Lithium Iodide	253.81s	3.494	0.67	0.2
Iodine	133.84	4.93	0.12	0.02

Table 5.5: Solvent based liquid electrolyte:

Figure 5.50 and Figure 5.51 show the impedance spectra of the nontemplated and 20% emulsion templated dye sensitized solar cells tested with liquid and quasi-solid electrolyte. In case of the nontemplated cells, the cell with gel electrolyte showed higher impedance of the TiO_2/dye/electrolyte interface, which was represented by the bigger semicircle in the Nyquist plot. After curve fitting the experimental data, the charge transfer resistance and the chemical capacitance values were extracted. These are shown in Table 5.6. The resistance associated with the TiO_2/dye/electrolyte interface was higher with the gel electrolyte as compared to the liquid electrolyte. This suggests that due to the higher viscosity and lower ionic conductivity of the gel electrolyte, the permeation through the nontemplated titania coating was not as effective. This resulted in the slower electron charge transfer. On the other hand, the emulsion templated solar cell had easily penetrable microstructure therefore even the viscous gel electrolyte did not get hindered and could be in contact with the titania nanoparticles/dye molecules in the interior part of the coating. This was reflected very well in the impedance plot of the templated cell, shown in Figure 5.51. There is not much difference in the impedances of the cells when comparing the liquid electrolyte and gel electrolyte.

This indeed is a very important result as it suggests that emulsion templating facilitates the use of quasi-solid electrolytes in the dye sensitized solar cell and could facilitate commercialization of DSSC's with a low-cost and relatively simple process. Although such electrolytes have lower conductivities, the

availability of broader pathways in the bulk of the titania coatings makes it easier for the electrolyte to reach to the titania particles and regenerate the dye rapidly.

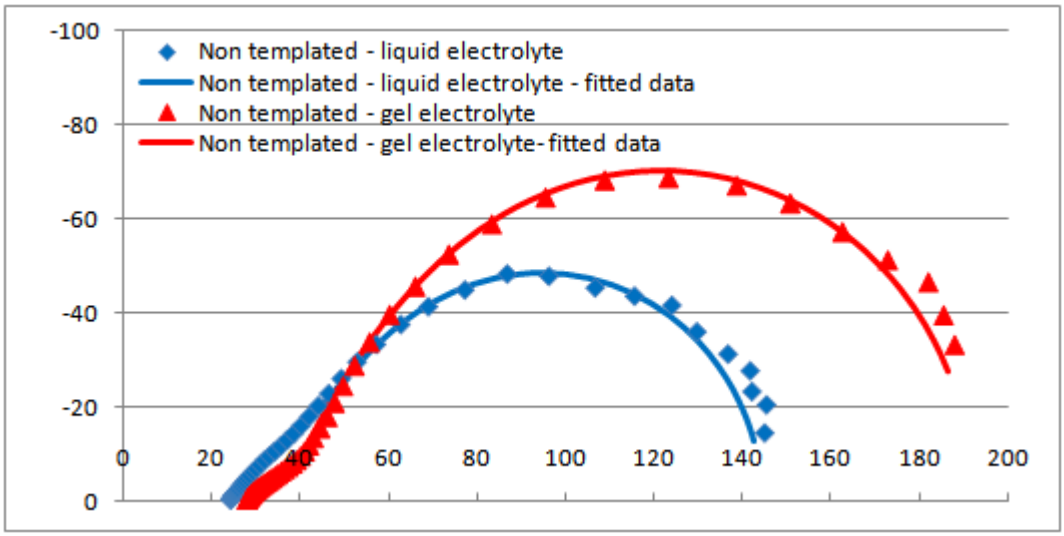

Figure 5.50: Impedance data of nontemplated dye solar cells. Solid line represents curve-fitted data and symbols represent the experimental data

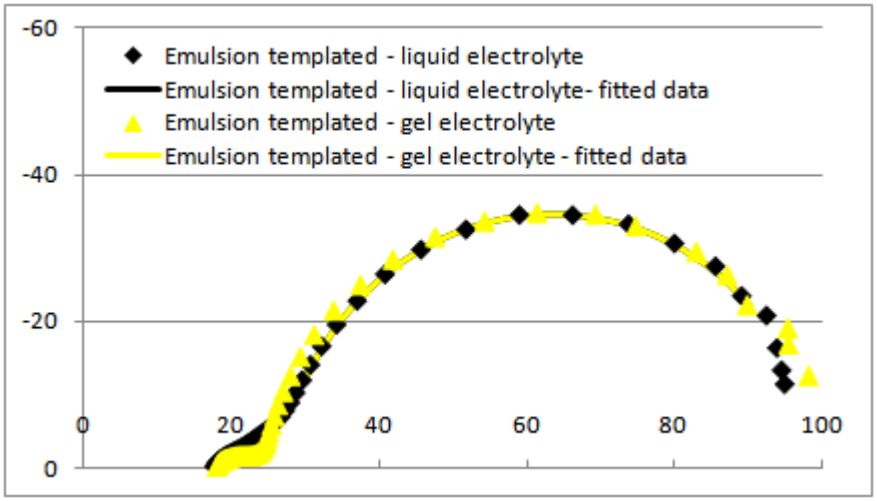

Figure 5.51: Impedance data of 20% emulsion templated dye solar cells. Solid line represents curve-fitted data and symbols represent the experimental data

Table 5.6: Charge transfer resistance and capacitance values extracted by curve fitting the impedance data shown in Figure 5.50 and Figure 5.51

Sample	R_1 (ohm)	R_2 (ohm)	C_2 (mF)
Nontemplated cell- liquid electrolyte	36	84	1.5
Nontemplated cell- gel electrolyte	34	127	1.9
Emulsion templated cell- liquid electrolyte	12	67	1.7
Emulsion templated cell- gel electrolyte	11	69	1.8

5.4 Testing the performance of the templated dye sensitized solar cells

The performance of the templated and nontemplated dye solar cells was tested by plotting the I-V curve and measuring the efficiency of the cells. Cells were tested under various configurations to understand the effect of different parameters on the cell operation. In every experiment 4 samples of each cell were prepared and tested. All the results presented here are average values for each type derived from the 4 samples.

5.4.1 Titania nanoparticles from different suppliers:

It has been mentioned in Chapter 4 that in all the experiments discussed so far, P25 titania nanoparticles purchased from Evonik-Degussa were used. However, in the initial phase of this research, three different types of titania nanoparticles from different suppliers were compared. Two types of titania particles, named Aeroxide P25 and Aeroxide P90, were obtained from Evonik-Degussa and another type of titania was obtained from Nanoamor Inc. The basic physical characteristics of these three types of titania have been listed in Table 5.7. To prepare the titania dispersion, the standard recipe as described in chapter 4, was followed. For this initial comparison, no emulsion was added into the titania. The dispersion pastes were blade coated onto the FTO glass and heat treated to 500 ^{0}C. The coatings were then soaked into the dye solution and assembled into the dye solar cells. The solar cell parameters and efficiency values of these solar cells are given in Table 5.8. It was observed that titania obtained from Nanoamor, Inc. showed best solar cell performance among the three samples. The Aeroxide-P90 showed lowest values of efficiency and Aeroxide-

P25 was in between. However, since Aeroxide-P25 nanopowder was supplied to us as a free sample in bulk it was used for the rest of this research.

Table 5.7: Physical properties of titania obtained from different suppliers

Titania sample	Primary particle size (nm)	Specific surface area (m^2/g)	Density (g/cm^3)	Morphology	Anatase
Aeroxide-P25	21	50	4	Spherical	70%
Aeroxide-P90	14	90	4	Spherical	70%
Nanoamor-TiO_2	15	240	3.9	Spherical	99%

Table 5.8: Solar cell performance comparison of titania obtained from different suppliers

Solar cell sample	Photocurrent (mA)	Photovoltage (V)	Fill factor	Efficiency (%)
Aeroxide-P25-A	1.25	0.55	0.67	2.05
Aeroxide-P25-B	1.25	0.56	0.70	2.21
Aeroxide-P90-A	0.67	0.61	0.91	1.66
Aeroxide-P90-B	0.68	0.61	0.70	1.31
Nanoamor-TiO_2-A	1.08	0.61	0.72	2.14
Nanoamor-TiO_2-B	2.14	0.64	0.53	3.22

5.4.2 Effect of templating on the dye solar cell performance:

In this experiment, the solar cell performance of the 20% and 40% emulsion templated cells were compared with the nontemplated dye solar cell. The results have been presented in Figure 5.52. All the tests were performed under 100 mW/cm^2 illumination. It was observed that the efficiency of the 20% emulsion templated solar cell was the highest, giving almost twice the efficiency as compared to the nontemplated solar cell. The photocurrent as well as the photovoltage was higher in the 20% emulsion templated cells.

The thickness of the nontemplated titania coating and 20% emulsion templated titania coating was in the range of 15 and 20 micron respectively. The 40% emulsion templated titania coating was much thicker, around 38 micron, due to the higher viscosity of the titania-emulsion dispersion. The lower efficiency of the 40% emulsion templated solar cell must partly be due to the higher thickness of the photoelectrode which caused loss of many photogenerated electrons before they got transported to the FTO electrode. In order to confirm this result several 40% emulsion templated cells were tested again and compared with the nontemplated cells. The results of all these cells are listed in Table 5.10. All the tests confirmed that templating the titania coating with 40% oil in water did not improve the solar cell performance. The SEM micrographs and porosimetry results had shown that 40% emulsion templated samples contained very big pores, some as large as 5 to 10 microns. Also the porosity of these coatings was above 80%. Such a high porosity decreases the light absorption of the coating, which in turn decreases the photocurrent [15].

To verify the effect of titania coating thickness on the performance of the solar cell, a detailed experiment was performed. In this experiment 20% emulsion templated titania coatings were deposited with different thickness. A thinner scotch tape was used to make thinner films and multiple layers of scotch tapes were used to make thicker coatings. Titania coatings with 5 different thicknesses such as 5 µm, 10 µm, 15 µm, 20 µm and 30 µm were deposited in this way. The thickness of the coatings was measured using a profilometer. Figure 5.53 plots the average efficiency of the solar cells made with these coatings. It was observed that 10 to 20 µm thick titania coatings gave higher solar cell efficiencies. The 5µm thick films were too thin to catch all the incident light, therefore had fewer photogenerated carriers. On the other hand, in the 30 µm thick films most of the photogenerated carriers in the outer part of the titania electrode might have got trapped before reaching to the FTO, therefore they did not contribute to the photocurrent of the solar cell.

While comparing the performance of the nontemplated, 20% templated and 40% templated cells (Table 5.9), any particular trend in the photovoltage was not seen. The electrolyte used for all the solar cell tests was the same, therefore ideally the photovoltage of the cells should be very similar. The differences in the photovoltage could be due to the influence of the electrical contacts made through the alligator clips. The fill factor of the solar cells showed dependence on the titania coating thickness. With increasing thicknesses, from nontemplated titania coating to 40 % templated titania coating, the series resistance of the solar cell increased, which reduced the fill factor. Most prominent effect of porosity

and microstructure of the titania coating was seen on the photocurrents of the cells. The photocurrents of the 20 % templated cells were highest. This result was consistent with the thickness, microscopy, porosimetry and impedance spectroscopy study of the 20 % templated cells. The porosity and microstructure of these coatings was well suited to the commercial P25 titania coating. This improved the electrolyte penetration and therefore charge transport though the titania coating.

In this research, titania from different sources or having a different morphologies, were not studied. But depending upon the primary particle size, shape and surface area properties the required pore structure for the titania photoelectrode may change. With emulsion templating method, it is very easy to modify the pore structure of the coating by changing the emulsion formulation. Thus emulsion templating method will be compatible with various types of titania.

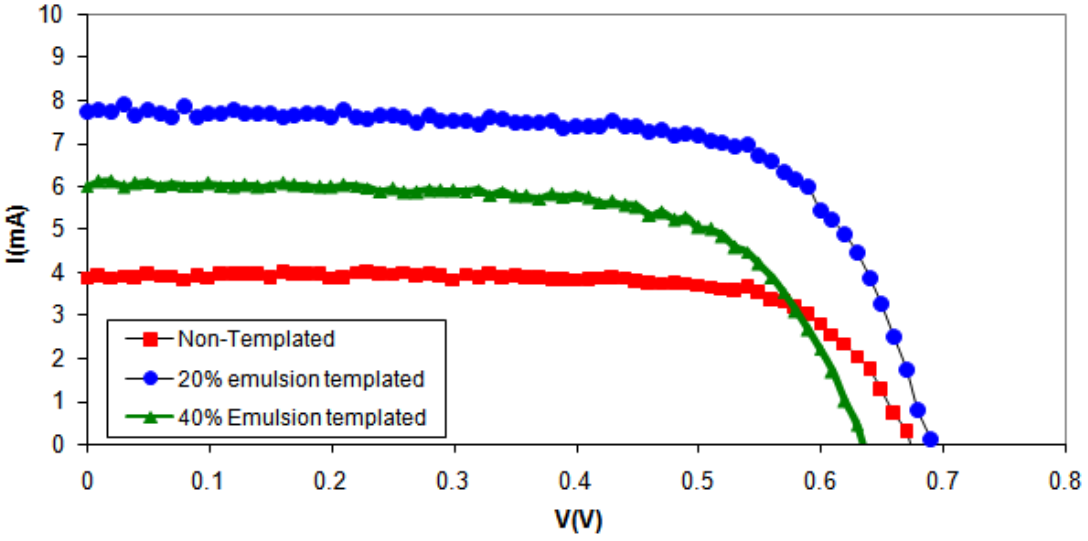

Figure 5.52: : I-V plot of dye sensitized solar cells with templated and nontemplated coatings under 100 mW/cm^2 illumination

Table 5.9: Solar cell parameters comparison of templated and nontemplated cells (under 100 mW/cm^2)

Sample	Photocurrent (mA.cm^{-2})	Photovoltage (V)	FF	Efficiency (%)	Thickness (micron)
Nontemplated	3.84	0.68	0.74	2.17	17
20% emulsion templated	7.72	0.7	0.69	4.17	20
40% emulsion templated	5.96	0.64	0.67	2.86	38

Table 5.10: Solar cell performance comparison between 40% emulsion templated and nontemplated dye solar cells

Sample	Photocurrent ($mA.cm^{-2}$)	Photovoltage (V)	FF	Efficiency (%)	Thickness (micron)
Nontemp-A	8.12	0.65	0.64	3.75	12
Nontemp-B	7.4	0.67	0.62	3.42	14
Nontemp-C	7.36	0.65	0.64	3.40	13
Nontemp-D	5.52	0.70	0.61	2.62	17
Nontemp-E	6.32	0.69	0.62	3.00	15
40temp-A	8.52	0.65	0.59	3.07	28
40temp-B	8.04	0.66	0.61	3.63	31
40temp-C	7.24	0.67	0.60	3.60	32
40temp-D	7.36	0.65	0.55	3.23	34
40temp-E	7.64	0.68	0.58	2.92	36

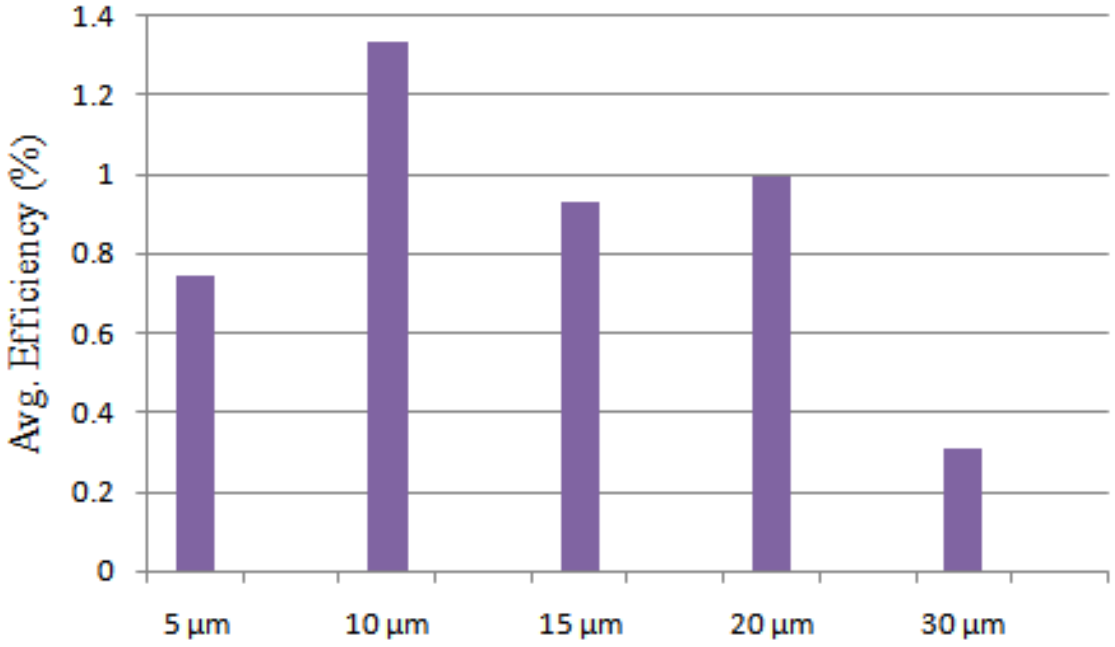

Figure 5.53: Effect of titania coating thickness on solar cell efficiency

5.4.3 The effect of templating on the sensitization time of the electrode

In the BET surface area measurements, it was observed that the surface area of the emulsion templated samples decreased with the increase in porosity. This suggests that at saturation the dye adsorbed onto the templated coatings will be less than for the nontemplated coatings. However, the interconnected pore channels in the templated coatings might provide better and faster access for dye molecules into the structure. To test this hypothesis, the effect of templating on the sensitization time of the titania coating was studied. For this study, the templated and nontemplated titania films were soaked in the dye solution over different duration of times (3, 6 and 9 hours). The films were then built into the dye sensitized solar cells and tested on the solar simulator system. Figure 5.54 plots the results of this experiment in terms of normalized photocurrents and the dye soaking time. It is interesting to note that the photocurrents of the templated cells, increased considerably within 3 to 6 hours of dye soaking. This effect was more pronounced for the 40% emulsion templated cells as compared to the 20% emulsion templated cells. On the other hand, the nontemplated cells showed slow improvement in the photocurrents and reached a plateau. It is evident from the plot that due to the interconnected pore channels in the emulsion templated solar cells, the dye solution could reach to the interior of the coatings more rapidly.

In a typical dye sensitized solar cell, the titania electrodes are soaked in the dye solution over 12 to 24 hours. The result showing that the emulsion templating process helps the titania films adsorb the dye molecules much

faster, is of great significance in the commercial sense because it suggests that by using porous titania electrodes the manufacturing time of the dye solar cells can be shortened.

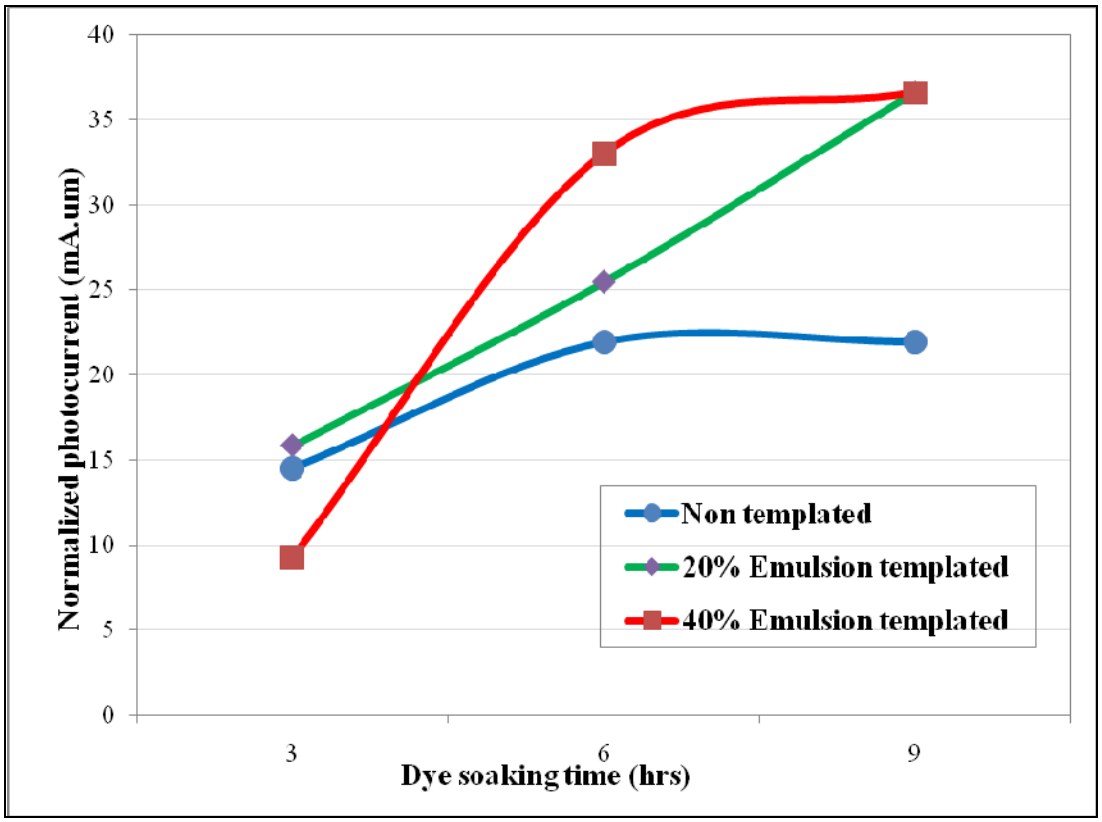

Figure 5.54: Effect of templating on the sensitization time of the dye solar cells

References

1. Mayerhofer, D. *Characteristics of resist film produced by spinning.* Journal of Applied Physics 1978, 49: p. 3993-3997.
2. Ohara, T., Matsumoto, Y., Ohashi, H. *The film formation dynamics in spin coating.* Physics of Fluids A. 1989, 1: p. 1949-1959.
3. Emslie, A. G., Bonner, F. T., Peck, L. G. *Flow of a viscous liquid on a rotating disk.* Journal of Pllied Physics 1958, 29: p. 858-862.
4. Bornside, D. E., Macosko, C. W., Scriven, L. E. *On the modeling of spin coating.* Journal of Imaging Technology 1987, 13: p. 122-130.
5. Przerwa, E., Sosnowski, S. *Deposition of poly(styrene/alpha-tert-butoxy-omega-vinyl-benzyl-polyglycidol) microspheres on mica plates crossing the liquid-air interface: Formation of stripe pattern.* Langmuir 2004, 20: p. 4684-4689.
6. Kralchevsky, P. A, Denkov, N. D. *Capillary forces and structuring in layers of colloid particles.* Current Opinion in Colloid & Interface Science 2001, 6: p. 383-401.
7. Denkov, N. D. *Mechanism of Formation of Two-Dimensional Crystals from Latex Particles on Substrates.* Langmuir 1992, 8: p. 3183-3190.
8. Gratzel, M. *Solar Energy Conversion by Dye-Sensitized Photovoltaic Cells.* Inorganic Chemistry 2005, 44: p. 6841-6851.
9. Gratzel, M. *Conversion of sunlight to electric power by nanocrystalline dye-sensitized solar cells.* Journal Of Photochemistry And Photobiology A-Chemistry. 2004, 168: p. 235-235.
10. Wang, Q., Moser, J. E., Grtzel, M. *Electrochemical Impedance Spectroscopic Analysis of Dye-Sensitized Solar Cells.* Journal of Physical Chemistry B 2005, 109: p. 14945-14953.
11. Hsua, C., Lee, K., Tai-Wei, J., Chia-Lin, Y. H., Lee, C., Wang, L., Tsai, S., Hoa, K. *EIS analysis on low temperature fabrication of TiO2 porous films for dye-sensitized solar cells.* Electrochimica Acta 2008, 53: p. 7514-7522.
12. Han, L., Koide, N., Chiba, Y., Mitate, T. *Modeling of an equivalent circuit for dye-sensitized solar cells.* Applied Physics Letters 2004, 84: p. 2433-2435.
13. Asano, T., Kubo, T., Nishikitani,Y. *Electrochemical properties of dye-sensitized solar cells fabricated with PVDF-type polymeric solid electrolytes.* Journal of Photochemistry and Photobiology A: Chemistry 2004, 164: p. 111-115.
14. DuPasquier, A. *An approach to laminated flexible Dye sensitized solar cells.* Electrochimica Acta 2007, 52: p. 7469-7474.
15. Ni, M., Leung, M. K. H., Leung, D. Y. C., Sumathy, K. *An analytical study of the porosity effect on dye-sensitized solar cell performance.* Solar Energy Materials & Solar Cells 2006, 90: p. 1331-1344.

CHAPTER 6: CONCLUSIONS

6.1 Use of emulsion templating for dye sensitized solar cells

Dye sensitized solar cells commonly use nanocrystalline titanium dioxide coatings as their photoanodes. The adsorption of the dye molecules on the titania coating surface and the permeation of the electrolyte through the titania coating have a great influence on the performance of the solar cell.

The goal of the present dissertation was to improve the permeation of the electrolyte in the titania coating. This was achieved through the creation of macropore channels in the coatings using emulsion templating. It was shown that the dye sensitized solar cells with improved porosity and microstructure of the titania coating had higher photocurrent and power outputs. The conclusions drawn in this research work are as follows:

- The templating method using either the polystyrene suspension or the oil-in-water emulsion provided a very convenient method to incorporate larger scale porosity into the titania coating. Emulsions with paraffin oil emulsified in water with Tween-80/Span-80 emulsifier mixture are projected to be more cost effective than suspensions made using the monodispersed polystyrene particles. Therefore the emulsion templating method has the potential to be employed in the commercial manufacturing of the dye sensitized solar cells as well as other structures where interconnected porosity is important for the device operation.
- The microstructure of the emulsion templated coatings was studied using scanning electron microscopy and other techniques. When compared to the nontemplated coatings, emulsion templated coatings clearly showed dual size-

scale porosity. The titania nanoparticles were pushed aside by the templating particles and sintered into framework structures around the pores left behind when the templates were removed. The cross-sectional SEM micrograph confirmed that the pores were not only present on the surface but also throughout the bulk of the titania coatings.

- Mercury porosimetry supported the results obtained by the electron microscopy. Nontemplated titania coatings contained pores of the order of 30 nm. The 20 % emulsion templated coatings had 30 nm mesopores as well as macropores with sizes ranging between 200-1000 nm. The 40 % templated coatings also contained some very big pores of the order of 5 to 10 microns (consistent with the SEM images), along with the smaller pores. The total porosity content of the nontemplated coatings was 53%. It increased to 69% in the 20 wt% emulsion templated coatings and to 82% in the 40 wt% emulsion templated coatings. Mercury porosimetry measures only the accessible interconnected pores by intruding liquid mercury in the coatings. This reconfirmed that the emulsion templating process created an interconnected network of pores throughout the bulk of the titania coatings.
- BET specific surface area measurements showed that the surface area of the templated coatings was smaller than the nontemplated coatings, however the total surface area was still similar to the starting material (about 80-90%). The 10-20% reduction in surface area could be due to some residual oil and impurities left in the mesopores in the coatings after firing to remove surfactant and oil constituents. However, the time required for dye sensitization of the titania

coatings was observed to be shorter in the templated coatings. This can also be attributed to the interconnected pore channels characterized above. This suggests that by employing porous titania electrodes, the manufacturing time of dye solar cells could be shortened.

- Electrochemical impedance spectroscopy was used to study the effect of the templating on the impedance related to the internal operation of the dye solar cell. The templated cells showed significantly lower impedances for the processes attributed to the TiO_2/dye/electrolyte interface within the devices. The charge transfer resistance of the TiO_2/dye/electrolyte interface showed a decreasing trend from nontemplated coatings to 20% and 40% emulsion templated coatings. At the same time, the chemical capacitance associated with the TiO_2/dye/electrolyte interface showed an increasing trend. This suggested that there was faster electron transfer at the TiO_2/dye/electrolyte interface of the emulsion templated cells.
- Electrochemical impedance spectroscopy of the emulsion templated and the nontemplated cells using liquid and quasi-solid electrolyte showed promising results. The difference in the conductivities of the electrolytes reflected clearly on the impedance data of the nontemplated cells showing higher impedances when the quasi-solid polymer gel electrolyte was used instead of the liquid electrolyte. On the other hand, the emulsion templated cells showed similar impedances for both electrolyte types. This result was a manifestation of the presence of the larger interconnected pore channels in the templated titania electrodes which

allowed the gel electrolyte to be in better contact with the titania structure compared to the liquid electrolyte.

- The 20 wt% emulsion templated solar cells showed better performance than nontemplated cells. This result was consistent with the microscopy and porosimetry results of 20 % templated coatings. These coatings had uniformly dispersed, interconnected and optimally sized (200 to 1000 nm) network of pores. The standard thickness of the 20 % templated titania coatings was around 15 to 20 microns, which was comparable to the nontemplated coatings.

6.2 Use of emulsion templated coatings in other applications

The emulsion templating method can be conveniently applied for the applications where materials with pore sizes in the range of 50 nm to 10 µm are needed and which require multiscale porous materials combining high diffusion, high surface area and high pore volume. The pore size and pore size distribution in these materials can be easily controlled by changing the emulsion formulation. Here are some applications where these materials might be suitable:

- **Photonic crystals with optical bandgaps:** Photonic crystals are materials composed of periodic dielectric nanostructures, which affect the propagation of light and create range of “forbidden” frequencies called a photonic bandgap. Depending on the wavelength, photons are either allowed or forbidden to pass through the structure which provides an opportunity to control the flow of the light for photonic information technology. V.N.Manoharan, et, al. [1] tried to produce photonic crystals with emulsion templated macroporous titania. In their work a high concentration emulsion was first added to a titania sol, containing TiO_2 oligomers in a polar liquid (formamide). A catalyst was then added to gel the sol followed by removal of the oil droplets. It was observed that very high degree of monodispersity of the emulsion is required to exhibit a bandgap. A sheared or fractioned emulsion can be used for this application in order to produce an emulsion with uniform oil droplets. Due to the deformability of the oil templates the material can easily withstand the stresses of shrinkage during the gelation process and is less likely to form cracks.

- **Catalytic materials:** For catalytic materials, the active sites are usually located in the meso or micropores. Introduction of larger, macro-sized pores improves the mass transfer in such materials, especially if the product or reactant molecules are large, such as biomolecules or polymers. Usually emulsions are polydispersed, therefore they have ability to create hierarchically bimodal mesoporous-macroporous materials in which larger pores are connected through smaller pores. Such interconnection is beneficial for increasing the diffusion rate in the catalytic materials.
- **HPLC separation:** The silica monolith with meso- and macropores, acting as the stationary phase in HPLC separation, shows much higher performance than the conventional columns with packed silica particles [2-3]. Ordered macroporous silica can be very successfully produced by emulsion templating with oil-in-formamide emulsion and silicon tetramethoxide [4-5]
- **Scaffolds and tissue engineering:** The emulsion templating method can produce highly interconnected macropores in the host material, therefore can be used as scaffolds for bioengineering applications if an appropriate biocompatible material is chosen [6-7].

The present successes using emulsion templating of materials for dye sensitized solar cells has demonstrated the high level of versatility and tunability of the technique and supports the suggestion that these other applications would benefit from using this process.

References:

1. Manoharan, V. N., Imhof, A., Thorne, J. D., Pine, D. J. *Photonic Crystals from Emulsion Templates.* Advanced Materials 2001, 6: p. 447-450.
2. Tanaka, N., Kobayashi, H., Nakanishi, K., Minakuchi, H., Ishizuka, N. *Peer Reviewed: Monolithic LC Columns.* Analytical chemistry 2001, 73: p. 420A-429A.
3. Ishizuka, N., Minakuchi, H., Nakanishi, K., Soga, N., Tanaka, N. *Designing monolithic double-pore silica for high-speed liquid chromatography.* Journal of Chromatography A 1998, 797: p. 133-137.
4. Imhof, A., Pine, D. J. *Uniform Macroporous Ceramics and Plastics by Emulsion Templating.* Chemical Enginerring Tehcnology 1998, 21: p. 682-685.
5. Imhof, A., Pine, D. J. *Ordered Macroporous Materials by Emulsion Templating.* Nature 1997, 389: p. 948-951.
6. Zhang, H., Cooper, A. *Synthesis and applications of emulsion-templated porous materials.* Soft Matter 2005, 1: p. 107-113.
7. Sohier, J., Haan, R. E., Groot, K., Bezemer, D. J. M. *A novel method to obtain protein release from porous polymer scaffolds: emulsion coating* Journal of Controlled Release 2003, 87: p. 57–68.

CHAPTER 7: FUTURE WORK

The main advantage of the dye sensitized solar cell technology is its potential for low material and processing cost as compared to the existing PV technologies. But it is apparent that the efficiency of this technology is far lower than the silicon solar cell and the other thin film technologies. Therefore, much of the future research in the dye sensitized solar cell field should be aimed at the performance and stability improvement of the solar cells. In the present research, the emulsion templating method was employed to produce macroporous titania coatings. It was demonstrated that the added macroporosity improved the electrolyte penetration in the titania photoelectrode and in turn improved the performance of the solar cell. In line with the presented study, I would like to propose the following areas in which this work could be further extended.

- Altering the template removal procedure

It was observed in this research, that the surface area of the emulsion templated titania coatings was somewhat lower than the nontemplated coatings. This could be due to the incomplete removal of oil templates from the tiny mesopores and residual impurities from the surfactants. Although the thermogravimetry data taken up to 500 ^{0}C showed a plateau from 430 ^{0}C onwards, a small percentage of oil and/or inorganic residue from the emulsion might still have been left behind in the tiny pores. An extended, higher temperature heat treatment or a chemical treatment can be employed to make sure that all the oil templates and other impurities are more completely removed while still keeping the surface area as high as possible. This

should increase the surface area of the templated coatings; its effect on the solar cell performance would be worth studying.

- Emulsion templating with different titania structures

In this research only commercial P25 titania nanoparticles, bought from Evonik-Degussa, were used. This was 70% anatase, spherical titania nanoparticle powder with average aggregate size of around 300 nm. It would be interesting to try titania with different nanoparticle size and morphology and see how the required pore structure might need to be altered compared to what we used for P25. For smaller titania particles, we may have to use an emulsion having smaller oil droplet size to incorporate pores from the range of 100 to 1000 nm.

For titania with different morphologies, most commonly with high aspect ratio particles, polydispersed template particles, again in the range of 100 to 1000 nm, might help align the nanoparticles in vertical direction to improve electron transport as well as electrolyte penetration through the titania structure.

- Emulsion templating with high internal phase (oil) ratio emulsions

In the presented research work, emulsions with only up to 40 wt % oil in water were used to template the titania coatings. At high internal phase ratio (IPR) (between 45 to 70 wt %), oil particles start interacting with each other and form continuous pathways even before drying of the coatings. It would be interesting to study the permeation of the quasi-solid electrolytes through the coating with such continuous pore paths. The diffusion of the ionic species will be much faster through such continuous pathways. It is very important to pay attention to the surface area while producing such coatings, because the titania particles might tend to get pushed

closer to each other, thus reducing the available surface area. This would have an adverse effect on the dye adsorption within the coating.

Another consideration is that a higher amount of emulsifier will have to be added in the formulation to produce higher IPR emulsions. The removal of these emulsifiers upon heat treatment will also add to the porosity of the coating. It is also very important to consider the effect on the thickness of the titania film with such high oil content. Some of the above mentioned effects of high IPR emulsion might not be beneficial for the overall solar cell performance but it would be worth trying, and the resulting data will improve our understanding of the coupled conduction processes in these devices.

- Inkjet printing of emulsion templated titania inks

It was mentioned in the results and discussion chapter (chapter 5) that the main drive behind choosing the emulsion templates over the polystyrene templates was the lower cost, easy availability and simplicity of the emulsion templating method. During this time of the research, I was also exploring the inkjet printing technique to print titania inks. The idea was to do a combinatorial study where different layers of the titania, the dye and the electrolyte could be deposited in a more controlled way with ink jet printing and a detailed study of the effect of different amounts of dye and electrolyte dosing could be performed. It would be interesting to try inkjet printing the mixture of emulsion and titania dispersions. Polydispersity of the emulsion should not cause any problem because the oil templates (being deformable) are less likely to clog the nozzle during droplet formation. Also the interaction of each ink droplet with the substrate will be different depending on the concentration of the oil

in each droplet. All these effects will have interesting influence on the microstructure of the printed coating.

CURRECULAM VITAE

Sarika Phadke: sarika.phadke@gmail.com

Education

- Ph.D. (Jan. 2010) Materials Science & Engineering, Rutgers University, NJ, USA GPA: 3.9
- MS (Jan. 2008) Materials Science & Engineering, Rutgers University, NJ, USA GPA: 3.9
- BE (June 2002), Instrumentation and Control Engineering, Government College of Engineering, Pune, India. First Class with Distinction

Research Experience

- Graduate Research Assistant (Sept. 2005 - present), Materials Science & Engineering, Rutgers University, NJ, USA.
- Teaching Assistant (Sept 2007 – Dec. 2007), Materials Science & Engineering, Rutgers University, NJ, USA.
- Part Time Research Scientist (Sept 2007 – Dec 2008), Honeywell Specialty Materials, NJ, USA.
- Full Time Research Scientist (June 2007–Sept 2007), Honeywell Specialty Materials, NJ, USA.
- BE, senior year project (June 1997-June 1998), Tata Institute of Fundamental Research, Pune, India

Industry Experience

- System Engineer (June 2002–Oct 2004), Emerson Process Management, Pune, India.

Publications

- S. Phadke, J. B. Stanley, J. D. Sorge, and D.P. Birnie III, “Clustering effects in solution based nanoparticle/template hybrid coatings”, Journal of the society for Information Display, 2007, 15, 1089.
- S. Phadke,Dunbar P. Birnie, III, “Emulsion templating to obtain dual-size-scale mesoporous titania coatings”, accepted at Materials Letters, 2009.
- S. Phadke, J. D. Sorge, S. Hachtmann and Dunbar P. Birnie, “Broadband optical characterization of sol-gel TiO_2 thin film microstructure evolution with temperature”, submitted at Thin Solid Films, 2009.
- S. Phadke, A. Du Pasquier and D. P. Birnie,III, “Enhanced conduction through template-derived pore channels in dye sensitized solar cells”, submitted at Electrochemica Acta, 2009.